

AD-A252 652



6571-AN-01

2

DTIC
ELECTE
JUL 8 1992
S C D

COMPOSITE BEAM ANALYSIS
LINEAR ANALYSIS OF NATURALLY
CURVED AND TWISTED ANISOTROPIC
BEAMS

Final Technical Report

by

Marco Borri, Full Professor
Gian Luca Ghiringhelli, Research Assistant
Teodoro Merlini, Associate Professor

May 1992

United States Army
EUROPEAN RESEARCH OFFICE OF THE U. S. ARMY
London, England

Contract DAJA45-90-C-0037

Politecnico di Milano
DIPARTIMENTO DI INGEGNERIA AEROSPAZIALE
Via C. Golgi 40, 20133 Milan, Italy

Approved for Public Release. Distribution unlimited.

92 7 00 0

92-17539



COMPOSITE BEAM ANALYSIS

LINEAR ANALYSIS OF NATURALLY CURVED AND TWISTED ANISOTROPIC BEAMS

by
Marco Borri, Gian Luca Ghiringhelli, Teodoro Merlini
Dipartimento di Ingegneria Aerospaziale
Politecnico di Milano
Via C. Golgi 40, 20133 Milan, Italy

Accession For	
DTIC GRA&I	<input checked="" type="checkbox"/>
DTIC TAB	<input type="checkbox"/>
Unannounced	<input type="checkbox"/>
Justification	
By	
Distribution/	
Availability Codes	
Avail and/or	
Dist	Special
A-1	

Abstract

The aim of this report is to present a consistent theory for the deformation of a naturally curved and twisted anisotropic beam. The proposed formulation naturally extends the classical Saint-Venant approach to the case of curved and twisted anisotropic beams. The mathematical model developed under the assumption of span-wise uniform cross-section, curvature and twist, can take into account any kind of elastic coupling due to the material properties and the curved geometry. The consistency of the math-model presented and its generality about the cross-sectional shape, make it a useful tool even in a preliminary design optimization context such as, for example, the aeroelastic tailoring of helicopter rotor blades.

The advantage of the present procedure is that it only requires a two-dimensional discretization: thus, very detailed analyses can be performed and interlaminar stresses between laminae can be evaluated. Such analyses would be extremely time consuming if performed with standard finite element codes: that prevents their recursive use as for example when optimizing a beam design.

Moreover, as a byproduct of the proposed formulation, one obtains the constitutive law of the cross-section in terms of stress resultant and moment and their conjugate strain measures. This constitutive law takes into account any kind of elastic couplings, e.g. torsion-tension, tension-shear, bending-shear, and constitutes a fundamental input in aeroelastic analyses of helicopter blades.

Four simple examples are given in order to show the principal features of the method.

1 Statement and Scope

The relevance of aeroelastic tailoring of helicopter blades is very well known in rotorcraft community. In fact, the elastic couplings can strongly influence the aeroelastic behavior of rotor systems and even control their stability. Stability analyses of helicopter rotors are often performed using special beam models to simulate the blade dynamic behavior, i.e. the blade is considered as a one-dimensional continuum with a general form of elastic couplings. Therefore, the constitutive law expressed in terms of stress resultant and moment on the cross-section and their conjugate strain measures is a fundamental input for aeroelastic analyses. In this regard, the elastic couplings, such as tension-torsion, tension-shear, bending-shear, etc., are of fundamental importance in performing aeroelastic tailoring.

Such couplings arise from two different sources, namely material properties and geometric shape of the blade. Obviously, a very general way in order to compute the elastic constitutive relations is using a general three-dimensional finite element code, but a drawback of this approach is the amount of computer time required that cannot be accepted during the preliminary design phases in which different fiber orientations and materials are to be analyzed in order to meet the design requirements.

An alternative approach, in order to circumvent this problem, is to take some suitable simplifying assumptions allowed by the blade geometry and by the aims of the preliminary design itself, as for example the constancy of the cross-section properties along the beam axis. This assumption leads to a dramatic improvement of the analysis since the three-dimensional problem can be easily reduced to a two-dimensional one. In fact the object of the analysis is now reduced to a simple beam slice instead of the entire blade. By the use of this simplified physical-mathematical model, the elastic properties of the blade cross-section can be optimized and properly tailored and only few three-dimensional analyses are required to assess the final design.

Solutions in closed form of composite cross-sections are not available and a two-dimensional finite element model of the blade section is required. This finite element model is a special one since it is able to recover the three-dimensional solution with the only assumption of constancy of the cross-section. This kind of analysis, developed by the writer and its colleagues, was already available for straight beams. The aim of this work is to extend this approach to naturally twisted and curved beams retaining the assumption of the constancy of the cross-section properties. The influence of the pre-twist become mandatory in the analysis of tilt helicopter rotors like the JVX, in which the amount of twist required in airplane mode by aerodynamic consideration is much larger than that usually required for conventional helicopter rotors: therefore a stronger influence can be also expected from a structural point of view.

The research work reported herein can be summarized as follows:

- Development of the mathematical formulation of the mechanics of a beam slice, based on the principle of virtual work and taking into account the effects of a constant pre-twist and pre-bending. The possibility of a cross-section tilted with respect to the axis has been investigated. This section extends the approach already available for straight beams. One result of such an analysis is the solution of the cross-section problem in terms of displacement and stress distribution due to six independent and equilibrated load conditions corresponding to the components of the cross-section stress resultant and moment. Moreover, as a byproduct of this analysis, the six by six compliance matrix of the cross-section is obtained. In addition, the eigenvalue analysis in terms of warping displacements is performed and the extremity solutions computed. The results of these analyses can be used as input in subsequent dynamic analyses in which the beam is treated as a one-dimensional continuum.
- Formulation of different finite elements in anisotropic material like the isoparametric plane element, the lamina element, the isoparametric panel and the stringer element.
- Modification of the pre-existing computer code for straight beam, in order to include the curved and tilted geometry. Description and organization of the computer code based on the finite element method.
- Development of some numerical test cases and comparison with NASTRAN results.

2 Theoretical Development

2.1 Introduction

The design of composite blades of helicopter rotors demands the analysis of three-dimensional stress states including interlaminar stresses. Despite the power of modern computers, standard three-dimensional finite element approximations of the entire rotor blade are not yet considered feasible, because of the huge computer effort required to achieve a reasonable degree of accuracy in modeling the material properties of the blade cross-section (Hodges, 1990b). In fact when dealing with composite beams, particular care must be taken in order to model the material properties, especially when interlaminar stresses must be evaluated. The example of the circular composite tube, see Fig. 1 (from Giavotto *et al.*, 1983), shows that the stress state is three-dimensional even under pure torsion, hence a detailed model of the cross-section is essential in order to correctly capture it. Moreover, the stacking sequence of different laminae may have a strong influence on the cross-section distortion and on the stress distribution, as shown for example by Ghiringhelli and Sala (1990): as a simple example refer to Fig. 2 (from Ghiringhelli and Sala, 1986), where the in-plane section distortions of a flat specimen loaded in uniform tension are shown for two different cross-ply laminates. These examples stress that for composite beams not only is the out-of-plane distortion, usually accounted for, significant, but also the in-plane distortion must be taken into account in order to correctly model the stress behavior. It is important to observe as well, that the interlaminar stresses between contiguous laminae must be continuous and, since the material properties are in general different, the conjugate strains are discontinuous. This fact constitutes a prerequisite of any displacement-based finite element approximation and, in order to model this strain discontinuity, the element size must not be greater than the thickness of the lamina.

The high degree of detail required to model such problems cannot be tolerated in a direct three-dimensional approach, since the high number of degrees of freedom prevents its use in preliminary design phases and in an optimization context. On the contrary, it would be better to face the problem in two consecutive steps dealing separately with the cross-sectional analysis and with the global-beam analysis. In the first step the three-dimensional stress analysis of the beam cross-section, modeled on a two-dimensional domain, is performed leading to a differential problem with respect to the span-wise coordinate of the beam. This step is generally performed with a finite element procedure, as proposed by Giavotto *et al.* (1983), although an analytical approach giving solutions in closed form could fit as well for very simple cross-sections. In this step particular solutions under prescribed stress resultants are obtained, giving the stiffness of the cross-section and its generalized warping, i. e. section out-of-plane and in-plane distortion. Moreover eigensolutions can be obtained giving the diffusion length of self-equilibrated modes, that can be

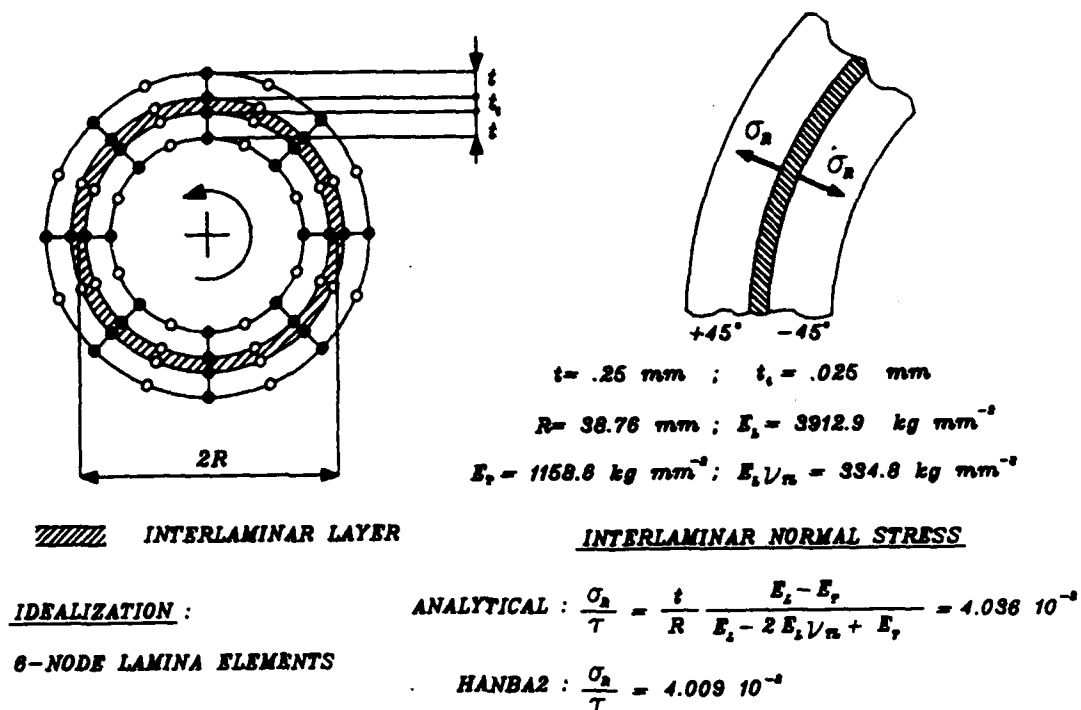
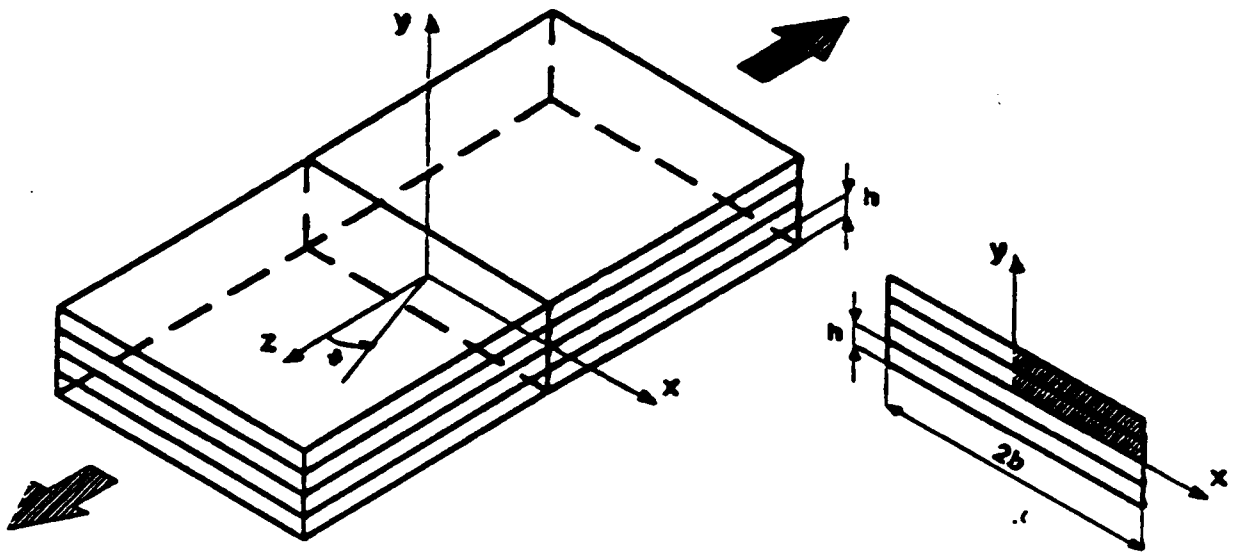


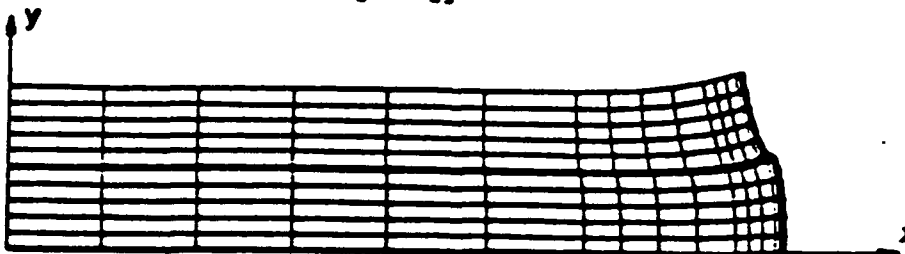
Figure 1: Thin-walled composite cylinder [+45/-45] loaded in torsion (not to scale).

superimposed to the central solutions to account for extremity effects, either at the beam ends or in the neighborhood of concentrated loads. These modes, as pointed out by Rehfield *et al.* (1990), could also be used as additional kinematical variables when modeling thin-walled beams, while their role in axially compressed beams and panels has been dealt with by Merlini (1988).

The second step is mainly devoted to the behavior of the entire beam, this in general being naturally curved and twisted: here the beam is considered as a one-dimensional continuum and its constitutive law is taken from the previous step. This kind of approach naturally extends the well known Saint-Venant approach to pretwisted and curved anisotropic beams, and it is gaining more and more attention in rotor blade modeling, as discussed in a review by Hodges (1990b). Moreover, this approach seems to be suitable for geometrically nonlinear beam analyses, both static and dynamic, where strains can be assumed to be small and nonlinearities confined within the one-dimensional beam model, as shown by Borri and Mantegazza (1985) and Borri and Merlini (1986). This idea can be found in the papers by Parker (1979a, b), who followed an asymptotic procedure and used the Saint-Venant warping function, and by Berdichevsky (1981) and Berdichevsky and Staroselsky (1983), who proposed a variational-asymptotical method. A general assessment of this approach has been set up by Hodges and his co-workers and is plainly described in some recent papers: Hodges (1990a), Atilgan and Hodges (1990), Atilgan *et al.*



$[90^\circ/0^\circ]_s$



$[0^\circ/90^\circ]_s$

Figure 2: Flat composite specimen loaded in axial tension and in-plane distortion for two different stacking sequences.

(1991) and Hodges *et al.* (1991a). An application to beam free-vibration analysis can be found in Hodges *et al.* (1991b).

It is not in the purpose of this report to review the intensive work towards comprehensive beam modeling found in the literature: an excellent review is found in Hodges (1990b). Nevertheless, at least the following papers must be mentioned for their significant contribution to the one-dimensional formulation and analysis of the nonlinear behavior of either rectilinear or space-curved beams: Reissner (1973, 1981), Simo (1985), Simo and Vu-Quoc (1988), Hodges (1987a, b), Danielson and Hodges (1987, 1988), Bauchau and Hong (1987), Cardona and Geradin (1988) and Iura and Atluri (1988, 1989). Other papers are mentioned here contributing to the three-dimensional analysis of the beam cross-section. Theories by Bauchau (1985) and Bauchau and Hong (1988) are demonstrated to behave well but the assumption of indeformability of the cross-section in its own plane seems too strong for a general-purpose analysis of composite beams. Kosmatka and Dong (1991) proposed an analytical model of the anisotropic cross-section yielding the global properties of the section, but their work is restricted to homogeneous beams. Finally, the work by Stemple and Lee (1988, 1989) is mentioned, though it is not relevant to any of the two steps stated above: they developed a particular fully three-dimensional finite element procedure accounting explicitly for warping of anisotropic sections, but it seems that the prerequisite of stress continuity and strain discontinuity between laminae could hardly be satisfied in practice by their approach.

The present report aims to contribute to the first step outlined above. A quite general theory is formulated for the three-dimensional cross-section analysis accounting for initial twist and curvature of anisotropic and nonhomogeneous beams. The constitutive law of the section obtained this way could then be used in most of the one-dimensional theories for space-curved beams proposed by many authors, such as those mentioned above. The generality of the proposed theory is only lacking in the sense that it allows for constant twist and curvature along the beam span: from a practical point of view, this restriction can be suitably overcome in the one-dimensional analysis by means of a spatial interpolation, using beam finite elements. Although this theory was motivated by the demands inherent to modeling helicopter rotor blades, it is believed that it constitutes a valid tool in many other structural fields. Thus it would be proper to begin to state what a *beam* is. It is worth noting that what is usually called a *beam* is not so univocally defined since there exist many different approximations. Therefore let us recall some basic definitions and restrictions.

There are at least two fundamental restrictions for a structural member to state that it is a beam: one involves only geometrical considerations, while the other concerns structural mechanics. From a geometrical point of view a beam can be defined as a solid traced by the rigid motion of a cross-section. One particular point of this section can be taken as the reference point and the line traced by this point as reference line, which is required to possess a certain level of continuity. The

geometric beam concept also includes some slenderness restrictions mainly related to the width of the cross-section that must be much smaller than the length of the reference line. Moreover, if the cross-section is not constant, its variation should be restricted to be only moderate.

From the structural point of view, in addition to the influence of the boundary conditions, we must mention at least two fundamental assumptions, one being relevant to the material properties and the other to the applied loads: these hypotheses concern the axial distribution of the material properties and the applied loads that must be very smooth. As a consequence, every structural variable like displacement or stress should have a gradient along the beam axis that is much lower than the gradient along the cross-section coordinates.

Now, it should be understood that if a solid must behave like a beam, the restrictions outlined above must hold not only before the deformation but also during the deformation and in the deformed configuration too. This issue leads to the concept of a reference cross-section which could be tilted with respect to the reference line, and even not exactly planar, in the undeformed configuration as well. Furthermore, this concept allows for an easy implementation of updated-Lagrangian incremental techniques. All these hypotheses allow us to consider a beam as a one-dimensional continuum, a point of which reacts against the deformation with one resultant and one moment, about the reference point, of the stresses acting upon the cross-section. With the previous restrictions in mind, these stress resultant and moment, for a specified reference line, should be independent of the orientation of the reference cross-section, which obviously cannot be too far from the normal one. Moreover, some freedom should also hold for the choice of the reference line: in fact, if we think about a beam which is naturally twisted, a section will be normal to only one reference line and it will not be normal to any other reference line.

Even if, in our opinion, the main difficulties related to this subject are not confined to the development of a consistent mathematical model, but instead in the correct identification of the elastic properties of composite materials, it still remains difficult to give a comprehensive definition of a *beam* and we can accept many of them, depending on a good judgment of what the goal is and what we can use to obtain it.

2.2 One-dimensional Beam Geometry

In a prescribed fixed orthogonal reference frame (O, \mathbf{E}_i) ($i = 1, 2, 3$), let \mathbf{x} be the position of a generic point P of a reference line l and let \mathbf{t} be the tangent to l at P . We can write

$$\mathbf{x} = \mathbf{x}(s) \quad \mathbf{t}(s) = \frac{d\mathbf{x}(s)}{ds} \quad (1)$$

where s denotes the arc length along l .

For simplicity let $A(s)$ be a plane cross-section. Associated to it define an orthogonal triad (P, e_i) : the unit vectors $e_1(s)$ and $e_2(s)$ belong to the cross-section while $e_3(s) = e_1(s) \times e_2(s)$ may be tilted with respect to $t(s)$; however, we assume that $e_3(s) \cdot t(s) > 0$ holds true anywhere. The orientation of the cross-section can be specified through a rotation of the section at $s = 0$,

$$e_i(s) = R(\mathbf{r}) \cdot e_i(0) \quad (2)$$

where $\mathbf{r}(s)$ is the rotation vector and $R(\mathbf{r})$ is the corresponding rotation tensor which by definition satisfies the orthonormality property $R(\mathbf{r}) \cdot R^T(\mathbf{r}) = I$. It is well known that the last can be given the following form

$$R(\mathbf{r}) = I + \sin \phi \mathbf{k} \times I + (1 - \cos \phi) \mathbf{k} \times \mathbf{k} \times I \quad (3)$$

where $\phi(s) = \sqrt{\mathbf{r}(s) \cdot \mathbf{r}(s)}$ is the magnitude of the rotation vector $\mathbf{r}(s) = \phi \mathbf{k}$ and \mathbf{k} the unit vector of the axis of the rotation.

The generalized curvature vector $c(s)$ of the beam can be introduced through the derivative of the rotation that can be cast in the form

$$\frac{dR(\mathbf{r})}{ds} = c(s) \times R(\mathbf{r})$$

due to the orthogonality property of the rotation itself. From eqn 2 it follows that

$$\frac{de_i(s)}{ds} = c(s) \times e_i(s). \quad (4)$$

In this report we confine ourselves to deal with the special case of a helicoidal beam for which the following limitations hold:

$$\frac{d}{ds}(t(s) \cdot e_i(s)) = 0 \quad \frac{d}{ds}(c(s) \cdot e_i(s)) = 0.$$

From these equations, taking into account eqn 4, we obtain

$$\frac{dt(s)}{ds} = c(s) \times t(s) \quad \frac{dc(s)}{ds} = 0$$

so that the curvature c is constant while the vector $t(s)$ rotates, i.e. it can be expressed in the following form:

$$t(s) = R(\mathbf{r}) \cdot t(0). \quad (5)$$

Moreover, since in this case it can be shown that $c = \frac{d\mathbf{r}(s)}{ds}$, it follows that

$$\mathbf{r}(s) = s\mathbf{c} = s\mathbf{c}\mathbf{k} \quad \phi(s) = sc, \quad (6)$$

i.e. the axis of rotation is constant and coincides with the axis of the curvature.

For such a helicoidal beam the equation of the line l can be written as the following:

$$\mathbf{x}(s) - \mathbf{a} = \phi(s)\alpha\mathbf{k} + \mathbf{R}(\mathbf{r}) \cdot (\mathbf{x}(0) - \mathbf{a}) \quad (7)$$

where

$$\alpha = \mathbf{k} \cdot \frac{\mathbf{t}(0)}{c} \quad \mathbf{a} = \mathbf{x}(0) + \mathbf{k} \times \frac{\mathbf{t}(0)}{c} + \lambda\mathbf{k}$$

and λ is an indeterminate scalar quantity which can arbitrarily be set to zero by choosing the vector \mathbf{a} such that $\mathbf{x}(0) - \mathbf{a}$ be orthogonal to \mathbf{k} . Equation 7 corresponds to the so called helicoidal decomposition of a rigid displacement into a rotation and a translation parallel to it. The tangent vector $\mathbf{t}(0)$ can be resolved in the following way,

$$\begin{aligned} \mathbf{t}(0) &= \mathbf{k} \otimes \mathbf{k} \cdot \mathbf{t}(0) + (\mathbf{I} - \mathbf{k} \otimes \mathbf{k}) \cdot \mathbf{t}(0) = \\ &= c(\alpha\mathbf{k} + \mathbf{k} \times (\mathbf{x}(0) - \mathbf{a})) \end{aligned} \quad (8)$$

where the identity $\mathbf{k} \times \mathbf{k} \times \mathbf{I} = \mathbf{k} \otimes \mathbf{k} - \mathbf{I}$ has been taken into account. From eqn 5, taking eqns 8 and 7 into account, we obtain the expression for the tangent vector $\mathbf{t}(s)$ to the reference line l :

$$\mathbf{t}(s) = c(\alpha\mathbf{k} + \mathbf{k} \times (\mathbf{x}(s) - \mathbf{a})).$$

Equation 7 can be easily obtained by integrating eqn 1 with eqn 5 on the curvilinear abscissa s . At first the tensor $\mathbf{S}(\mathbf{r})$ is introduced,

$$\mathbf{S}(\mathbf{r}) = \frac{1}{s} \int_0^s \mathbf{R}(\mathbf{r}) ds = \mathbf{I} + \frac{1 - \cos \phi}{\phi} \mathbf{k} \times \mathbf{I} + (1 - \frac{\sin \phi}{\phi}) \mathbf{k} \times \mathbf{k} \times \mathbf{I}$$

leading to

$$\mathbf{x}(s) = \mathbf{x}(0) + s\mathbf{S}(\mathbf{r}) \cdot \mathbf{t}(0).$$

Then recalling eqns 8 and 6 and taking the following property into account,

$$\mathbf{R}(\mathbf{r}) = \mathbf{I} + \mathbf{S}(\mathbf{r}) \cdot \mathbf{r} \times \mathbf{I}$$

eqn 7 is obtained.

It is worthwhile noting that this description of helicoidal beams is invariant with respect to the choice of the reference line. In order to clear up this concept, let l^* denote a new reference line different from l , and let $\mathbf{x}^*(s)$ and $\mathbf{x}(s)$ be the position vectors of two points P^* and P belonging to those lines and to the same cross-section. Hence the line l^* can be defined through the equation

$$\mathbf{x}^*(s) = \mathbf{x}(s) + \mathbf{e}_\alpha(s)\eta^\alpha \quad (9)$$

with η^α ($\alpha = 1, 2$) constant. Recalling eqn 2 we can write

$$\mathbf{x}^*(s) - \mathbf{x}(s) = \mathbf{R}(\mathbf{r}) \cdot (\mathbf{x}^*(0) - \mathbf{x}(0)).$$

Then eqn 7 transforms to

$$\mathbf{x}^*(s) - \mathbf{a} = \phi(s)\alpha\mathbf{k} + \mathbf{R}(\mathbf{r}) \cdot (\mathbf{x}^*(0) - \mathbf{a}).$$

In order to completely change the reference line we should also change the independent variable to the new arc length s^* on l^* . By definition, we have

$$ds^* = \sqrt{d\mathbf{x}^*(s) \cdot d\mathbf{x}^*(s)} = j ds$$

and since in the present case the the jacobian j is constant, implying $s^* = js$, from eqn 6 we can obtain the new curvature $c^* = \frac{c}{j}$. Hence, by the definition

$\mathbf{t}^*(s) = \frac{d\mathbf{x}^*(s)}{ds^*} = \frac{1}{j} \frac{d\mathbf{x}^*(s)}{ds}$, we easily obtain the tangent vector to the new reference line l^* :

$$\mathbf{t}^*(s) = c^* (\alpha\mathbf{k} + \mathbf{k} \times (\mathbf{x}^*(s) - \mathbf{a})).$$

Although the tangent and the curvature vectors depend on the choice of the reference line, the parameters α and \mathbf{a} describing the elicoidal beam are invariant: with reference to the new line l^* , they can be written as

$$\alpha = \mathbf{k} \cdot \frac{\mathbf{t}^*(0)}{c^*} \quad \mathbf{a} = \mathbf{x}^*(0) + \mathbf{k} \times \frac{\mathbf{t}^*(0)}{c^*} + \lambda^* \mathbf{k}$$

where $\lambda^* = \lambda - \mathbf{k} \cdot (\mathbf{x}^*(0) - \mathbf{x}(0))$ is a new indeterminate scalar.

2.3 One-dimensional Beam Equations

In a generic deformed position of the beam, let $\mathbf{T}(s)$ and $\mathbf{M}(s)$ denote respectively the resultant and the moment of the stresses acting upon the cross-section $A(s)$. In the small-displacement linear theory, the equilibrium equations of the beam are written as

$$\begin{aligned} \frac{d\mathbf{T}(s)}{ds} &= 0 \\ \frac{d\mathbf{M}(s)}{ds} - \mathbf{T}(s) \times \mathbf{t}(s) &= 0 \end{aligned} \tag{10}$$

where the explicit influence of the distributed external forces is omitted, since our interest is confined to homogeneous solutions. These equations can be immediately integrated leading to:

$$\begin{aligned} \mathbf{T}(s) &= \mathbf{T}(0) \\ \mathbf{M}(s) &= \mathbf{M}(0) + \mathbf{T}(0) \times (\mathbf{x}(s) - \mathbf{x}(0)). \end{aligned} \tag{11}$$

Both of eqn 11 have a very well-known and clear physical meaning. Looking at the expression for $\mathbf{x}(s) - \mathbf{x}(0)$ in eqn 7 we can see that the general solution depends on s by means of linear and circular functions.

Moreover it is interesting to obtain the solutions of eqn 10 in terms of cross-sectional components, i.e. $\hat{T}_i(s) = \mathbf{T}(s) \cdot \mathbf{e}_i$ and $\hat{M}_i(s) = \mathbf{M}(s) \cdot \mathbf{e}_i$. For simplicity we assume the fixed reference triad to be oriented as the cross-section triad at $s = 0$, so that $\mathbf{E}_i = \mathbf{e}_i(0)$, and define $\hat{\mathbf{T}}(s) = \hat{T}_i(s)\mathbf{E}_i$, $\hat{\mathbf{M}}(s) = \hat{M}_i(s)\mathbf{E}_i$, i.e. $\hat{\mathbf{T}}(s) = \mathbf{R}^T(\mathbf{r}) \cdot \mathbf{T}(s)$, $\hat{\mathbf{M}}(s) = \mathbf{R}^T(\mathbf{r}) \cdot \mathbf{M}(s)$. This is equivalent to pulling back the stress resultant and moment to the cross-section at $s = 0$. By observing that

$$\begin{aligned}\frac{d\mathbf{T}(s)}{ds} &= \mathbf{R}(\mathbf{r}) \cdot \left(\frac{d\hat{\mathbf{T}}(s)}{ds} + \hat{\mathbf{c}} \times \hat{\mathbf{T}}(s) \right) \\ \frac{d\mathbf{M}(s)}{ds} &= \mathbf{R}(\mathbf{r}) \cdot \left(\frac{d\hat{\mathbf{M}}(s)}{ds} + \hat{\mathbf{c}} \times \hat{\mathbf{M}}(s) \right)\end{aligned}$$

where $\hat{\mathbf{c}} = \mathbf{R}^T(\mathbf{r}) \cdot \mathbf{c} = \mathbf{c}$, the one-dimensional beam equilibrium equations in terms of $\hat{\mathbf{T}}(s)$ and $\hat{\mathbf{M}}(s)$ are easily written as

$$\begin{aligned}\frac{d\hat{\mathbf{T}}(s)}{ds} + \hat{\mathbf{c}} \times \hat{\mathbf{T}}(s) &= 0 \\ \frac{d\hat{\mathbf{M}}(s)}{ds} + \hat{\mathbf{c}} \times \hat{\mathbf{M}}(s) + \hat{\mathbf{t}} \times \hat{\mathbf{T}}(s) &= 0\end{aligned}$$

where $\hat{\mathbf{t}} = \mathbf{R}^T(\mathbf{r}) \cdot \mathbf{t}(s) = \mathbf{t}(0)$. These equations can be grouped into one equation of the form

$$\frac{d\hat{\mathbf{S}}(s)}{ds} + \hat{\mathbf{T}} \cdot \hat{\mathbf{S}}(s) = 0 \quad (12)$$

where

$$\hat{\mathbf{S}}(s) = (\hat{\mathbf{T}}(s), \hat{\mathbf{M}}(s)) \quad \hat{\mathbf{T}} = \begin{bmatrix} \hat{\mathbf{c}} \times \mathbf{I} & 0 \\ \hat{\mathbf{t}} \times \mathbf{I} & \hat{\mathbf{c}} \times \mathbf{I} \end{bmatrix}$$

Observing that the operator $\hat{\mathbf{T}}$ is constant and the following property holds,

$$\hat{\mathbf{T}}^6 + 2c^2\hat{\mathbf{T}}^4 + c^4\hat{\mathbf{T}}^2 = 0,$$

as it can be easily seen, by differentiating eqn 12 we obtain $\frac{d^2\hat{\mathbf{S}}(s)}{ds^2} = \hat{\mathbf{T}}^2 \cdot \hat{\mathbf{S}}(s)$,

$\frac{d^4\hat{\mathbf{S}}(s)}{ds^4} = \hat{\mathbf{T}}^4 \cdot \hat{\mathbf{S}}(s)$ and $\frac{d^6\hat{\mathbf{S}}(s)}{ds^6} = \hat{\mathbf{T}}^6 \cdot \hat{\mathbf{S}}(s)$, whence

$$\frac{d^6\hat{\mathbf{S}}(s)}{ds^6} + 2c^2\frac{d^4\hat{\mathbf{S}}(s)}{ds^4} + c^4\frac{d^2\hat{\mathbf{S}}(s)}{ds^2} = 0. \quad (13)$$

The peculiarity of this equation is that each component of the vector $\hat{\mathbf{S}}(s)$ is governed by the same differential equation. Thus, the eigenvalues are immediately found to be the solutions of the characteristic equation

$$\lambda^2(\lambda - ic)^2(\lambda + ic)^2 = 0 \quad i = \sqrt{-1}.$$

As a consequence, eqn 12 admits a solution of the following form:

$$\hat{S}(s) = (\hat{A}_0 + \phi \hat{B}_0) + (\hat{A}_c + \phi \hat{B}_c) \cos \phi + (\hat{A}_s + \phi \hat{B}_s) \sin \phi. \quad (14)$$

Imposing the initial condition at $s = 0$, by means of subsequent derivatives of eqn 12 at $s = 0$ we can obtain:

$$\begin{aligned} \hat{A}_0 &= (I + 2c^{-2}\hat{T}^2 + c^{-4}\hat{T}^4) \cdot \hat{S}(0) \\ \hat{A}_c &= -c^{-2}\hat{T}^2 \cdot (2I + c^{-2}\hat{T}^2) \cdot \hat{S}(0) \\ \hat{A}_s &= 1/2c^{-3}\hat{T}^3 \cdot (5I + 3c^{-2}\hat{T}^2) \cdot \hat{S}(0) \\ \hat{B}_0 &= -c^{-1}\hat{T} \cdot (I + 2c^{-2}\hat{T}^2 + c^{-4}\hat{T}^4) \cdot \hat{S}(0) \\ \hat{B}_c &= -1/2c^{-3}\hat{T}^3 \cdot (I + c^{-2}\hat{T}^2) \cdot \hat{S}(0) \\ \hat{B}_s &= -1/2c^{-2}\hat{T}^2 \cdot (I + c^{-2}\hat{T}^2) \cdot \hat{S}(0) \end{aligned} \quad (15)$$

Then we can express eqn 14 in the following form:

$$\hat{S}(s) = \left[I + \sum_{k=1}^5 (-c)^{-k} \psi_k(\phi) \hat{T}^k \right] \cdot \hat{S}(0) \quad (16)$$

where

$$\begin{aligned} \psi_1 &= \phi \\ \psi_2 &= 2 - 2 \cos \phi - \frac{1}{2} \phi \sin \phi \\ \psi_3 &= \frac{1}{2} \phi \cos \phi - \frac{5}{2} \sin \phi + 2\phi \\ \psi_4 &= 1 - \cos \phi - \frac{1}{2} \phi \sin \phi \\ \psi_5 &= \phi + \frac{1}{2} \phi \cos \phi - \frac{3}{2} \sin \phi. \end{aligned}$$

It is interesting to derive an approximation of these expressions for small curvature. This is easily obtained observing that:

$$\lim_{c \rightarrow 0} (-c)^{-k} \psi_k = \frac{(-s)^k}{k!}.$$

Then $\hat{S}(s)$ can be approximated by

$$\hat{S}(s) = \left[I + \sum_{k=1}^5 \frac{(-s)^k}{k!} \hat{T}^k \right] \cdot \hat{S}(0). \quad (17)$$

This is a consistent approximation since for small curvature the differential equilibrium eqn 13 is approximated by $\frac{d^6 \hat{S}(s)}{ds^6} = 0$, which admits eqn 17 as solution.

Moreover, since for $c = 0$ also $\hat{T}^2 = 0$, for this particular case we have

$$\hat{A}_0 = \hat{S}(0) \quad \phi \hat{B}_0 = -s \hat{T} \cdot \hat{S}(0) \quad \hat{A}_c = \hat{A}_s = \hat{B}_c = \hat{B}_s = 0$$

so that we obtain a linear solution for the generalized stress resultant in the form

$$\hat{\mathbf{S}}(s) = (\mathbf{I} - s\hat{\mathbf{T}}) \cdot \hat{\mathbf{S}}(0).$$

2.4 Three-dimensional Beam Deformation

In order to obtain the constitutive equations of the cross-section, i.e. the cross-sectional rigidity matrix, let us consider the beam as a three-dimensional continuum.

The position vector \mathbf{x}_Q of a generic material point Q in the cross-section can be expressed as

$$\mathbf{x}_Q(\xi^\alpha, s) = \mathbf{x}(s) + \xi^\alpha \mathbf{e}_\alpha(s)$$

where $\mathbf{x}(s)$ is the position of the point P on l and ξ^α ($\alpha = 1, 2$) are the cartesian coordinates along the cross-sectional axes $\mathbf{e}_\alpha(s)$. This representation induces curvilinear coordinates ξ^k ($k = 1, 2, 3$), $\xi^3 = s$, with covariant basis vectors

$$\mathbf{g}_\alpha = \mathbf{e}_\alpha \quad \mathbf{g}_3 = \mathbf{t} + \mathbf{c} \times \mathbf{b}$$

where $\mathbf{b} = \mathbf{x}_Q - \mathbf{x}$ is the vector from point P to point Q . Moreover, denoting by g the determinant of the metric tensor such that $\sqrt{g} = \mathbf{g}_1 \times \mathbf{g}_2 \cdot \mathbf{g}_3$, the contravariant basis vectors are given by

$$\mathbf{g}^\alpha = -\frac{\mathbf{g}_3 \times \mathbf{e}_3 \times \mathbf{e}_\alpha}{\sqrt{g}} \quad \mathbf{g}^3 = \frac{\mathbf{e}_3}{\sqrt{g}}.$$

In the following, in order to compute the strain tensor, we need the expression for the displacement gradient tensor. Let $\nabla \mathbf{s}$ denote the gradient of the displacement vector \mathbf{s} , i.e. $\nabla \mathbf{s} = \mathbf{g}^k \frac{\partial \mathbf{s}}{\partial \xi^k}$, and let $\nabla_d \mathbf{s}$ denote the covariant derivative of \mathbf{s} along the direction \mathbf{d} , i.e. $\nabla_d \mathbf{s} = \mathbf{d} \cdot \nabla \mathbf{s}$. In the same way the covariant derivatives of \mathbf{s} along the cross-sectional basis vectors \mathbf{e}_i are denoted by $\nabla_{\mathbf{e}_i} \mathbf{s}$ and are given by

$$\nabla_{\mathbf{e}_i} \mathbf{s} = \mathbf{e}_i \cdot \nabla \mathbf{s} = \mathbf{e}_i \cdot \mathbf{g}^k \frac{\partial \mathbf{s}}{\partial \xi^k}.$$

Substituting in this equation the expressions for the contravariant basis vectors we easily obtain

$$\begin{aligned} \nabla_{\mathbf{e}_\alpha} \mathbf{s} &= \frac{\partial \mathbf{s}}{\partial \xi^\alpha} \\ \nabla_{\mathbf{e}_3} \mathbf{s} &= \frac{1}{\sqrt{g}} \left(\frac{\partial \mathbf{s}}{\partial \xi^3} - \mathbf{e}_\alpha \cdot \mathbf{g}_3 \frac{\partial \mathbf{s}}{\partial \xi^\alpha} \right) \\ &= \frac{1}{\sqrt{g}} \left(\frac{\partial^\circ \mathbf{s}}{\partial \xi^3} + \mathbf{c} \times \mathbf{s} - \mathbf{e}_\alpha \cdot \mathbf{g}_3 \frac{\partial \mathbf{s}}{\partial \xi^\alpha} \right) \end{aligned}$$

where $\frac{\partial^\circ \mathbf{s}}{\partial \xi^3} \equiv \frac{\partial \mathbf{s}}{\partial \xi^3} - \mathbf{c} \times \mathbf{s}$ denotes the corotational derivative with the cross-sectional triad, with respect to the arc length.

Within the approximation of small displacements the strain tensor is the symmetric part of the displacement gradient tensor, i.e. $\epsilon = \frac{1}{2}(\nabla \mathbf{s} + \nabla^T \mathbf{s})$, and there is no need to distinguish among the various nonlinear stress tensors. Then let σ denote the stress tensor at the generic point Q , corresponding to the displacement field \mathbf{s} and let us assume the validity of Hooke's law, i.e. $\sigma = \mathbf{D} \cdot \epsilon$ where \mathbf{D} is the elasticity tensor. We do not specify any restriction to the nature of the elastic tensor \mathbf{D} except that it is symmetrical and positive definite and its corotational derivative is zero. Moreover, let \mathbf{n} denote the unit normal to the cross-section and $\mathbf{p} = \sigma \cdot \mathbf{n}$ the corresponding stress vector.

For the sake of simplicity, we assume that the external loads are applied only at the end sections of the beam, and the distributed loads are negligible or absent. For our purposes, these hypotheses do not affect the results we are looking for.

2.5 Virtual Work Principle and F.E.M. Approximation

Using the notation of the previous paragraphs, the principle of virtual work written for an infinitesimal beam slice reads

$$\int \text{tr}(\delta \epsilon \cdot \mathbf{D} \cdot \epsilon) \sqrt{g} dA = \frac{d}{ds} \int \delta \mathbf{s} \cdot \mathbf{p} dA \quad (18)$$

where $\delta \mathbf{s}$ denotes the virtual displacement of the generic point Q and $\delta \epsilon = \frac{1}{2}(\nabla \delta \mathbf{s} + \nabla^T \delta \mathbf{s})$ is the corresponding virtual strain tensor. This principle obviously includes the one-dimensional beam equations as a special case; in fact for a virtual rigid displacement of the form

$$\delta \mathbf{s} = \delta \mathbf{u}(s) - \mathbf{b} \times \delta \phi(s)$$

the virtual strain tensor vanishes identically and from eqn 18 we obtain

$$\frac{d}{ds} (\delta \mathbf{u} \cdot \mathbf{T} + \delta \phi \cdot \mathbf{M}) = 0 \quad (19)$$

where

$$\mathbf{T} = \int \mathbf{p} dA \quad \mathbf{M} = \int \mathbf{b} \times \mathbf{p} dA$$

are respectively the cross-sectional stress resultant and moment. Moreover, since $\delta \mathbf{s}$ is rigid, we must have

$$\frac{d\delta \mathbf{u}}{ds} = \delta \phi \times \mathbf{t} \quad \frac{d\delta \phi}{ds} = 0$$

and substituting these expressions into eqn 19 we can easily obtain the one-dimensional beam equations

$$\frac{d\mathbf{T}}{ds} = 0 \quad \frac{d\mathbf{M}}{ds} + \mathbf{t} \times \mathbf{T} = 0$$

which show the consistency of the three-dimensional and one-dimensional approaches.

In order to perform a finite element approximation of eqn 18 it is much easier to rewrite it in the pulled-back form,

$$\int \text{tr}(\delta \hat{\epsilon} \cdot \hat{D} \cdot \hat{\epsilon}) \sqrt{g} dA = \frac{d}{ds} \int \delta \hat{s} \cdot \hat{p} dA \quad (20)$$

in which the hat denotes the pull-back operation to the cross-section at $s = 0$, i.e.

$$\begin{aligned} \delta \hat{s} &= \mathbf{R}^T \cdot \delta s & \hat{p} &= \mathbf{R}^T \cdot p \\ \delta \hat{\epsilon} &= \mathbf{R}^T \cdot \delta \epsilon \cdot \mathbf{R} & \hat{\epsilon} &= \mathbf{R}^T \cdot \epsilon \cdot \mathbf{R} \end{aligned}$$

and \hat{D} is the pulling back at $s = 0$ of the elastic tensor, which is constant with respect to s by our assumption. This is equivalent to refer all vectors and tensors to the cross-sectional components.

The finite element approximation of eqn 20 is easily obtained by means of the following displacement representation:

$$\hat{s}(\xi^k) = \hat{N}(\xi^\alpha) \cdot \hat{S}(s)$$

where \hat{S} denotes the vector array of the displacement at the nodes of the finite element mesh of the discretized cross-section, and \hat{N} denotes the matrix of the shape functions.

Using the definition previously given of covariant derivative along the cross-sectional axes, the independent components of the strain tensor $\hat{\epsilon}$ can be given the form $\hat{A}(\xi^\alpha) \cdot \hat{S}'(s) + \hat{B}(\xi^\alpha) \cdot \hat{S}(s)$ where \hat{A} , \hat{B} are suitable given functions of the cross-sectional coordinates and (\prime) denotes the differentiation along the beam axis. Discretization of eqn 20 then leads to the following set of ordinary differential equations:

$$\begin{aligned} \hat{M} \cdot \hat{S}' + \hat{C}^T \cdot \hat{S} &= \hat{P} \\ \hat{C} \cdot \hat{S}' + \hat{E} \cdot \hat{S} &= \hat{P}' \end{aligned} \quad (21)$$

where

$$\begin{aligned} \hat{M} &= \int \hat{A}^T \cdot \hat{D} \cdot \hat{A} dA \\ \hat{C} &= \int \hat{B}^T \cdot \hat{D} \cdot \hat{A} dA \\ \hat{E} &= \int \hat{B}^T \cdot \hat{D} \cdot \hat{B} dA \\ \hat{P} &= \int \hat{N}^T \cdot \hat{p} dA. \end{aligned}$$

The variables \hat{P} can be called nodal stresses in the sense that they represent the discretized stresses acting upon the cross-sectional surface. Equation 21 constitutes a set of first-order ordinary differential equations in the variables \hat{S} and \hat{P} and can be put in a second-order form by eliminating the nodal stress variables. After differentiation of the first of eqn 21 and substitution into the second, we obtain

$$\hat{M} \cdot \hat{S}'' + (\hat{C}^T - \hat{C}) \cdot \hat{S}' - \hat{E} \cdot \hat{S} = 0. \quad (22)$$

Equations 21 and 22 are the discretized differential homogeneous equations of equilibrium with constant coefficients and symplectic structure, hence the eigenvalues are of the type: $\lambda = \mp a \mp ib$. From physical considerations, according to Saint-Venant's principle, we expect six eigenvalues with zero real part, representing the solutions corresponding to nonzero stress resultants, and eigenvalues with nonzero real part, corresponding to the exponentially decaying self-equilibrated modes. Following Giavotto *et al.* (1983), the non-decaying solutions are called central solutions while the decaying ones are called extremity solutions.

Considering the beam as a one-dimensional continuum, we are interested in the cross-sectional constitutive equations, i.e. in finding out the cross-sectional rigidity matrix. In this case, it is common to understand the strain energy as a function of the stress resultant and moment only, so that we are mainly interested in central solutions which can be viewed as a particular solution under a prescribed combination of the stress resultant and moment at a given cross-section, and subjected to particular boundary conditions that avoid the existence of any extremity solution. This goal can be achieved with the procedure shown in the subsequent paragraphs.

Before continuing, it is extremely important to establish some fundamental properties of the operators \hat{M} , \hat{C} and \hat{E} . These properties come from the consideration that for rigid displacement of the entire beam, the stress vector \mathbf{p} is identically zero so that the nodal stress vector $\hat{\mathbf{P}}$ is also zero. For our purposes the displacement $\hat{\mathbf{s}}$ can be expressed as an infinitesimal rigid displacement of the form

$$\hat{\mathbf{s}} = \hat{\mathbf{u}}(s) - \hat{\mathbf{b}} \times \hat{\phi}(s) \quad \hat{\mathbf{b}} = \mathbf{R}^T \cdot \mathbf{b}$$

so that the nodal displacements can be expressed as

$$\hat{\mathbf{S}}(s) = \hat{\mathbf{Z}} \cdot \hat{\mathbf{X}}(s) \quad \hat{\mathbf{X}}(s) = (\hat{\mathbf{u}}(s), \hat{\phi}(s))$$

where $\hat{\mathbf{Z}}$ collects the constant operators $\hat{\mathbf{Z}}_i$ of the nodes Q_i .

$$\hat{\mathbf{Z}}_i = [\mathbf{I}, -\hat{\mathbf{b}}_i \times \mathbf{I}] \quad \hat{\mathbf{b}}_i = \mathbf{R}^T \cdot \mathbf{b}_i.$$

Recalling that for rigid displacement we have

$$\hat{\mathbf{u}}' = -\hat{\mathbf{c}} \times \hat{\mathbf{u}} - \hat{\mathbf{t}} \times \hat{\phi} \quad \hat{\phi}' = -\hat{\mathbf{c}} \times \hat{\phi}$$

or

$$\hat{\mathbf{X}}' = \hat{\mathbf{T}}^T \cdot \hat{\mathbf{X}},$$

from eqn 21 it follows that the operators \hat{M} , \hat{C} and \hat{E} must satisfy the properties

$$\begin{aligned} \hat{M} \cdot \hat{\mathbf{Z}} \cdot \hat{\mathbf{T}}^T + \hat{C}^T \cdot \hat{\mathbf{Z}} &\equiv 0 \\ \hat{C} \cdot \hat{\mathbf{Z}} \cdot \hat{\mathbf{T}}^T + \hat{E} \cdot \hat{\mathbf{Z}} &\equiv 0 \end{aligned}$$

and since the operator \hat{M} is nonsingular we also obtain:

$$\begin{aligned} \hat{M}^{-1} \cdot \hat{C}^T \cdot \hat{\mathbf{Z}} &\equiv -\hat{\mathbf{Z}} \cdot \hat{\mathbf{T}}^T \\ \hat{E} \cdot \hat{\mathbf{Z}} &\equiv \hat{C} \cdot \hat{M}^{-1} \cdot \hat{C}^T \cdot \hat{\mathbf{Z}} \end{aligned} \quad (23)$$

2.6 Displacement Resolution

Since it is well known that the central solutions entail cross-sectional distortion, it is extremely significant to resolve the displacement \mathbf{s} into a rigid part that does not strain the cross-section and into a residual part \mathbf{w} called warping, which is responsible for the cross-sectional distortion. This resolution, in pulled-back notation, reads

$$\hat{\mathbf{s}}(\xi^k) = \hat{\mathbf{u}}(s) - \hat{\mathbf{b}} \times \hat{\boldsymbol{\phi}}(s) + \hat{\mathbf{w}}(\xi^k) \quad \hat{\mathbf{w}} = \mathbf{R}^T \cdot \mathbf{w}. \quad (24)$$

It is immediately seen that this resolution is six times indeterminate, meaning that the warping itself needs further specification. Obviously, the specification of the warping entails the specification also of the translation $\hat{\mathbf{u}}$ and the rotation $\hat{\boldsymbol{\phi}}$ because, according to eqn 24, they must represent the same displacement $\hat{\mathbf{s}}$. Moreover, irrespectively of the particular warping determination adopted, the stress distribution over the cross-section is not affected.

If the same kind of resolution is adopted for the virtual displacement, the virtual work principle, eqn 20 is rewritten as:

$$\begin{aligned} \int \text{tr}(\delta \hat{\boldsymbol{\epsilon}} \cdot \hat{\mathbf{D}} \cdot \hat{\boldsymbol{\epsilon}}) \sqrt{g} dA = \frac{d}{ds} \int \delta \hat{\mathbf{w}} \cdot \hat{\mathbf{p}} dA + \\ + (\delta \hat{\mathbf{u}}' + \hat{\mathbf{c}} \times \delta \hat{\mathbf{u}} + \hat{\mathbf{t}} \times \delta \hat{\boldsymbol{\phi}}) \cdot \hat{\mathbf{T}} + (\delta \hat{\boldsymbol{\phi}}' + \hat{\mathbf{c}} \times \delta \hat{\boldsymbol{\phi}}) \cdot \hat{\mathbf{M}}. \end{aligned} \quad (25)$$

It can be seen that in general, the warping contributes directly to the internal virtual work, but, if the interest is focused on central solutions only, there is a great interest in defining the internal energy, the warping $\hat{\mathbf{w}}$ and the stress vector $\hat{\mathbf{p}}$, as a function of the stress resultant and moment only. To this end, eqn 25 suggests an intrinsic definition of the warping as a particular displacement $\hat{\mathbf{w}}$ satisfying the following orthogonality condition:

$$\int \hat{\mathbf{w}} \cdot \hat{\mathbf{p}} dA = 0 \quad (26)$$

as proposed by Borri and Merlini (1986). By doing so, the associated quantities $\hat{\mathbf{u}}' + \hat{\mathbf{c}} \times \hat{\mathbf{u}} + \hat{\mathbf{t}} \times \hat{\boldsymbol{\phi}}$ and $\hat{\boldsymbol{\phi}}' + \hat{\mathbf{c}} \times \hat{\boldsymbol{\phi}}$, which can be grouped in the following vector,

$$\hat{\boldsymbol{\epsilon}} = (\hat{\mathbf{u}}' + \hat{\mathbf{c}} \times \hat{\mathbf{u}} + \hat{\mathbf{t}} \times \hat{\boldsymbol{\phi}}, \hat{\boldsymbol{\phi}}' + \hat{\mathbf{c}} \times \hat{\boldsymbol{\phi}}) = \hat{\mathbf{X}}' - \hat{\mathbf{T}}^T \cdot \hat{\mathbf{X}} \quad (27)$$

assume the meaning of intrinsic measures of the cross-sectional deformation, being conjugate of the generalized stress resultant $\hat{\mathbf{S}}$: that becomes evident from eqn 25, here written in the form

$$\int \text{tr}(\delta \hat{\boldsymbol{\epsilon}} \cdot \hat{\mathbf{D}} \cdot \hat{\boldsymbol{\epsilon}}) \sqrt{g} dA = \delta \hat{\boldsymbol{\epsilon}} \cdot \hat{\mathbf{S}}.$$

The meaning of the orthogonality condition in eqn 26 is clear: it allows one to obtain the one-dimensional expression of the strain energy in a straightforward manner.

Indeed, it could be observed that that condition is too strong, since an arbitrary constant value for that integral would suffice: for our purposes, let choose a null value for such constant.

In practice, the *a priori* imposition of the orthogonality condition in eqn 26 is a difficult task. Hence it is better to compute a particular warping, which does not satisfy eqn 26, and then recover the intrinsic warping by means of a special projection as shown later on.

2.7 Central Solution

Let us perform a finite element approximation of the warping by writing

$$\hat{w}(\xi^k) = \hat{N}(\xi^\alpha) \cdot \hat{W}(s)$$

where \hat{W} denotes the vector of the warping displacement at the nodes of the finite element mesh. The vector of the nodal displacements assumes the form:

$$\hat{S} = \hat{Z} \cdot \hat{X} + \hat{W}.$$

The discretized counterpart of the virtual work principle eqn 25 leads to the following set of ordinary differential equations:

$$K \cdot Y = L \quad (28)$$

where

$$Y = (\hat{W}', \hat{W}, \hat{X}', \hat{X})$$

$$L = (\hat{P}, \hat{P}', \hat{Z}^T \hat{P}, \hat{Z}^T \hat{P}')$$

and the matrix K has the following structure:

$$\begin{bmatrix} \hat{M} & \hat{C}^T & \hat{M} \hat{Z} & \hat{C}^T \hat{Z} \\ \hat{C} & \hat{E} & \hat{C} \hat{Z} & \hat{E} \hat{Z} \\ \hat{Z}^T \hat{M} & \hat{Z}^T \hat{C}^T & \hat{Z}^T \hat{M} \hat{Z} & \hat{Z}^T \hat{C}^T \hat{Z} \\ \hat{Z}^T \hat{C} & \hat{Z}^T \hat{E} & \hat{Z}^T \hat{C} \hat{Z} & \hat{Z}^T \hat{E} \hat{Z} \end{bmatrix}$$

Taking into account the properties of the operators \hat{M} , \hat{C} and \hat{E} previously obtained, eqn 23, and the definition of the cross-sectional deformation, eqn 27, eqn 28 transforms to

$$\hat{K} \cdot \hat{Y} = \hat{L}$$

where

$$\hat{Y} = (\hat{W}', \hat{W}, \hat{E}, \hat{X})$$

$$\hat{L} = (\hat{P}, \hat{P}', \hat{S}, 0)$$

and the matrix \tilde{K} has the following structure:

$$\begin{bmatrix} \hat{M} & \hat{C}^T & \hat{M} \cdot \hat{Z} & 0 \\ \hat{C} & \hat{E} & \hat{C} \cdot \hat{Z} & 0 \\ \hat{Z}^T \cdot \hat{M} & \hat{Z}^T \cdot \hat{C}^T & \hat{Z}^T \cdot \hat{M} \cdot \hat{Z} & 0 \\ 0 & 0 & 0 & 0 \end{bmatrix}$$

which clearly shows that the rigid displacement parameter \hat{X} will remain indeterminate.

From this equation the cross-sectional deformation vector \hat{E} is easily eliminated, leading to

$$\begin{aligned} \tilde{M} \cdot \hat{W}' + \tilde{C}^T \cdot \hat{W} &= \hat{P} - \hat{M} \cdot \hat{Z} \cdot \hat{F}^{-1} \cdot \hat{S} \\ \tilde{C} \cdot \hat{W}' + \tilde{E} \cdot \hat{W} &= \hat{P}' - \hat{C} \cdot \hat{Z} \cdot \hat{F}^{-1} \cdot \hat{S} \\ \hat{E} &= \hat{F}^{-1} \cdot (\hat{S} - \hat{Z}^T \cdot \hat{M} \cdot \hat{W}' - \hat{Z}^T \cdot \hat{C}^T \cdot \hat{W}) \end{aligned}$$

where:

$$\begin{aligned} \hat{F} &= \hat{Z}^T \cdot \hat{M} \cdot \hat{Z} \\ \tilde{M} &= \hat{M} - \hat{M} \cdot \hat{Z} \cdot \hat{F}^{-1} \cdot \hat{Z}^T \cdot \hat{M} \\ \tilde{C} &= \hat{C} - \hat{C} \cdot \hat{Z} \cdot \hat{F}^{-1} \cdot \hat{Z}^T \cdot \hat{M} \\ \tilde{E} &= \hat{E} - \hat{C} \cdot \hat{Z} \cdot \hat{F}^{-1} \cdot \hat{Z}^T \cdot \hat{C}^T \end{aligned}$$

Eliminating \hat{P} and \hat{P}' by differentiation of the first group and by substitution into the second group, taking eqn 12 into account, the following second-order differential equation set is obtained:

$$\tilde{M} \cdot \hat{W}'' + (\tilde{C}^T - \tilde{C}) \cdot \hat{W}' - \tilde{E} \cdot \hat{W} = \hat{G} \cdot \hat{S} \quad (29)$$

where $\hat{G} = \hat{C} \cdot \hat{Z} \cdot \hat{F}^{-1} + \hat{M} \cdot \hat{Z} \cdot \hat{F}^{-1} \cdot \hat{T}$.

This set of equations is six times redundant since we know that the warping is six times indeterminate and in fact it can be recognized that the following properties hold:

$$\begin{aligned} \hat{Z}^T \cdot \tilde{M} &\equiv 0 & \hat{Z}^T \cdot \tilde{C}^T &\equiv 0 \\ \hat{Z}^T \cdot \tilde{C} &\equiv 0 & \hat{Z}^T \cdot \tilde{E} &\equiv 0 \\ \hat{Z}^T \cdot \hat{G} &\equiv 0. \end{aligned}$$

Then it is possible to eliminate six rows from the previous set of equations, set six components of \hat{W}'' , \hat{W}' , \hat{W} to zero, and solve the remaining equations. This is equivalent to putting six independent single-point constraints on the warping: a common practice to do this in finite element procedures is to add extremely high artificial rigidities to the diagonal terms of six independent equations and set the corresponding right-hand side to zero. The warping \hat{W} so determined will be

denoted with an overbar, and the same notation will be adopted for the operators involved.

Looking at the form of \hat{S} given in eqn 16, a particular solution for \overline{W} can be computed along with the corresponding cross-sectional strain \overline{E} and the nodal stress vector \hat{P} . This solution can be concisely written in the following form:

$$\overline{W} = \overline{W} \cdot \hat{S} \quad \overline{E} = \overline{C} \cdot \hat{S} \quad \hat{P} = \Pi \cdot \hat{S}$$

where the operators \overline{W} , \overline{C} and Π are constant. Moreover, since by definition we have $\hat{S} = \hat{Z}^T \cdot \hat{P}$, the following property holds:

$$\hat{Z}^T \cdot \Pi = I. \quad (30)$$

It must be noted that \overline{W} , \overline{C} strictly depend on the particular set of single-point constraints imposed on the warping. On the contrary, the stress distribution is not affected; consequently, Π does not depend on this particular choice. As it will be shown in the next paragraph, from the knowledge of these quantities it is possible to determine an intrinsic warping and an intrinsic cross-sectional strain, as proposed by Borri and Merlini (1986).

The particular solution previously mentioned is obtained recalling the form 17 of the stress resultant and moment, and expression 15 of the integration constants. This form suggests one should single out the particular solution of the warping displacement in the following form:

$$\overline{W} = \overline{U}_0 + \phi \overline{V}_0 + (\overline{U}_c + \phi \overline{V}_c) \cos \phi + (\overline{U}_s + \phi \overline{V}_s) \sin \phi.$$

Then from eqn 29 the following sets of linear algebraic equations in terms of $\overline{U}_0, \overline{V}_0, \overline{U}_c, \overline{V}_c, \overline{U}_s, \overline{V}_s$ are obtained:

$$\begin{aligned} \overline{E} \cdot \overline{V}_0 &= -\overline{G} \cdot \hat{B}_0 \\ \overline{E} \cdot \overline{U}_0 &= -\overline{G} \cdot \hat{A}_0 + c\overline{H} \cdot \overline{V}_0 \\ (c^2\overline{M} + \overline{E}) \cdot \overline{V}_c + c\overline{H} \cdot \overline{V}_s &= -\overline{G} \cdot \hat{B}_c \\ c\overline{H}^T \cdot \overline{V}_c + (c^2\overline{M} + \overline{E}) \cdot \overline{V}_s &= -\overline{G} \cdot \hat{B}_s \\ (c^2\overline{M} + \overline{E}) \cdot \overline{U}_c + c\overline{H} \cdot \overline{U}_s &= -\overline{G} \cdot \hat{A}_c - c\overline{H} \cdot \overline{V}_c + 2c^2\overline{M} \cdot \overline{V}_s \\ c\overline{H}^T \cdot \overline{U}_c + (c^2\overline{M} + \overline{E}) \cdot \overline{U}_s &= -\overline{G} \cdot \hat{A}_s + 2c^2\overline{M} \cdot \overline{V}_c + c\overline{H}^T \cdot \overline{V}_s \end{aligned} \quad (31)$$

where for sake of coinciseness we have defined $\overline{H} = -\overline{H}^T = \overline{C} - \overline{C}^T$. Recalling expressions 15, these equations lead to the solution in terms of the stress resultant and moment corresponding to the section at $s = 0$, i.e. $\hat{S}(0)$, and, in particular,

we obtain $\bar{W}(0) = \bar{U}_0 + \bar{U}_c$ and $\bar{W}'(0) = c(\bar{V}_0 + \bar{V}_c + \bar{U}_s)$, that can be used in order to compute the global section strain $\bar{\epsilon}(0)$. The particular case of straight beams, i.e. $c = 0$, can be recovered considering that in this case $\frac{\phi}{c}\bar{V}_0 = s\bar{V}_0$ and $\bar{U}_c = \bar{U}_s = \bar{V}_c = \bar{V}_s \equiv 0$.

It is extremely interesting to observe the symmetry of eqns 31 and that they can be solved in sequence, i.e. at first for \bar{V}_0 then for \bar{U}_0 , subsequently for \bar{V}_c and \bar{V}_s , and at last for \bar{U}_c and \bar{U}_s . In addition, due to the symmetry of these equations, we observe the possibility of stacking the equations for \bar{V}_c, \bar{V}_s , and for \bar{U}_c, \bar{U}_s , in complex form, which can be more efficient for computational purposes. To this end let us define the following complex constants:

$$\begin{aligned} \hat{A} &= \hat{A}_c + i\hat{A}_s, & \hat{B} &= \hat{B}_c + i\hat{B}_s, \\ \bar{U} &= \bar{U}_c + i\bar{U}_s, & \bar{V} &= \bar{V}_c + i\bar{V}_s. \end{aligned}$$

Then the complex equations for \bar{U} and for \bar{V} are written in the following form that replaces the last four equations 31:

$$\begin{aligned} (c^2\bar{M} + ic\bar{H} + \bar{E}) \cdot \bar{V} &= -\bar{G} \cdot \hat{B} \\ (c^2\bar{M} + ic\bar{H} + \bar{E}) \cdot \bar{U} &= -\bar{G} \cdot \hat{A} + c(\bar{H} - 2ic\bar{M}) \cdot \bar{V}. \end{aligned}$$

2.8 Intrinsic Warping

As intrinsic warping \hat{w} , according to eqn 26, we defined that particular warping which is orthogonal to the stress distribution. Then we have $\hat{P} \cdot \hat{W} = 0$ for any independent set of stress resultants and moments, which entails $\Pi^T \cdot \hat{W} = 0$. Using this property allows us to recover from the warping \bar{w} the intrinsic warping \hat{w} . In fact, the nodal displacement vector \hat{S} can be written both in terms of \bar{W} and in terms of the intrinsic warping \hat{W} in the following way:

$$\hat{S} = \hat{Z} \cdot \bar{X} + \bar{W} = \hat{Z} \cdot \hat{X} + \hat{W}$$

from which we easily see that the two warpings differ by a rigid displacement of the cross-section. In fact we have

$$\bar{W} - \hat{W} = -\hat{Z} \cdot (\bar{X} - \hat{X})$$

and since both warpings refer to the same loading conditions we also have

$$\bar{W} - \hat{W} = (\bar{W} - \hat{W}) \cdot \hat{S} = \hat{Z} \cdot (\hat{X} - \bar{X}) = \hat{Z} \cdot \bar{Q} \cdot \hat{S}$$

where \bar{Q} is the constant operator that takes into account the dependency relation between the warping distributions:

$$\bar{W} - \hat{W} = \hat{Z} \cdot \bar{Q}.$$

Left-multiplying this equation by Π^T , we obtain the final result

$$\bar{Q} = \Pi^T \cdot \bar{W}$$

where the property 30 has been taken into account. Finally, the intrinsic warping distribution is expressed in the form

$$\hat{W} = \bar{W} - \hat{Z} \cdot \bar{Q} = \mathcal{P} \cdot \bar{W}$$

where $\mathcal{P} = I - \hat{Z} \cdot \Pi^T$ is the particular projection needed to recover the intrinsic warping. That the operator \mathcal{P} is a true projector, in fact, is easily verified since $\mathcal{P}^2 = \mathcal{P}$. Moreover, this projector is orthogonal to the rigid displacement of the cross-section since we have $\mathcal{P} \cdot \hat{Z} = 0$, and its transpose is orthogonal to the stress distribution since $\mathcal{P}^T \cdot \Pi = 0$.

After the intrinsic warping is determined, the intrinsic cross-sectional strain can be recovered. This is obtained observing that

$$\hat{\epsilon} - \bar{\epsilon} = \hat{X}' - \bar{X}' - \hat{T}^T \cdot (\hat{X} - \bar{X}) = \bar{Q} \cdot \hat{S}' - \hat{T}^T \cdot \bar{Q} \hat{S}.$$

Hence, taking the equilibrium equation 12 into account and setting $\hat{\epsilon} = \hat{C} \cdot \hat{S}$, we obtain the cross-sectional compliance matrix in the form:

$$\hat{C} = \bar{C} - \bar{Q} \cdot \hat{T} - \hat{T}^T \cdot \bar{Q}.$$

An alternative approach is also possible, as indicated by Giavotto *et al.* (1983): this consists of computing the internal energy stored in the section for each independent component of the generalized stress resultant \hat{S} .

The compliance matrix \hat{C} is not singular, thus the cross-section rigidity \hat{K} is obtained by inversion.

3 Formulation of Finite Elements

The Finite Elements developed for the cross-sectional analysis are depicted in Fig. 3: they are isoparametric elements on the cross-section domain. The most general element is the *Plane Element*: it is a full three-dimensional solid element, whose view on the cross-section is a quadrilateral polygon; the *Lamina Element* is quite similar to it and is designed to model very thin solids. The *Panel Element* is a plane stress element whose view on the cross-section is an arc of line: it is used to model walls in hollow beams; the *Joint Element* is quite similar to it and only works in shear. Finally, the *Stringer Element* is a one-dimensional element which is seen on the cross-section as a point.

3.1 Plane Element

This element is a quadrilateral element used to model the cross-section of solid beams. The formulation of this element is based on an analytical expression of the strain and stress tensors in terms of cross-sectional components, that is given in the following.

From the programmer's point of view it is easier to adopt a little different notation than that used so far: in particular let us denote with $\{\hat{\mathbf{V}}\}$ the vector array of the cross sectional components of a generic vector $\hat{\mathbf{V}}$, i.e. $\{\hat{\mathbf{V}}\}^T = [\hat{V}_1, \hat{V}_2, \hat{V}_3]$ where $\hat{V}_k = \mathbf{e}_k \cdot \hat{\mathbf{V}}$. Following the same kind of notation, we denote with $\hat{\epsilon}_{ik} = \mathbf{e}_i \cdot \hat{\epsilon} \cdot \mathbf{e}_k$ the cross-sectional components of the strain tensor $\hat{\epsilon}$, and for convenience we introduce the strain array vector $\{\hat{\epsilon}\}^T = [\hat{\epsilon}_O^T, \hat{\epsilon}_I^T]$ where

$$\{\hat{\epsilon}_O\}^T = [2\hat{\epsilon}_{13}, 2\hat{\epsilon}_{23}, \hat{\epsilon}_{33}] \quad \{\hat{\epsilon}_I\}^T = [\hat{\epsilon}_{11}, \hat{\epsilon}_{22}, 2\hat{\epsilon}_{12}]$$

represent the *out-of-plane* and *in-plane* strain tensor arrays.

Taking into account the expressions of the displacement gradient tensor reported above, we can write

$$\{\hat{\epsilon}_O\} = \frac{1}{\sqrt{g}} \left(\left\{ \frac{\partial \hat{\mathbf{s}}}{\partial \xi^3} \right\} + [\mathcal{D}_O] \{\hat{\mathbf{s}}\} \right)$$

and

$$\{\hat{\epsilon}_I\} = [\mathcal{D}_I] \{\hat{\mathbf{s}}\}$$

where $\{\hat{\mathbf{s}}\}$ is the displacement vector array and the differential operators $[\mathcal{D}_O]$ and $[\mathcal{D}_I]$ have the following definition:

$$[\mathcal{D}_O] = \begin{bmatrix} \mathcal{D} & -\hat{c}_3 & \hat{c}_2 + \sqrt{g} \frac{\partial}{\partial \xi^1} \\ \hat{c}_3 & \mathcal{D} & -\hat{c}_1 + \sqrt{g} \frac{\partial}{\partial \xi^2} \\ -\hat{c}_2 & \hat{c}_1 & \mathcal{D} \end{bmatrix} \quad [\mathcal{D}_I] = \begin{bmatrix} \frac{\partial}{\partial \xi^1} & 0 & 0 \\ 0 & \frac{\partial}{\partial \xi^2} & 0 \\ \frac{\partial}{\partial \xi^2} & \frac{\partial}{\partial \xi^1} & 0 \end{bmatrix}$$

ELEMENT LIBRARY	
NAME	TOPOLOGY
PLANE ELEMENT	
LAMINA ELEMENT	
STRINGER ELEMENT	
JOINT ELEMENT	
THIN PANEL ELEMENT	

Figure 3: Element library.

with \mathcal{D} defined as follows:

$$\mathcal{D} = -(\hat{t}_1 - \hat{c}_3 \xi^2) \frac{\partial}{\partial \xi^1} - (\hat{t}_2 + \hat{c}_3 \xi^1) \frac{\partial}{\partial \xi^2}.$$

The metric determinant \sqrt{g} can be computed by

$$\sqrt{g} = \hat{t}_3 - \hat{c}_2 \xi^1 + \hat{c}_1 \xi^2,$$

and we recall that, within the approximation of a helicoidal beam, the vector arrays $\{\hat{t}\}$ and $\{\hat{c}\}$ are constants.

Assuming the following finite element discretization

$$\{\hat{s}(\xi^k)\} = [\hat{N}(\xi^\alpha)] \cdot \{\hat{S}(s)\}$$

and letting $\hat{S}' = \frac{\partial \hat{S}}{\partial \xi^3}$, we can write

$$\{\hat{\epsilon}_0\} = [\mathcal{A}_0] \{\hat{S}'\} + [\mathcal{B}_0] \{\hat{S}\} \quad \{\hat{\epsilon}_1\} = [\mathcal{B}_1] \{\hat{S}\},$$

where:

$$[\mathcal{A}_0] = \frac{1}{\sqrt{g}} [\hat{N}(\xi^\alpha)] \quad [\mathcal{B}_0] = \frac{1}{\sqrt{g}} [\mathcal{D}_0] [\hat{N}(\xi^\alpha)] \quad [\mathcal{B}_1] = [\mathcal{D}_1] [\hat{N}(\xi^\alpha)].$$

Collecting the previous formulae we obtain

$$\{\hat{\epsilon}\} = [\mathcal{A}] \{\hat{S}'\} + [\mathcal{B}] \{\hat{S}\}$$

where:

$$[\mathcal{A}] = \begin{bmatrix} \mathcal{A}_0 \\ 0 \end{bmatrix} \quad [\mathcal{B}] = \begin{bmatrix} \mathcal{B}_0 \\ \mathcal{B}_1 \end{bmatrix}$$

The numerical evaluation of the matrices $[\mathcal{B}_0]$ and $[\mathcal{B}_1]$ requires the differentiation of the shape functions $[\hat{N}(\xi^\alpha)]$ with respect to the cross-sectional coordinates ξ^α : this is easily performed according to the particular type of finite element used. The element implementation follows an isoparametric formulation based upon 2 to 4 nodes for each side and allows for linear, parabolic and cubic displacement interpolation. The total number of nodes ranges from 4 to 12. The shape functions are reported in Table 1, where p and q denote non-dimensional cartesian coordinates on the parent domain, as shown in Fig. 4.

The constitutive equation $\sigma = \mathcal{D} \cdot \epsilon$ can be written in terms of *out-of-plane* and *in-plane* components, with reference to the cross-section triad, in the following way:

$$\begin{aligned} \{\hat{\sigma}_0\} &= [\hat{D}_{00}] \{\hat{\epsilon}_0\} + [\hat{D}_{01}] \{\hat{\epsilon}_1\} \\ \{\hat{\sigma}_1\} &= [\hat{D}_{10}] \{\hat{\epsilon}_0\} + [\hat{D}_{11}] \{\hat{\epsilon}_1\} \end{aligned}$$

Element order	Shape function
Linear	$\hat{N}_1 = \frac{1}{4}(1+p)(1+q)$ $\hat{N}_2 = \frac{1}{4}(1-p)(1+q)$ $\hat{N}_3 = \frac{1}{4}(1-p)(1-q)$ $\hat{N}_4 = \frac{1}{4}(1+p)(1-q)$
Quadratic	$\hat{N}_1 = \frac{1}{4}(1+p)(1+q) + \frac{1}{2}(\hat{N}_5 + \hat{N}_8)$ $\hat{N}_2 = \frac{1}{4}(1-p)(1+q) + \frac{1}{2}(\hat{N}_5 + \hat{N}_6)$ $\hat{N}_3 = \frac{1}{4}(1-p)(1-q) + \frac{1}{2}(\hat{N}_8 + \hat{N}_7)$ $\hat{N}_4 = \frac{1}{4}(1+p)(1-q) + \frac{1}{2}(\hat{N}_7 + \hat{N}_8)$ $\hat{N}_5 = \frac{1}{2}(1-p^2)(1+q)$ $\hat{N}_6 = \frac{1}{2}(1-p)(1-q^2)$ $\hat{N}_7 = \frac{1}{2}(1-p^2)(1-q)$ $\hat{N}_8 = \frac{1}{2}(1+p)(1-q^2)$
Cubic	$\hat{N}_1 = \frac{1}{32}(1+p)(1+q)(-10+9(p^2+q^2))$ $\hat{N}_2 = \frac{1}{32}(1-p)(1+q)(-10+9(p^2+q^2))$ $\hat{N}_3 = \frac{1}{32}(1-p)(1-q)(-10+9(p^2+q^2))$ $\hat{N}_4 = \frac{1}{32}(1+p)(1-q)(-10+9(p^2+q^2))$ $\hat{N}_5 = \frac{9}{32}(1+q)(1-p^2)(1+3p)$ $\hat{N}_6 = \frac{9}{32}(1+q)(1-p^2)(1-3p)$ $\hat{N}_7 = \frac{9}{32}(1-p)(1-q^2)(1+3p)$ $\hat{N}_8 = \frac{9}{32}(1-p)(1-q^2)(1-3p)$ $\hat{N}_9 = \frac{9}{32}(1-q)(1-p^2)(1-3p)$ $\hat{N}_{10} = \frac{9}{32}(1-q)(1-p^2)(1+3p)$ $\hat{N}_{11} = \frac{9}{32}(1+p)(1-q^2)(1-3p)$ $\hat{N}_{12} = \frac{9}{32}(1+p)(1-q^2)(1+3p)$

Table 1: Shape functions of the Plane Element.

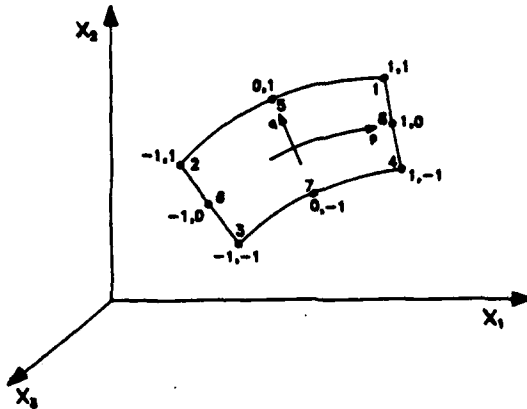


Figure 4: Parent domain of the Plane Element.

The array vectors $\{\hat{\sigma}_O\}$ ¹ and $\{\hat{\sigma}_I\}$ are the *out-of-plane* and *in-plane* stress tensor arrays, while the matrices $[\hat{D}_{OO}]$, $[\hat{D}_{OI}]$, $[\hat{D}_{IO}]$, $[\hat{D}_{II}]$, group the cross-sectional components of the elasticity tensor D . Since D is symmetric, the equivalence $[\hat{D}_{OI}] = [\hat{D}_{IO}]^T$ is assumed. These matrices depend on the particular material: the user may supply the elasticity tensor D directly or its inverse, or he can supply the elastic properties along the orthotropy directions for orthotropic materials. Orthotropic materials are allowed with an orthotropy plane normal to the cross-section: the user must supply the orientation of this plane on the cross-section and the orientation of the orthotropy directions in this plane by means of two angles. These angles are unique for each element and can be supplied with reference to either the physical or the parent domain.

The standard integration procedure uses Gauss-Legendre points and weights to compute the stiffness matrices $[\hat{M}]$, $[\hat{C}]$ and $[\hat{E}]$ of the element. In the case of linear and parabolic interpolation functions it is possible to force the use of integration points located at the nodes of the element: this allows us recovering stresses at the nodes themselves.

3.2 Lamina Element

This element is very similar to the plane element and has been designed to model very thin structural elements, as for example interlaminar layers. It can be considered as a degeneration of the plane element, in fact the formulation is almost the same, except the strain which is kept constant through the element thickness. The shape functions along the lamina direction are the same as the plane element, while a linear interpolation is used in the transverse direction. A relaxed integration can be used through the thickness. The geometry of the lamina element is defined by

¹The array vector $\{\hat{\sigma}_O\}$ represents the stress vector acting at the generic point on the cross-section and coincides with the vector elsewhere called \hat{p} .

means of 2 to 4 nodes on its reference line and by means of its thickness at each node. This element can only be orthotropic with an orthotropy plane tangent to its reference line.

3.3 Panel Element

The panel element can be used to model thin-walled beams: it is a thin element of constant thickness, defined from a geometrical point of view as a surface which intersects the cross section along a line $f(\xi^\alpha)$. An isoparametric description, with a number of nodes ranging from 2 to 4, is assumed for this line.

From a mechanical point of view the panel is a membrane working in plane stress; then letting ν be the unit normal to the line $f(\xi^\alpha)$, the identity $\sigma \cdot \nu = 0$ is trivially satisfied. Moreover, letting μ be the unit tangent to the line $f(\xi^\alpha)$, the significant components of the stress tensor can be grouped in the stress array vector

$$\{\hat{\sigma}_P\}^T = [\hat{\sigma}_{\mu\mu}, \hat{\sigma}_{\mu 3}, \hat{\sigma}_{33}]$$

being $\hat{\sigma}_{\mu\mu} = \mu \cdot \hat{\sigma} \cdot \mu$, $\hat{\sigma}_{\mu 3} = \mu \cdot \hat{\sigma} \cdot e_3$ and $\hat{\sigma}_{33} = e_3 \cdot \hat{\sigma} \cdot e_3$. Following the same kind of notation, we define the strain tensor array $\{\hat{\epsilon}_P\}$ as

$$\{\hat{\epsilon}_P\}^T = [\hat{\epsilon}_{\mu\mu}, 2\hat{\epsilon}_{\mu 3}, \hat{\epsilon}_{33}]$$

and the plane stress state constitutive equation as

$$\{\hat{\sigma}_P\} = [\hat{D}_P] \cdot \{\hat{\epsilon}_P\}$$

where $[\hat{D}_P]$ denotes the elasticity matrix typical of the plane stress state.

The expression of the components $\hat{\epsilon}_{\mu\mu}$, $2\hat{\epsilon}_{\mu 3}$ and $\hat{\epsilon}_{33}$ comes from the general expression of the strain tensor taking into account that in this case we have

$$g^\alpha \frac{\partial s}{\partial \xi^\alpha} = \mu \frac{\partial s}{\partial s_\mu}$$

where ds_μ represents the differential of the curvilinear abscissa along the line f . Then the partial derivatives with respect to the cross section coordinates are to be replaced by

$$\frac{\partial}{\partial \xi^\alpha} = \mu \cdot e_\alpha \frac{\partial}{\partial s_\mu}$$

and from the general expression of the displacement gradient tensor we obtain:

$$\nabla_{\mu} s = \frac{\partial s}{\partial s_\mu} \quad \nabla_{e_3} s = \frac{1}{\sqrt{g}} \left(\frac{\partial s}{\partial \xi^3} - \mu \cdot g_3 \frac{\partial s}{\partial s_\mu} \right)$$

Assuming the following finite element discretization

$$\{\hat{s}\} = [\hat{N}(s_\mu)] \cdot \{\hat{S}(s)\}$$

Element order	Shape function
Linear	$\hat{N}_1 = \frac{1}{2}(1 - p)$ $\hat{N}_2 = \frac{1}{2}(1 + p)$
Quadratic	$\hat{N}_1 = \frac{1}{2}(p^2 - p)$ $\hat{N}_2 = \frac{1}{2}(p^2 + p)$ $\hat{N}_3 = (1 - p^2)$
Cubic	$\hat{N}_1 = \frac{1}{16}(-1 + p(1 + p(9 - 9p)))$ $\hat{N}_2 = \frac{1}{16}(-1 + p(-1 + p(9 + 9p)))$ $\hat{N}_3 = \frac{1}{16}(9 + p(-27 + p(-9 + 27p)))$ $\hat{N}_4 = \frac{1}{16}(9 + p(+27 + p(-9 - 27p)))$

Table 2: Shape functions of the Panel Element.

we can write

$$\{\epsilon_P\} = [\mathcal{A}_P][\hat{N}(s_\mu)]\{\hat{S}'\} + [\mathcal{B}_P][\hat{N}(s_\mu)]\{\hat{S}\}$$

where, as it is easily verified,

$$[\mathcal{A}_P] = \begin{bmatrix} 0 & 0 & 0 \\ \frac{\hat{\mu}_1}{\sqrt{g}} & \frac{\hat{\mu}_2}{\sqrt{g}} & 0 \\ 0 & 0 & \frac{1}{\sqrt{g}} \end{bmatrix}$$

$$[\mathcal{B}_P] = \begin{bmatrix} \hat{\mu}_1 \frac{\partial}{\partial s_\mu} & \hat{\mu}_2 \frac{\partial}{\partial s_\mu} & 0 \\ \hat{\mu}_2 \hat{c}_3 - a \hat{\mu}_1 \frac{\partial}{\partial s_\mu} & -\hat{\mu}_1 \hat{c}_3 - a \hat{\mu}_2 \frac{\partial}{\partial s_\mu} & \hat{\mu}_1 \hat{c}_2 - \hat{\mu}_2 \hat{c}_1 + \frac{\partial}{\partial s_\mu} \\ -\hat{c}_2 & \hat{c}_1 & -a \frac{\partial}{\partial s_\mu} \end{bmatrix}$$

and $a = \frac{\boldsymbol{\mu} \cdot \mathbf{g}_3}{\sqrt{g}}$, $\hat{\mu}_\alpha = \hat{\boldsymbol{\mu}} \cdot \mathbf{e}_\alpha$. The shape functions for linear, parabolic and cubic interpolation are reported in Table 2, where p denotes non-dimensional cartesian coordinates on the parent domain, as shown in Fig. 5.

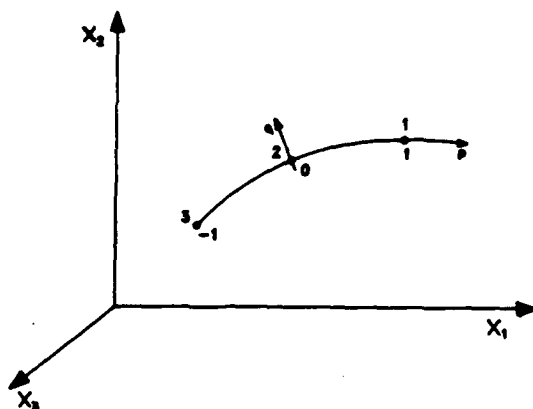


Figure 5: Parent domain of the Panel Element.

When using a curvilinear element, care must be taken for two reasons. First, the matrix $[\hat{D}_P]$ has constant components referred to the local directions μ , ν and e_3 , hence it is not a constant matrix when referred to the cross section triad. Second, due to the component $\hat{\sigma}_{\mu\mu}$ this element requires $\hat{\sigma}_{\nu\nu}$ different from zero in order to be equilibrated: this stress component can be provided by other elements. The program takes care of the first problem: the user is allowed to supply the elasticity matrix $[\hat{D}_P]$ with reference to the parent domain. About the second problem, it is left to the user to judge the opportunity of using curvilinear elements. Nevertheless, it is always possible to supply singular data for $[\hat{D}_P]$ so that $\hat{\sigma}_{\mu\mu}$ will be zero. Furthermore, in order to emulate semi-monocoque behavior the user can set to zero both the extensional rigidities.

The panel element can be also used in order to model a thin laminate: its stiffness matrix can be evaluated stacking the characteristics of a sequence of layers that can be made each of different material with different orthotropy orientations. Obviously this element can be used only if the interlaminar stresses are considered not to be important.

3.4 Joint Element

The joint element has been implemented to model an elastic link between an offset stringer and a thin panel. It is a two-node shear element obtained as a degeneration of a panel element, with both the extensional rigidities set to zero.

3.5 Stringer Element

The stringer element is mainly used to model stiffeners in thin-walled beams: on the cross-section domain, this element can be classified as a *point* element. A stringer is modeled by a line element which is able to sustain an axial load N along the direction λ of the stringer itself with an axial rigidity K . Letting s_λ be the

curvilinear abscissa along the stringer, the constitutive equation of the stringer is obviously given by

$$N = K \lambda \otimes \lambda \cdot \frac{ds}{ds_\lambda}$$

where s is the displacement of the stringer.

In order to use this element in the context of the present approach, we have to specify the derivative of the displacement with respect to the curvilinear abscissa in terms of the derivative along the beam axis and evaluate the virtual change of the potential energy of the stringer. To this end, let Q be the point of the intersection of the stringer with the generic cross-section and let ξ^α be the cross-sectional coordinates of the point Q . Moreover, if dQ denotes an infinitesimal length vector along the stringer, we have

$$dQ = g_k d\xi^k = \lambda ds_\lambda,$$

(standing on the cross-section, this element can be classified as *point element*) and obviously $ds_\lambda = \sqrt{dQ \cdot dQ}$. Along the line element of the stringer the coordinate differentials $d\xi^k$ can be expressed in terms of ds_λ as follows,

$$d\xi^k = g^k \cdot \lambda ds_\lambda,$$

and assuming the stringer intersect the cross-section (i.e. $\lambda \cdot e_3$ different from zero) we obtain the relationship between $d\xi^3$ and ds_λ in the form

$$d\xi^3 = g^3 \cdot \lambda ds_\lambda = \frac{e_3 \cdot \lambda}{\sqrt{g}} ds_\lambda,$$

whence

$$\frac{ds}{ds_\lambda} = \frac{e_3 \cdot \lambda}{\sqrt{g}} \frac{ds}{d\xi^3}.$$

Then, the virtual change of the potential energy of an infinitesimal length of stringer is given by:

$$\delta V = \frac{ds}{ds_\lambda} \cdot N ds_\lambda = \frac{ds}{d\xi^3} \cdot N d\xi^3 = K \frac{e_3 \cdot \lambda}{\sqrt{g}} \lambda \otimes \lambda \cdot \frac{ds}{d\xi^3}.$$

This equation shows that the contribution of the stringer to the virtual change of the potential energy depends on the position of the stringer itself within the cross-section, due to the different lengths of $d\xi^3$ and ds_λ .

In terms of cross-sectional components, since the shape function reduces in this case to the identity, we have $\hat{s} = \hat{S}$ and therefore

$$\delta V = (\{\hat{S}'\} + [\hat{c} \times I]\{\hat{S}\})^T [\hat{M}] (\{\hat{S}'\} + [\hat{c} \times I]\{\hat{S}\}),$$

where $[\hat{M}]$ is given by:

$$[\hat{M}] = K \frac{e_3 \cdot \lambda}{\sqrt{g}} \{\hat{\lambda}\} \{\hat{\lambda}\}^T.$$

The other finite element stiffness matrices $[\hat{C}]$ and $[\hat{E}]$ are then computed by the formulae:

$$[\hat{C}] = [\hat{c} \times I]^T [\hat{M}] \quad [\hat{E}] = [\hat{c} \times I]^T [\hat{M}] [\hat{c} \times I].$$

4 The Computer Code

This section draws the basic ideas of the organization of the computer code as it should be for an efficient analysis of the cross-section of curved and twisted anisotropic beams. The numerical examples discussed later on have been obtained by an early program written to analyze only straight beams then modified for the present scope. The modifications performed, even if correct, are not the best from the point of view of program architecture and modularity: in particular, in the present version the displacement resolution is performed at element level and should be brought outside, following the formulation given above. Thus, most but not all the features discussed herein are actually implemented in the present code.

4.1 Input Data

Input data are grouped into three main blocks:

- Control data:
 - case description;
 - execution flags and parameters, curvature data;
 - outputs required and node/element selection;
 - eigenvalue solution parameters.
- Node data:
 - node identifier and coordinates;
 - nodal renumbering sequence;
 - single point constraints;
 - multiple point constraints.
- Element data:
 - material properties;
 - element properties;
 - element connections.

4.2 Disk and Memory Data Management System

The computer program interfaces with mass storage units by means of a home-made disk manager based on a paging technique similar to that used by virtual operating systems. Only few physical files are required by the disk manager: that has the nice effect to allow the user handling simple procedures to perform start, restart, backup

and restore operations. On the contrary, several logical files are allowed within the program and can be accessed both in sequential and in direct mode.

A memory manager is also implemented allowing memory dynamic allocation, memory packing and other features. This memory manager is fully integrated with the disk manager to get a high programming flexibility. The performances of this system can be tuned at installation time, according to the specific hardware configuration, by means of a set of parameters grouped in a block data.

4.3 Organization of the Computer Code

The program is organized in several main modules:

- *Case Input.* This module reads the data for the execution control:
 - Case description, execution flags, parameter values and restart options;
 - Outputs required: echo of input data, displacements, stresses, strains, intermediate results;
 - Node/element data selection for warping, stress and strain printouts;
 - Reference systems for input data.
- *Data Input.* This module performs the following items:
 - Node data input. The nodal data are rearranged in ascending order with regard to the node identifier; index vectors for external/internal numbering correspondence are prepared, accounting for possible external reordering sequence.
 - Constraint input. Single and multiple point constraints are available. An automatic procedure is implemented for eliminating any singularity due to rigid body motions; a table of constrained DOFs is printed. Single point constraints are handled as very strong springs: the default spring rigidity can be modified in input. Each multiple point constraint generate a kinematic equation that is added to the analysis by means of a Lagrange Multiplier.
 - Equations numbering. The equations related to each node are numbered, accounting for the presence of multi-point constraints: each constraint equation is automatically inserted after the first degree of freedom involved in order to ensure any singularity to be removed. The equations related to the generalized cross-section deformation parameters are numbered as last ones.
 - Element Data input. The element data are stored in a logical file structured with variable length records: each record contains the element identifier, the element type, the connected nodes, the material data and physical properties and other informations specific to the element.

- Equation pointer array. For each element an array of pointers to the equations involved is set and stored on disk.
- *Element Matrix Computation.* The matrices \bar{M} , \bar{C} , \bar{E} and P are computed for each element and stored on a disk file.
- *Assembling Module.* The matrices of the cross-section finite element analysis are assembled by this module. The assembling process can be performed either with an in-core procedure or with an out-of-memory one. The out-of-memory procedure runs with a frontal technique which is very effective for large problems. The in-core procedure is based on a skyline assembler/solver routine which can speed up the execution when large amount of core memory is available. The assembler/solver package can work either in real or complex mode, for the analysis of straight or curved beams respectively.
- *Solution Module.* This module performs the solution iterations according to the execution options: two solution steps on a real matrix are run for straight beams, while six steps are required on a Hermitian matrix for curved beams. In any case the coefficient matrix is the same for each step, thus only one decomposition is needed. The right-hand side vector is setup at each step, then the frontal or skyline solution is performed. Both the implemented solvers contain an automatic procedure for singularity elimination that can be turned off with an input option. Finally, the section intrinsic warping is recovered, as discussed in the theoretical section of this report.
- *Cross-section Stiffness and Mass Module.* The 6×6 stiffness matrix of the cross-section is computed and it is evaluated also with reference to the principal axes of the normal stress. By integrating the density on the area of each element the mass matrix of the cross-section is also computed. Then the center of gravity of the cross-section and its inertial properties and principal axes are computed.
- *Stress and Strain Recovery.* Stresses and strains can be recovered either with reference to the element frames or to the cross-section global frame.
- *Extremity Solution.* The solution of the extremity problem can be performed with two different formulations: a full analysis to extract all the eigenvalues and a reduced one, based on the Lanczo's algorithm, to extract only a few eigenvalues of interest. This module computes eigenvalues and eigenvectors and can recover the eigenstresses too.
- *Printout Module.* It performs any output selected by the user and prints the cross-section global characteristics.

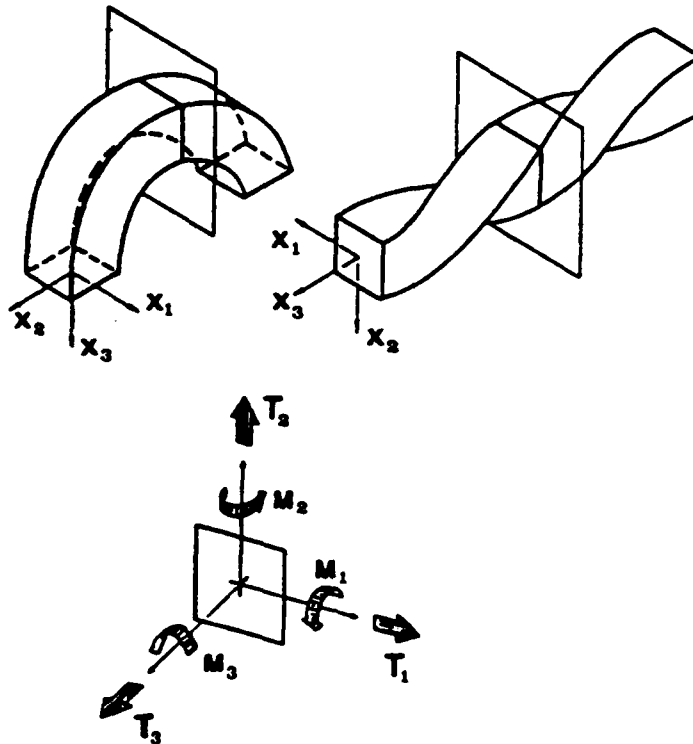


Figure 6: Elementary study cases. Simply curved and twisted beams.

5 Numerical Examples

5.1 A Curved or Twisted Isotropic Solid Beam

The first study case presented is very simple and aims to only determine the feasibility of the method presented without any claim to be exhaustive. An isotropic square cross-section of 120x120 mm is analyzed and results are presented for two cases, see Fig. 6: a simply curved beam with radius of curvature of 200 mm (Case A) and a simply twisted beam with a twist of 90° degrees over 314.5 mm of length (Case B).

The beam cross-section has been modeled with 25 square 8-node isoparametric elements for a total of 294 DOFs. The analysis by the present approach is compared with theoretical results, when available, and with three-dimensional numerical analyses by MSC-NASTRAN. The three-dimensional discretization of half a beam is composed of 10 or 12 slices of 25 20-node isoparametric solid elements (CHEXA), for a total of 250 elements and 4248 DOFs for case A, and 300 elements and 5040 DOFs for case B. These models, see Fig. 7, are loaded at the free extremity with suitable nodal forces giving the desired resultants. Note that the present approach involves more than one order of magnitude reduction of the problem size relative to MSC-NASTRAN.

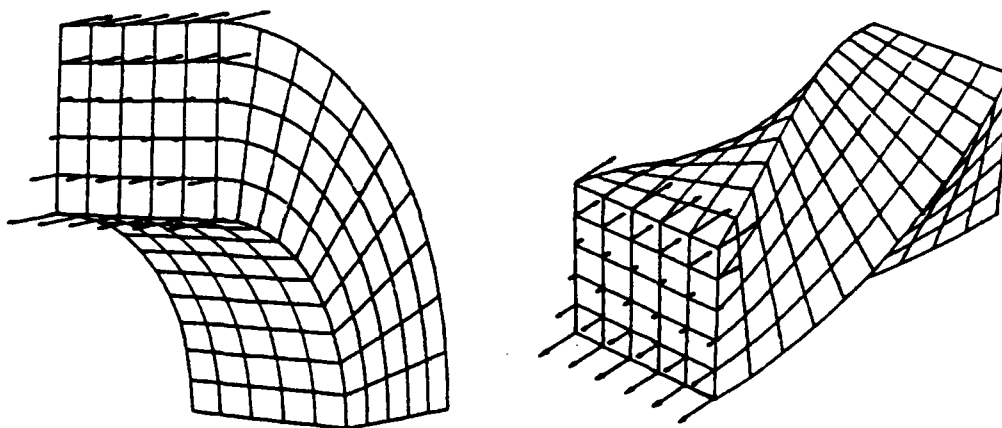


Figure 7: Elementary study cases. MSC-NASTRAN mesh.

Case A: Curved Beam

Theoretical results are only available for a simply curved beam acted upon by a bending moment in the curvature plane. A comparison of the normal stress is given in Fig. 8: it can be seen that the present analysis and the three-dimensional one agree very well and discrepancies are confined within 0.3%. We also observe that the maximum value of the compression stress is about 30% greater than the straight beam with the same cross-section.

Figures 9, 10 and 11 report some stress distributions for different load conditions, showing significant effects due to the curvature. As expected, the stress distributions are different from the corresponding ones of the straight-beam case: for example, the in-plane stress component σ_{11} is different from zero, the shear stress distribution σ_{13} due to T_1 is not symmetric and the shear center is closer to the curvature center. A comparison with MSC-NASTRAN results is given in Fig. 12: the difference in computed stresses is under 2%.

Case B: Twisted Beam

Also in the twisted beam case is the difference with respect to the rectilinear beam with the same cross-section very significant. In Fig. 13 the shear stress under four elementary load conditions is plotted: shear stresses arise at the four corners even under bending and tension loading, thus satisfying the boundary conditions on the lateral surface.

For this case only a comparison of the present analysis vs a three-dimensional one is reported, as theoretical results were not found: the stress distributions on the cross-section, see Fig. 14, are quite similar for the two analyses even if discrepancies are more evident than for case A. A more detailed discretization would reduce these differences.

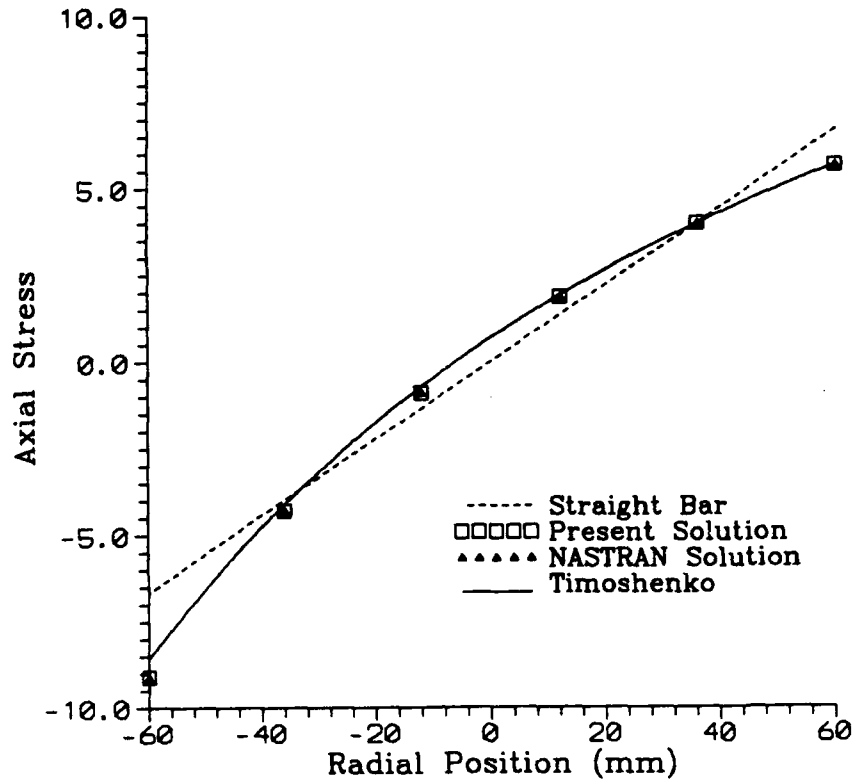


Figure 8: Case A. Normal stress due to bending.

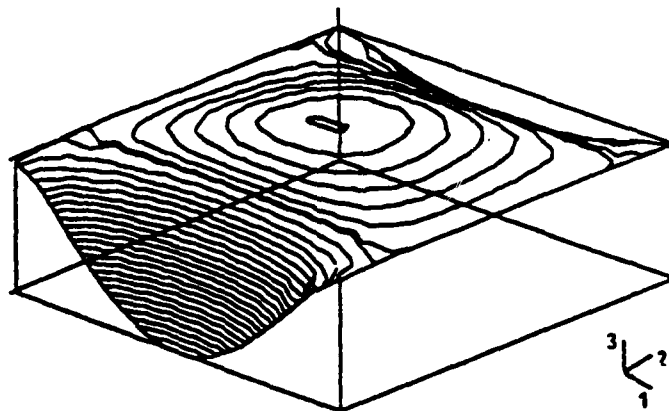


Figure 9: Case A. Stress σ_{11} contour plot due to M_1 .

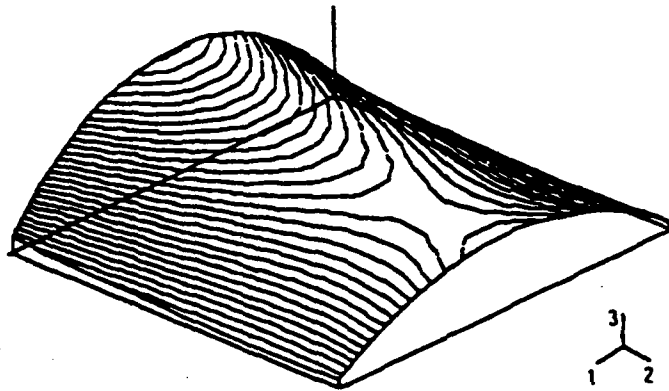


Figure 10: Case A. Stress σ_{13} contour plot due to T_1 .

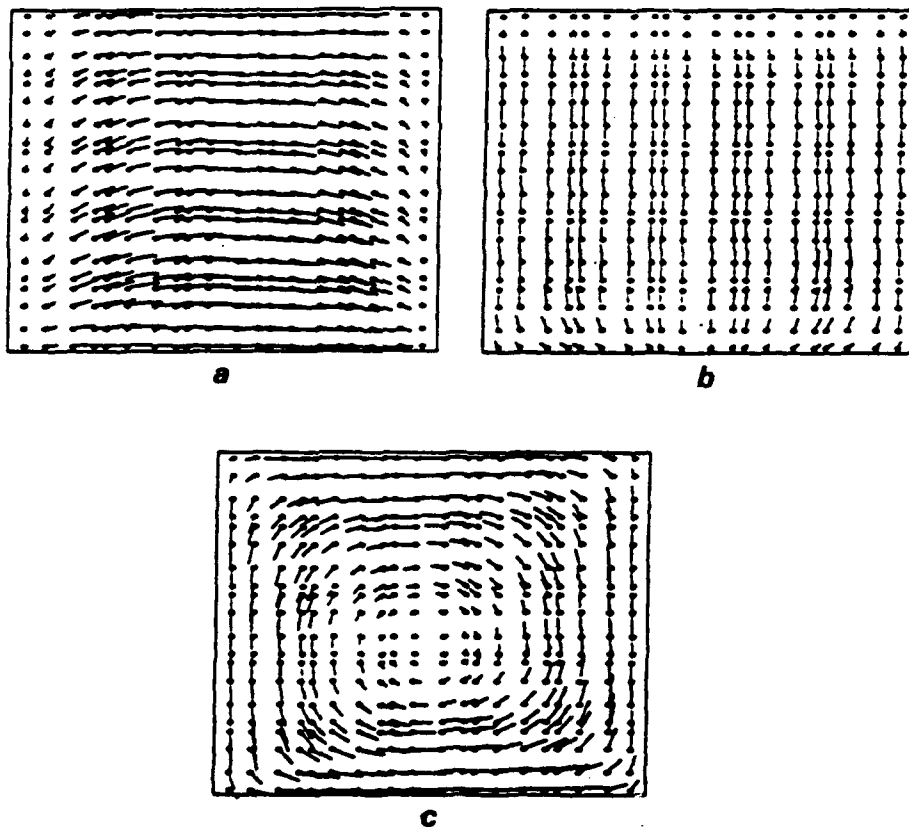


Figure 11: Case A. Shear stresses due to: (a) T_1 , (b) T_2 , (c) M_3 .

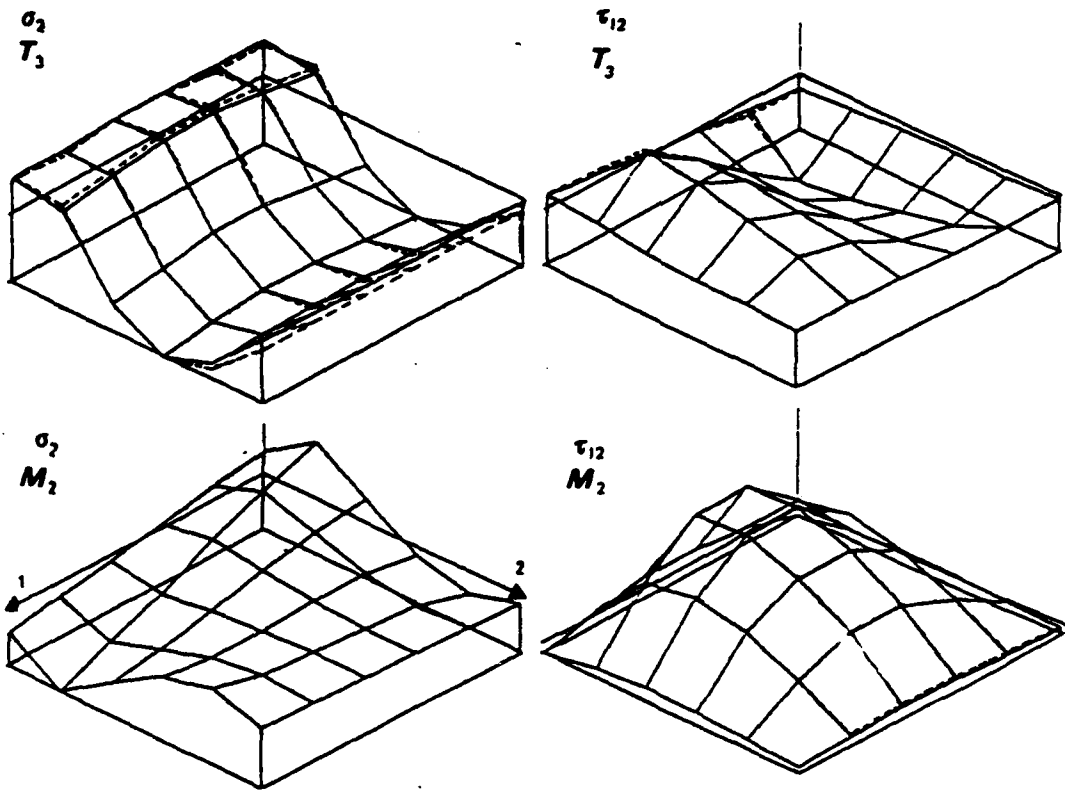


Figure 12: Case A. Some stress distributions due to different section resultants. Comparison with MSC-NASTRAN (dotted lines) results.

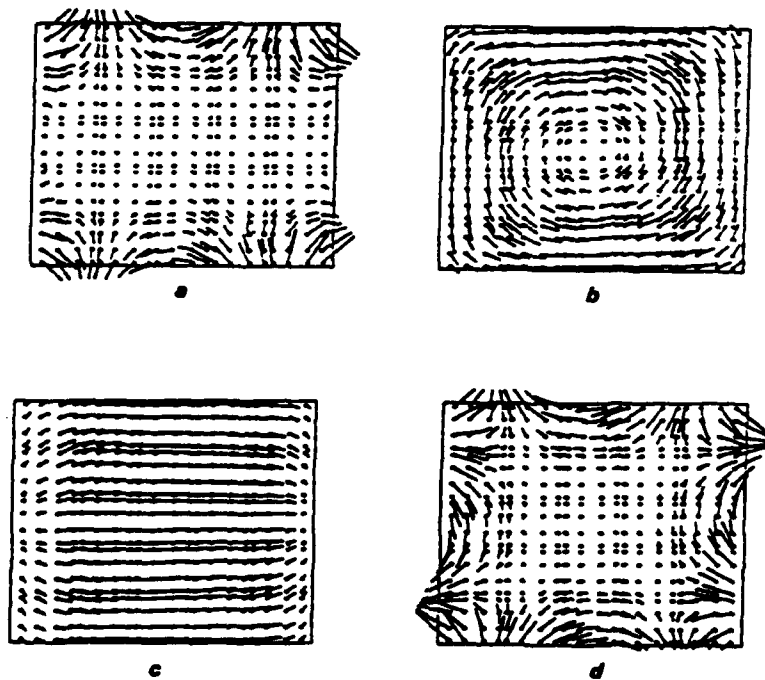


Figure 13: Case B. Shear stresses due to: (a) M_1 , (b) M_3 , (c) T_1 , (d) T_3 .

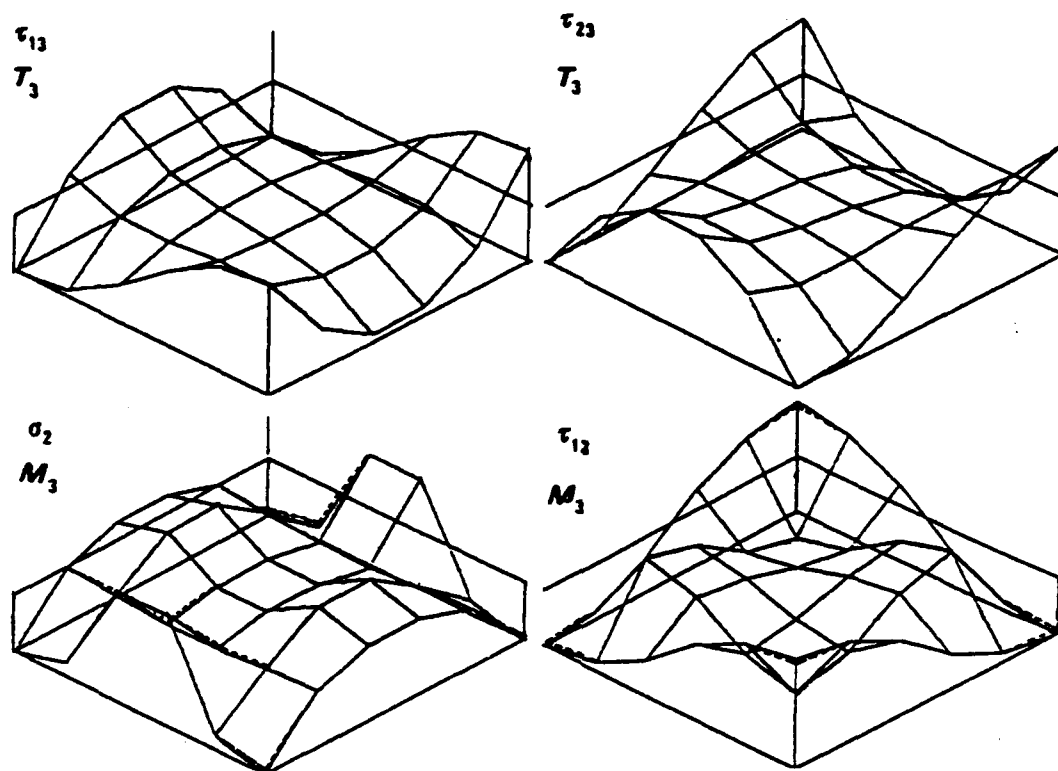


Figure 14: Case B. Some stress distributions due to different section resultants. Comparison with MSC-NASTRAN (dotted lines) results.

5.2 A Rectilinear Composite Box-Beam

As a second example, the rectilinear composite box-beam already investigated by Smith and Chopra (1990) is considered (see Fig. 15): the experimental and numerical results they present give the opportunity to compare the performances of different approaches to the analysis of composite beams. Ten specimens have been analyzed having two different aspect ratios and several laminations: the geometric data, the stacking sequences and the elastic properties of the material, unidirectional GR/EP AS4/3501-6, are reported in Tables 3, 4 and 5. The stacking sequences

	Case A	Case B
L	30. in.	30. in.
c	2.060 in.	.0953 in.
d	1.025 in.	.0537 in.
L/d	29	56
ply thickness	.005 in.	.005 in.
wall thickness (6 plies)	.030 in.	.030 in.

Table 3: Box-beam. Geometric data.

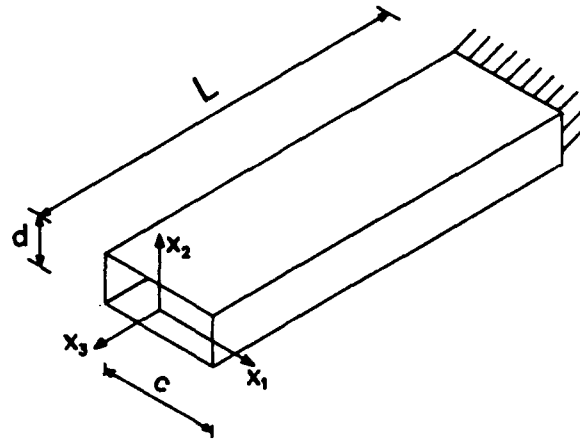


Figure 15: The rectilinear composite box-beam.

Specimen #	Case	Configuration	Upper and lower walls	Side walls
1	A	symmetrical	0/90	0/90
2	B	anti-symm.	15	15/15
3	B	anti-symm.	0/30	0/30
4	B	anti-symm.	0/45	0/45
5	A	symmetrical	15	15/-15
6	A	symmetrical	30	30/-30
7	A	symmetrical	45	45/-45
8	B	symmetrical	15	15/-15
9	B	symmetrical	30	30/-30
10	B	symmetrical	45	45/-45

Table 4: Box-beam. Stacking sequences.

Orthotropic Young's modulus	E_L	=	20.59 msi
Transversal Young's modulus	E_T	=	1.42 msi
Tangential modulus	G_{LT}	=	0.87 msi
Poisson's ratio	ν_{LT}	=	0.42

Table 5: Box-beam. Elastic properties.

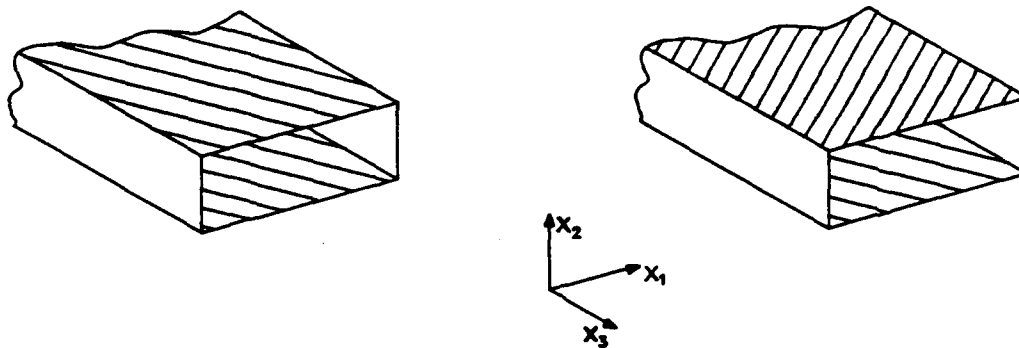


Figure 16: Box-beam. Symmetric and anti-symmetric configurations.

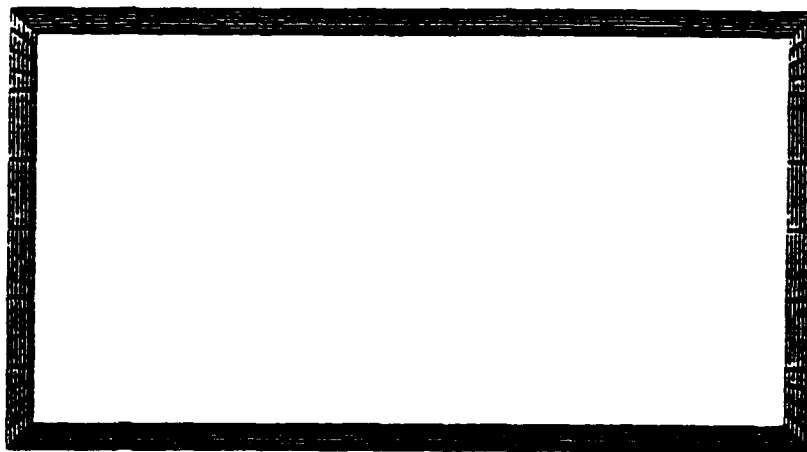


Figure 17: Box-beam. Mesh of the cross-section.

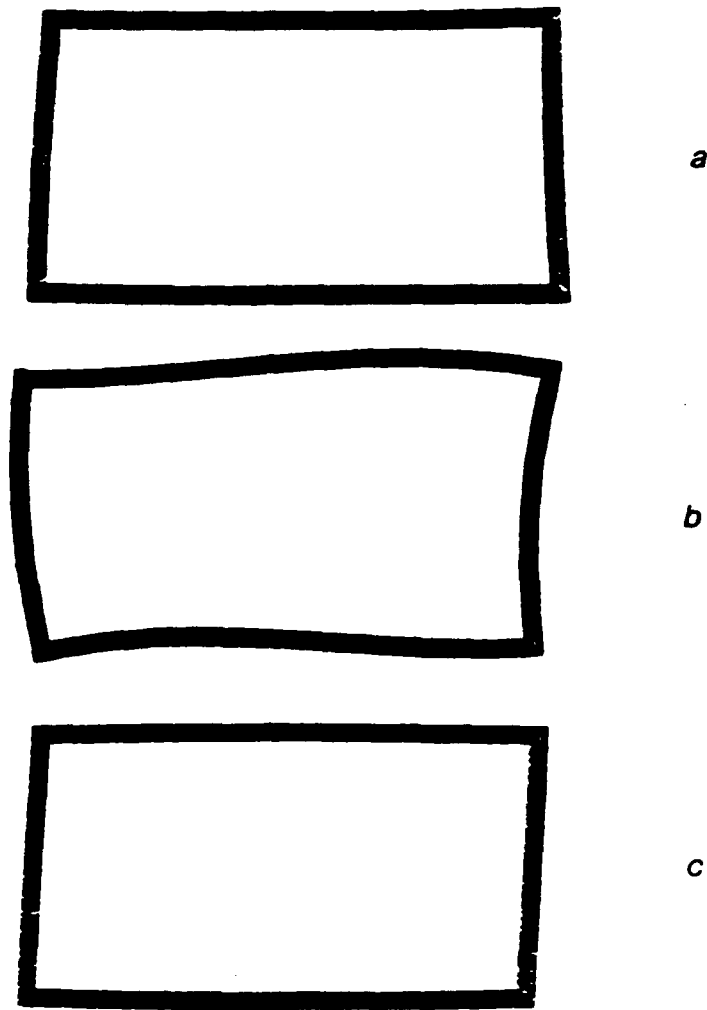


Figure 18: Box-beam, Specimen 3. Deformed cross-section due to: (a) bending moment M_1 , (b) torque M_3 and (c) axial force T_3 .

considered allow us to analyze either uncoupled behavior or symmetric or anti-symmetric couplings: refer to Fig. 16 for the orientation of the laminations. The model of the cross-section, see Fig. 17, stands on 288 8-node isoparametric plane elements, each bounded within a single ply: the analysis DOFs amount to 2886.

The deformed cross-sections under a few elementary load conditions are shown in Fig. 18. Some diagonal terms of the flexibility matrix of the cross-section, namely flexure about X_1 and torsion, are given in Table 6 for all the specimens and plotted in Fig. 19 versus the characteristic angle of lamination.

Some coupling effects are given in Table 7: two off-diagonal terms of the flexibility matrix are reported for all the specimens. The section torsion under axial load and bending is also plotted in Fig. 20 versus the characteristic angle of lamination. These plots show that, as it is expected, for the symmetric specimens (1 and 5 to 10) axial extension does not couple with torsion while flexure does; the opposite

Specimen #	Flexure due to M_1 (rad/in)	Torsion due to M_3 (rad/in)
1	1.042×10^{-6}	1.406×10^{-5}
2	2.665×10^{-5}	1.125×10^{-4}
3	1.844×10^{-5}	6.445×10^{-5}
4	2.018×10^{-5}	6.836×10^{-5}
5	2.890×10^{-6}	9.790×10^{-6}
6	6.860×10^{-6}	7.260×10^{-6}
7	1.250×10^{-5}	6.960×10^{-6}
8	2.380×10^{-5}	8.332×10^{-5}
9	5.620×10^{-5}	6.120×10^{-5}
10	1.060×10^{-4}	5.903×10^{-5}

Table 6: Box-beam. Flexure and torsion due to unit moments.

Specimen #	Flexure due to T_3 (rad/in)	Torsion due to M_1 (rad/in)
1	0.0	0.0
2	8.34×10^{-6}	0.0
3	2.70×10^{-6}	0.0
4	1.41×10^{-6}	0.0
5	0.0	3.03×10^{-6}
6	0.0	3.42×10^{-6}
7	0.0	4.39×10^{-6}
8	0.0	2.47×10^{-5}
9	0.0	3.60×10^{-5}
10	0.0	3.61×10^{-5}

Table 7: Box-beam. Some coupling effects.

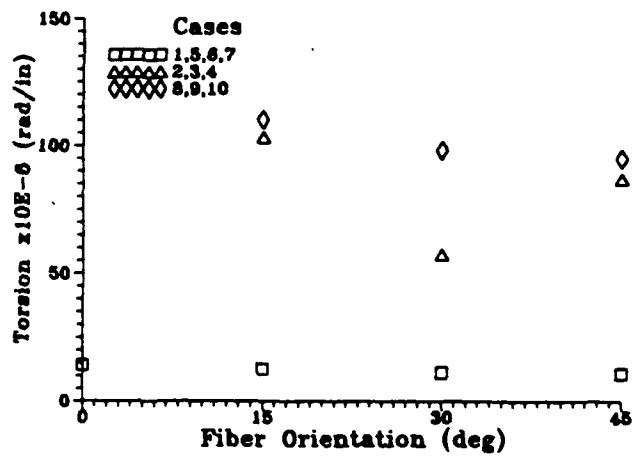
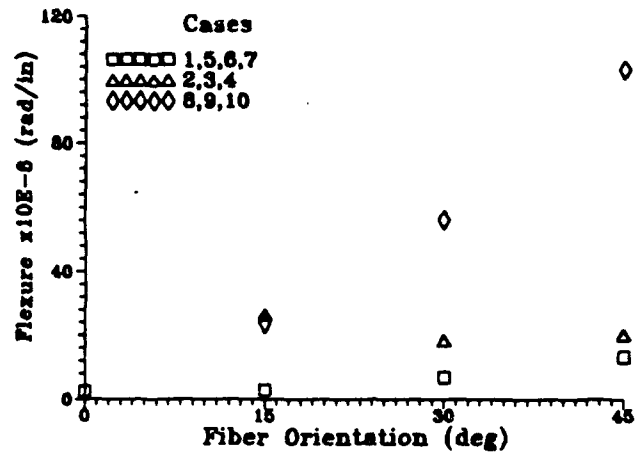


Figure 19: Box-beam. Flexure and torsion due to unit moments.

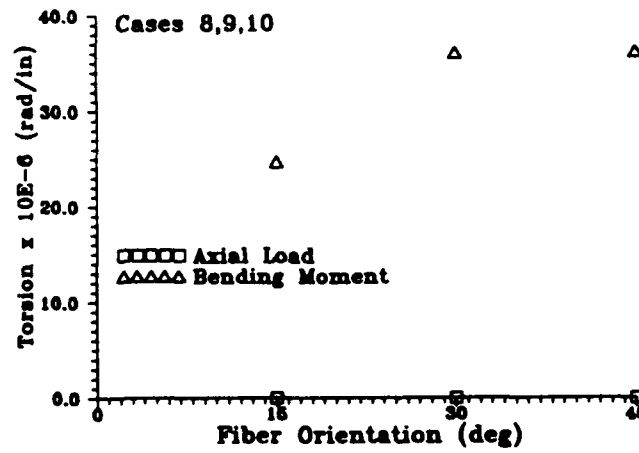
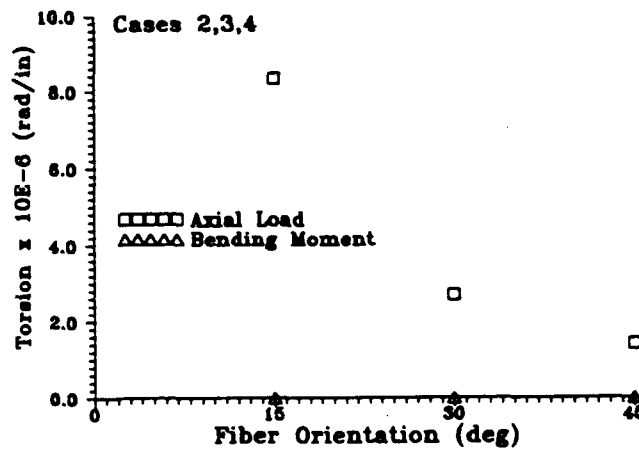
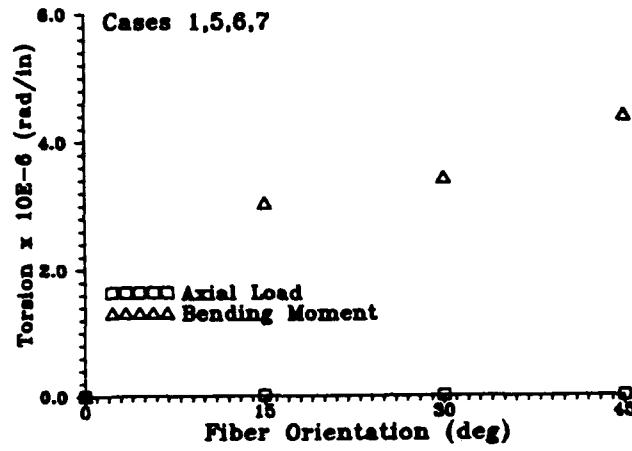


Figure 20: Box-beam. Some couplings effects.

happens for the anti-symmetric specimens (2 to 4). Moreover, the influence on these couplings of the fiber orientation and of the specimen aspect ratio can be observed. It is well known that the knowledge of results like these ones would be a valuable support while tailoring a real beam, for example for aeroelastic purposes: all the elastic effects must be taken into account in order to achieve a desired coupling level, and this can be a very difficult task for a complex beam if adequate tools are not at hand, as this quite simple example of a box-beam can demonstrate.

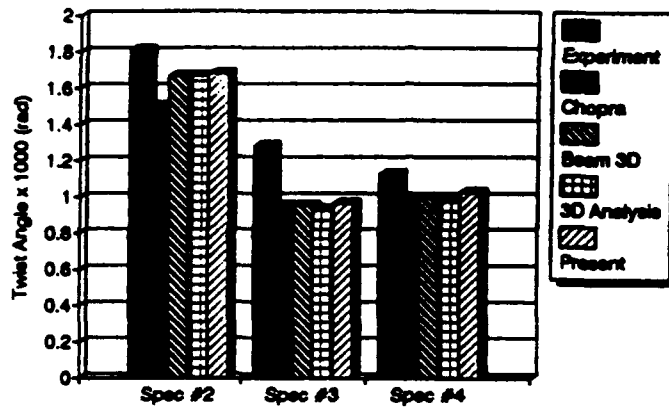
The cross-section stiffness has been integrated along the beam span to obtain a beam model for the experiments reported by Smith and Chopra (1990): that allows us to extend the comparison among different analysis methods, presented in that work. Figure 21 shows the results obtained: the effectiveness of the present approach with respect to others methods can be appreciated even if we cannot point out a best one.

Hereafter the strain and stress distributions across the wall thickness are presented for two points of the cross-section of specimen 3, chosen at the mid-side of the upper and right walls, for two load conditions, namely axial load and torque. As it will be observed, some stress or strain components are discontinuous between laminae: accounting for these discontinuities is implicit in the present formulation based on a fully three-dimensional stress state. Obviously discontinuous elastic properties must be reproduced with an adequate finite element model of the composite cross-section.

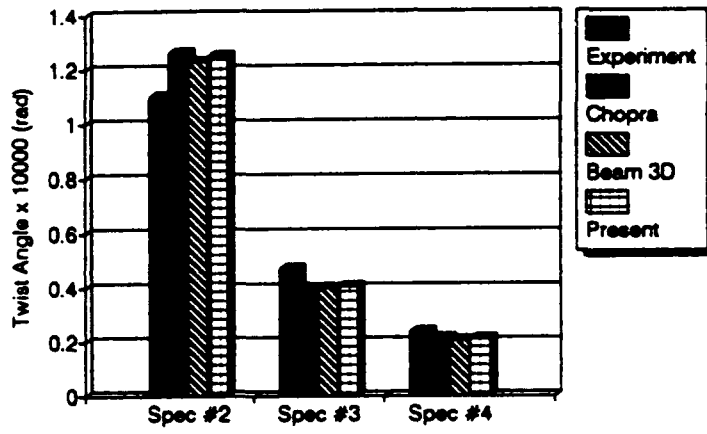
In the case of axial load, Figs. 22 to 25, the stress component σ_{33} is discontinuous between layers at 0° and layers at 30° , while strain ϵ_{33} keeps constant. As a consequence, alternate shear stresses σ_{13} in the upper-side wall and σ_{23} in the right-side one arise: the corresponding strains ϵ_{13} and ϵ_{23} are continuous and linearly varying across the thickness. A transverse stress state can be observed: the extensional stress σ_{11} in the upper-side wall and σ_{22} in the right-side one are alternate, while the corresponding strains ϵ_{11} and ϵ_{22} are linearly varying. Transverse strains ϵ_{22} or ϵ_{11} are present, while stresses σ_{22} or σ_{11} are zero. The transverse shear stress σ_{12} and strain ϵ_{12} are zero.

In the case of torque, Figs. 26 to 29, the results are qualitatively similar: the stress components σ_{13} in the upper-side wall and σ_{23} in the right-side one are discontinuous between the layers, while the corresponding strains ϵ_{13} and ϵ_{23} are linearly varying, and an axial stress σ_{33} arises, with null strain ϵ_{33} . A discontinuous behavior of the extensional stress σ_{11} in the upper-side wall and σ_{22} in the right-side one can be observed, while the corresponding strains ϵ_{11} and ϵ_{22} are linearly varying. Transverse strains ϵ_{22} or ϵ_{11} are present, while stresses σ_{22} or σ_{11} are zero. The transverse shear stress σ_{12} and strain ϵ_{12} are again zero.

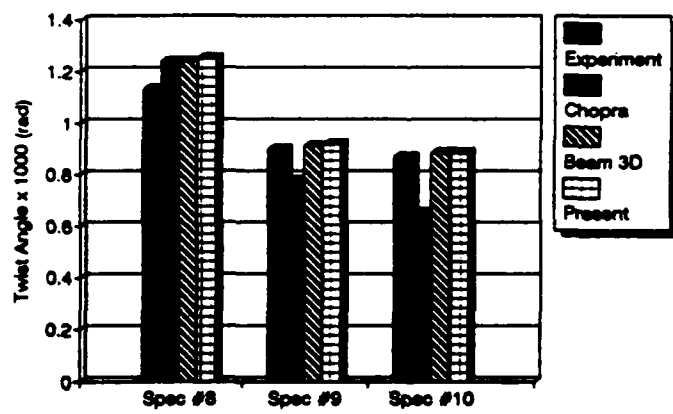
Even if, in this example, the rectilinear shape of the beam walls prevents any interlaminar stress to arise, it is expected that the presence of a transverse stress state would induce interlaminar stresses in the case of curved walls. Indeed, interlaminar stresses are also present in this example in the corner areas, but a more



a



b



c

Figure 21: Box-beam. Twist angle under: (a, b) unit tip torque, (c) unit axial load.

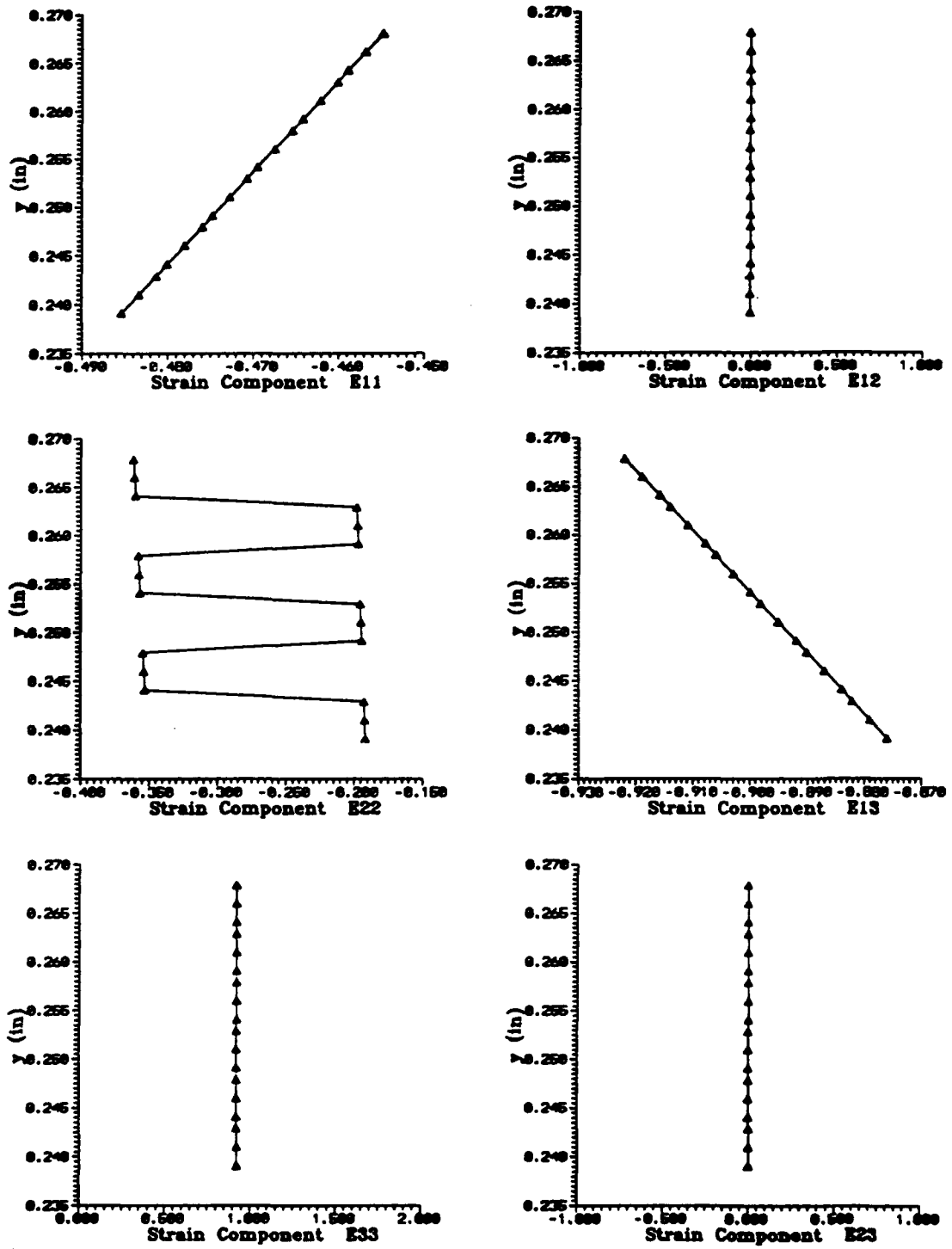


Figure 22: Box-beam, upper-side wall. Strain under axial load.

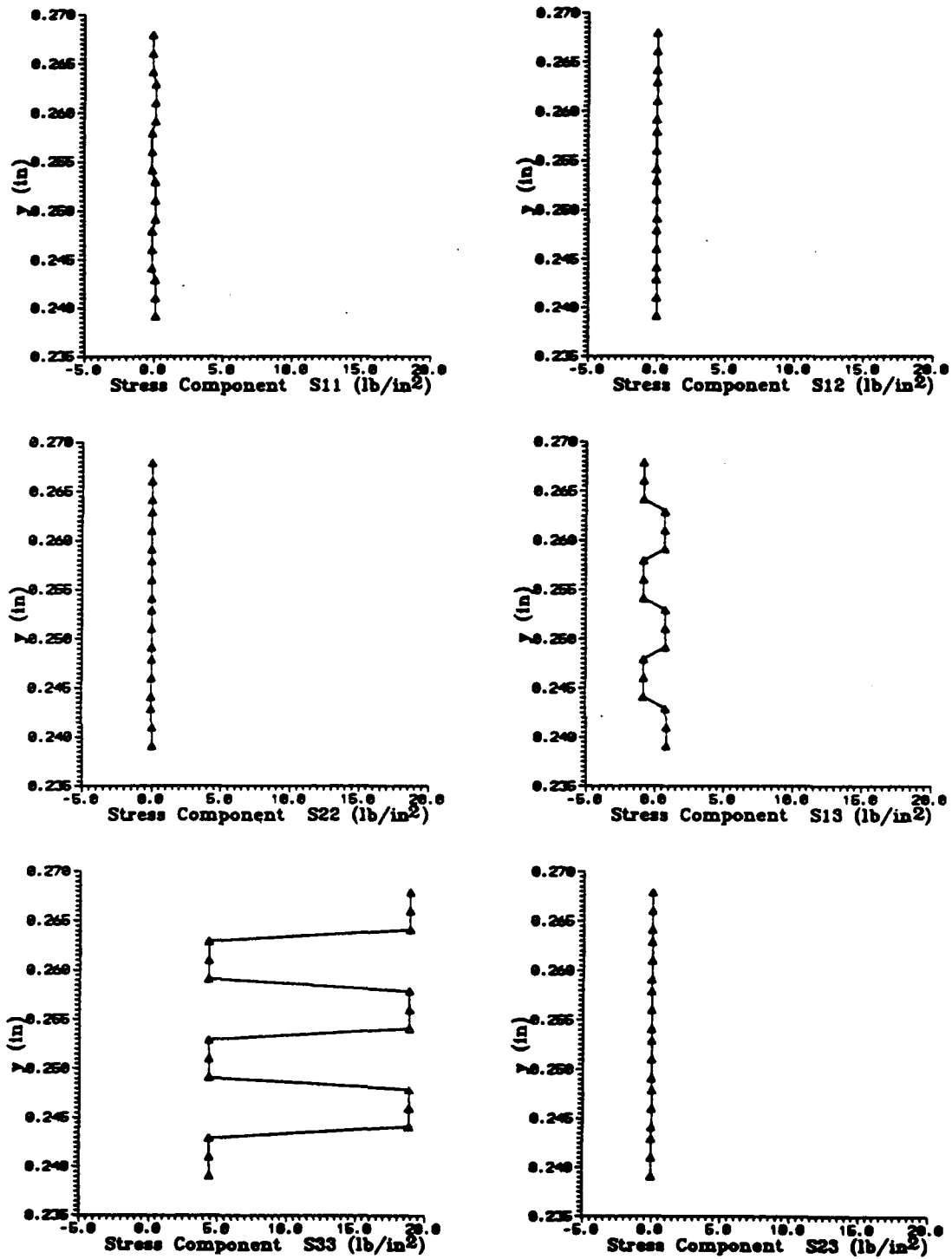


Figure 23: Box-beam, upper-side wall. Stress under axial load.

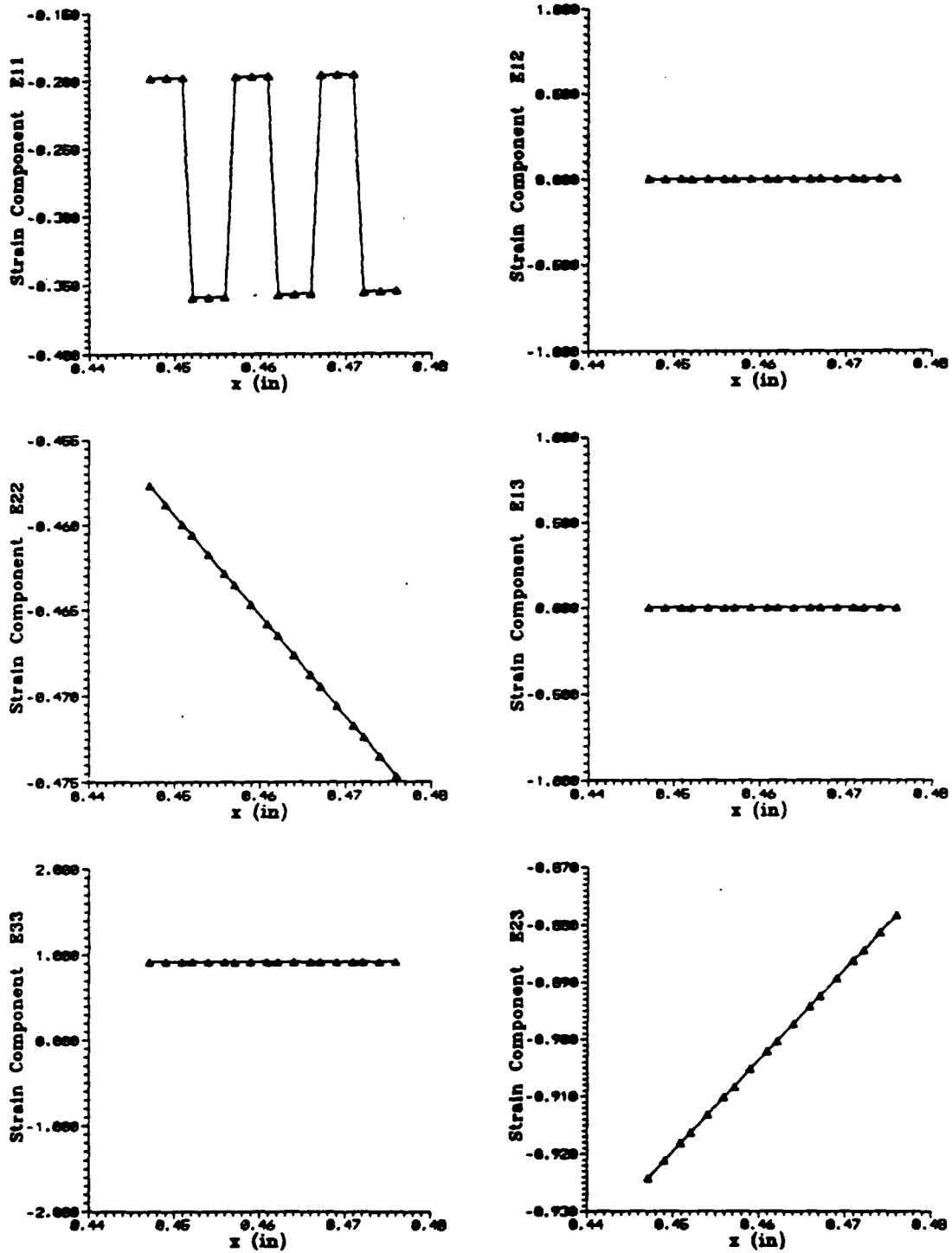


Figure 24: Box-beam, right-side wall. Strain under axial load.

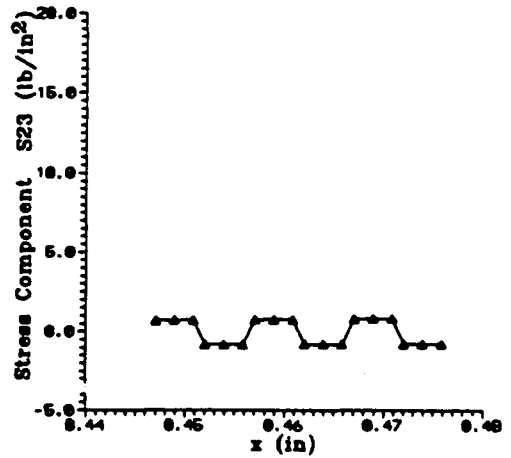
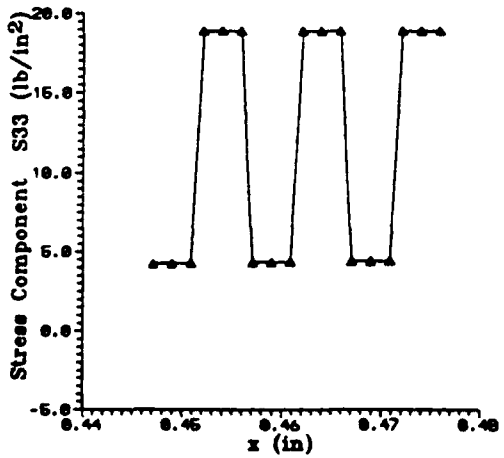
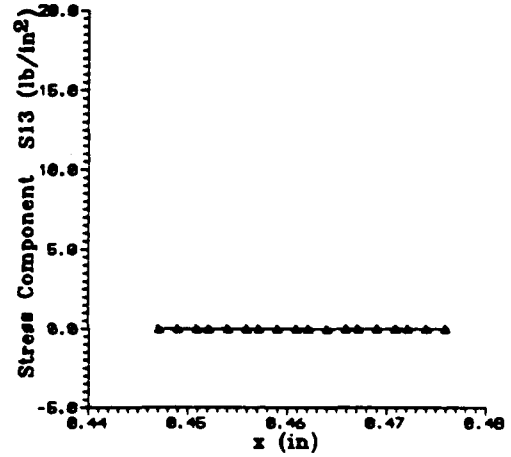
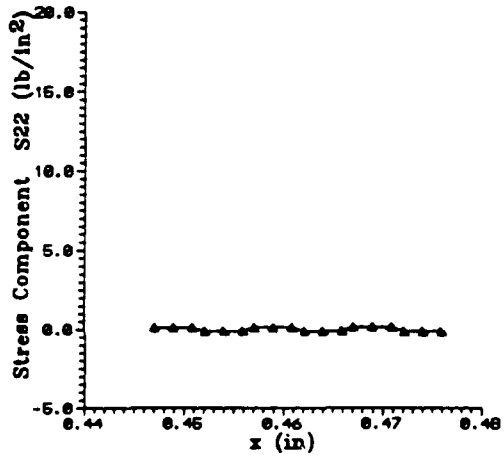
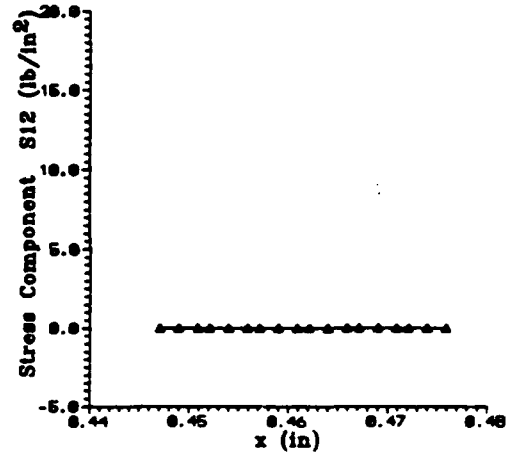
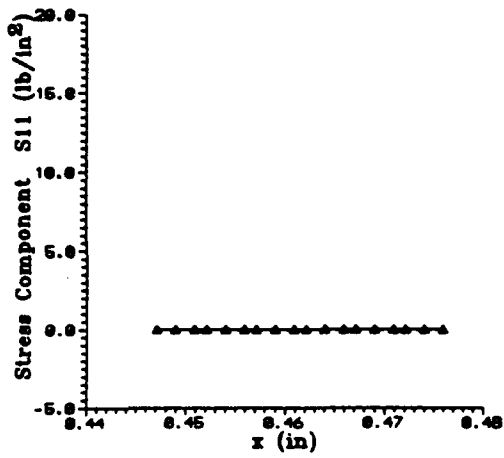


Figure 25: Box-beam, right-side wall. Stress under axial load.

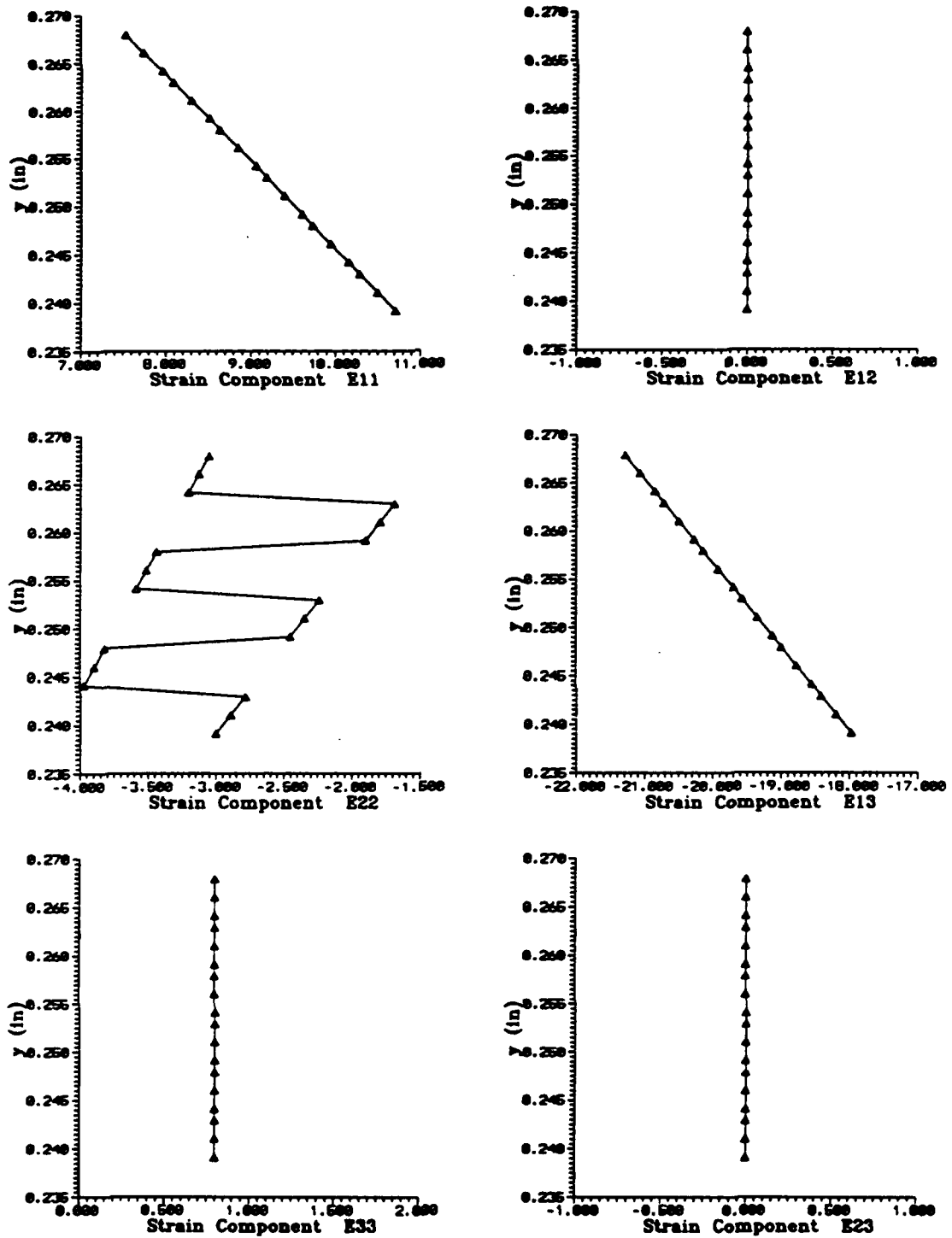


Figure 26: Box-beam, upper-side wall. Strain under torque.

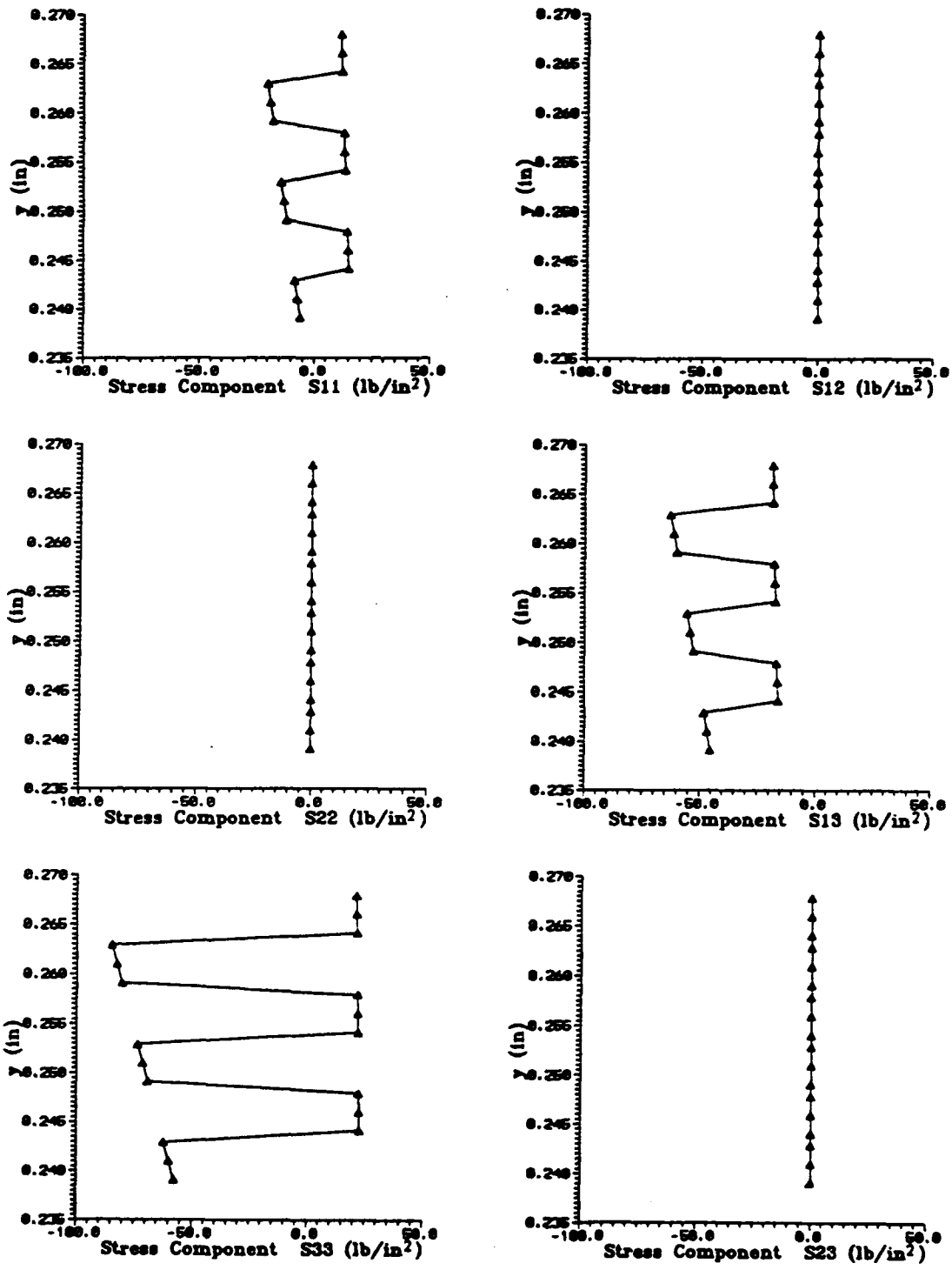


Figure 27: Box-beam, upper-side wall. Stress under torque.

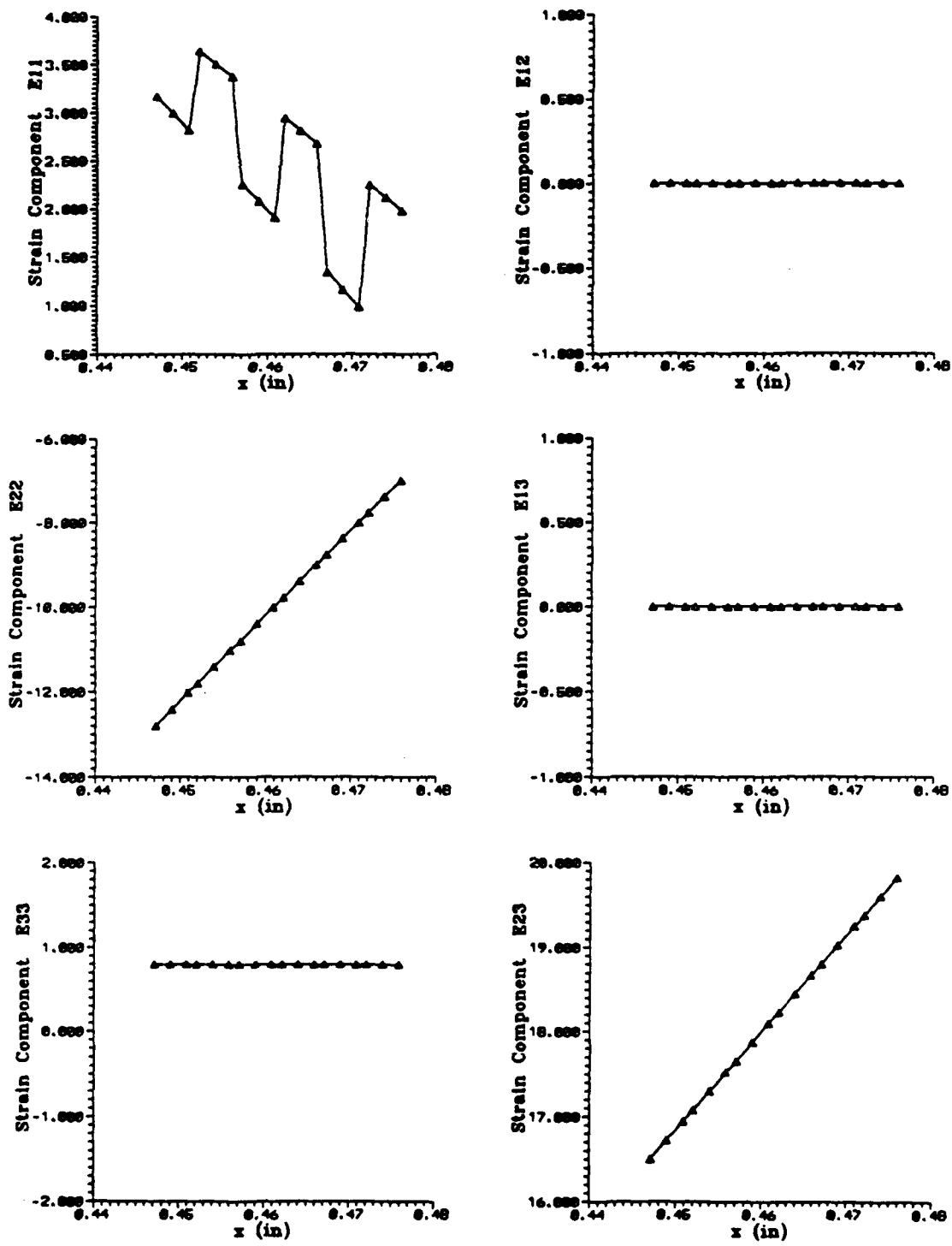


Figure 28: Box-beam, right-side wall. Strain under torque.

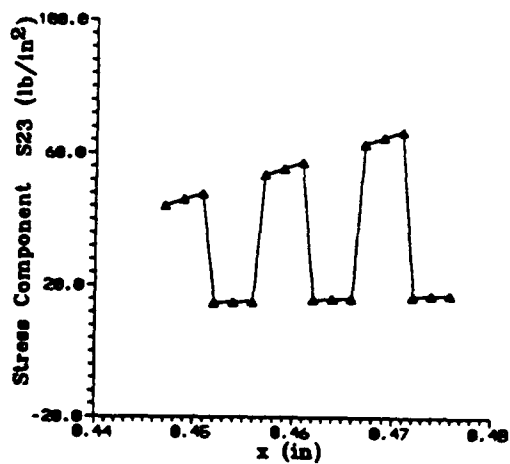
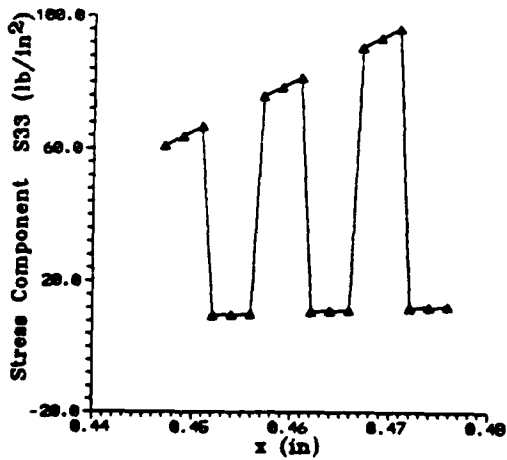
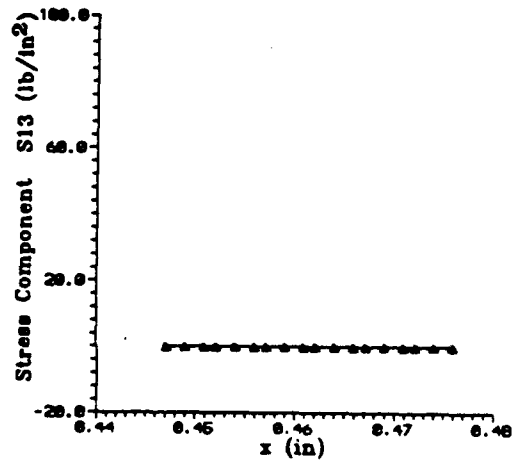
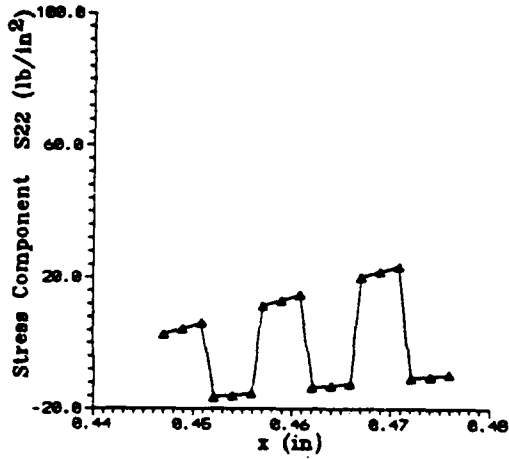
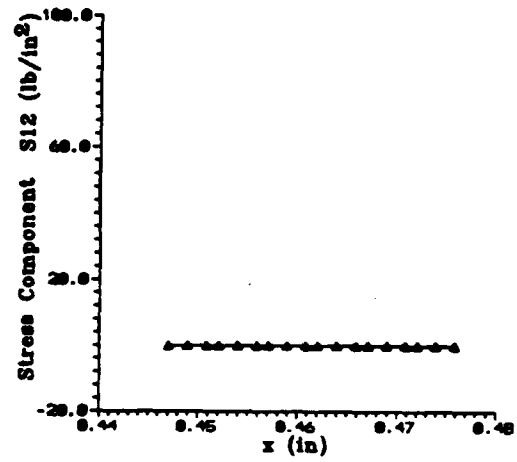
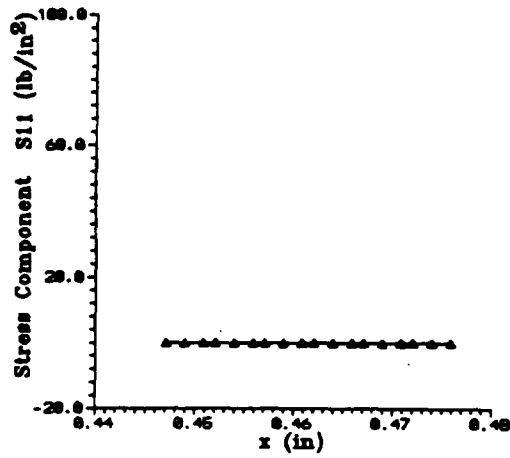


Figure 29: Box-beam, right-side wall. Stress under torque.

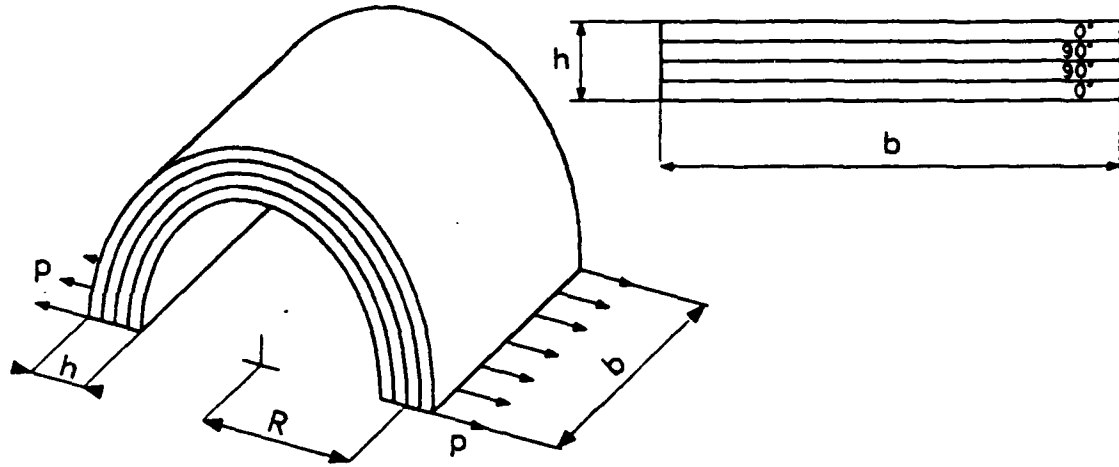


Figure 30: The curved cross-ply specimen.

Geometric dimensions	Elastic properties
$R = 4.5 \text{ mm}$	$E_{11} = 14074 \text{ kg/mm}^2$
$h = 1.0 \text{ mm}$	$E_{22} = E_{33} = 1478 \text{ kg/mm}^2$
$b = 6.0 \text{ mm}$	$\nu_{12} = \nu_{13} = .21 \quad \nu_{23} = .3$
stacking sequence: $[0/90]_s$	$G_{12} = G_{13} = G_{23} = 598 \text{ kg/mm}^2$

Table 8: Cross-ply specimen. Geometric and material data.

detailed mesh would be necessary in order to correctly capture them, and that was beyond the scope of this test case.

5.3 A Curved Cross-ply Specimen

A comparison with a fully three-dimensional approach has been attempted analyzing a curved composite specimen made of four symmetric graphite-epoxy cross-ply layers. This specimen, see Fig. 30 and Table 8, is characterized by a strong curvature ($R/h=4.5$, $R/b=.75$) and extends over 180° : the mid cross-section is considered when the specimen is loaded as shown with a resultant force of 1000 kg.

The three-dimensional mesh is made with 20-node isoparametric brick elements to model each ply; because of symmetry, a quarter of the specimen has been modeled for a total of 432 elements, see Fig. 31. For the two-dimensional analysis of the cross-section three meshes have been modeled as shown in Fig. 32: a coarse one equivalent to the 3-D model as far as the section is concerned (4×6 parabolic plane elements for half a section); a medium one with 2 elements for each layer and still 6 elements on the section half-span; and a refined one with 3 elements for each layer

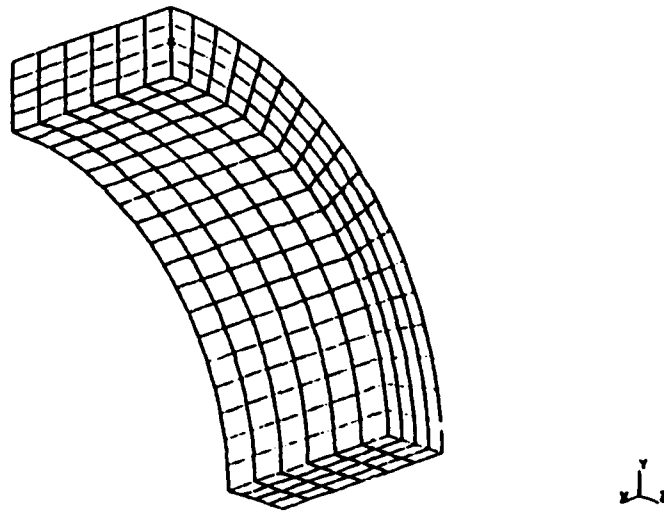


Figure 31: Cross-ply specimen. 3-D mesh of a quarter of the specimen.

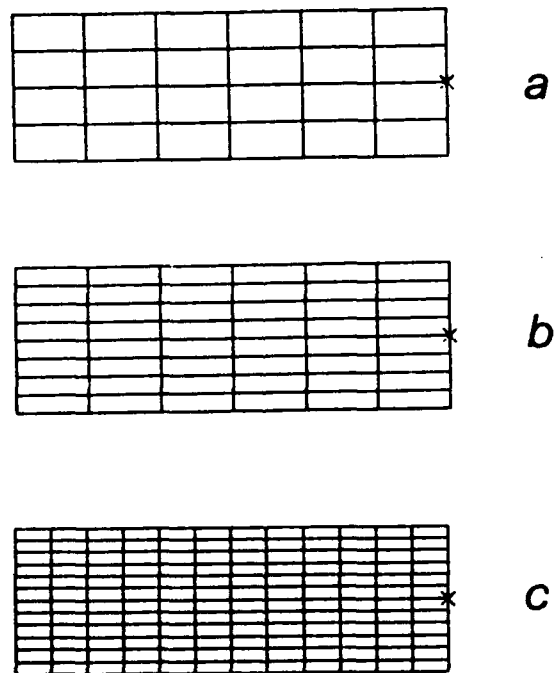


Figure 32: Cross-ply specimen. 2-D meshes of a half of the cross-section: (a) coarse, (b) medium, (c) fine.

Mesh	Nodes	DOFs	Elements
3-D	2397	7191	432
2-D coarse	93	285	24
2-D medium	159	483	96
2-D fine	481	1449	144

Table 9: Cross-ply specimen. Sizes of the finite element models.

and 12 elements on the section half-span. Using these three models ensures reaching convergence of results. The sizes of the finite element models are given in Table 9: these data stress once more the effectiveness of the present approach.

Results are compared in terms of stress and strain across the thickness at the center of the specimen. The stress state near the end sides of the specimen section is under free edge effect and it is not reported here: interlaminar layers should have been modeled in order to study these effects and this was not the purpose of this example. As shown in Fig. 33, the three 2-D models yield the same results, showing that even the coarse mesh is adequate. Moreover, both the 2-D and 3-D analyses are able to handle the discontinuities in the material elastic properties: the stress σ_{33} and strain ϵ_{33} normal to the cross-section are in good agreement. On the contrary, the two transverse stress and strain components differ in magnitude in 2-D and 3-D models. This discrepancy would probably reduce with a more refined discretization along the curved beam in the 3-D model: in fact, the displacement representation along the beam axis in the present approach must be considered *exact*.

5.4 A Curved Composite I-Beam

The last numerical example refers to a curved I-shaped beam: this beam was first analyzed, using a different approach, by Peck (1991) and it constitutes a good numerical test for the present method. The analysis target is to calculate the axial force and the curling moment acting upon the flange elements of the beam loaded independently with a bending moment and an axial load. A peculiarity of this example is the high shear force transferred between the flanges and web due to the curvature, even under bending moment and axial loads: therefore the curling moment of the flanges becomes a significant test quantity.

The geometric data of this example are reported in Fig. 34, and sign conventions in Fig. 35. Four different laminations have been tested, as described in Table 10: the elastic properties of the material, graphite-epoxy GR/EP T300/5208, are reported in Table 11. The finite element discretization of the cross-section is summarized as follows, see Fig. 36: 8×2 elements across the thickness of the web (two plane elements averaging each one 6 layers), and 12×22 elements across the thickness of

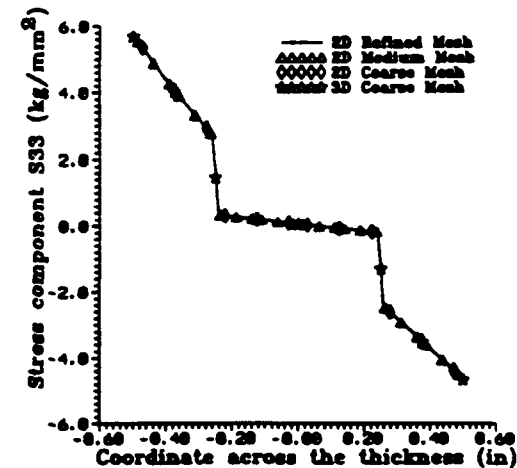
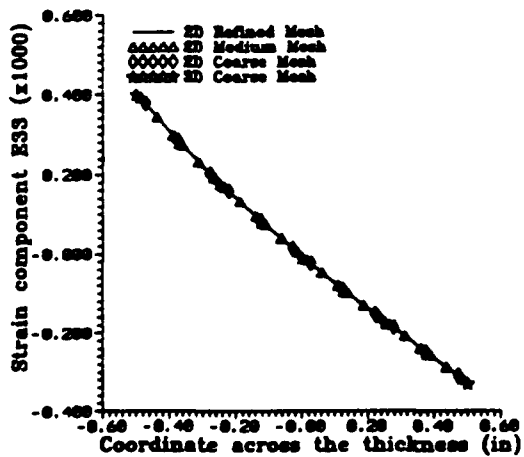
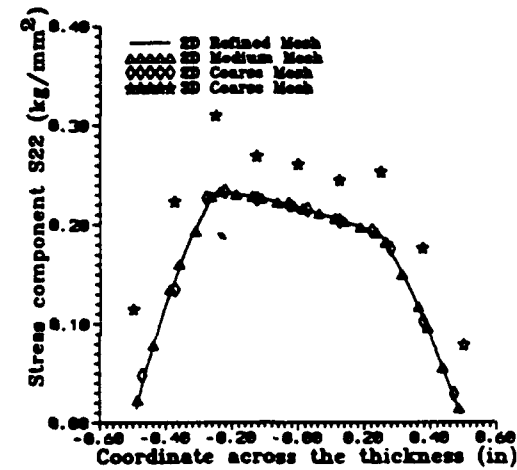
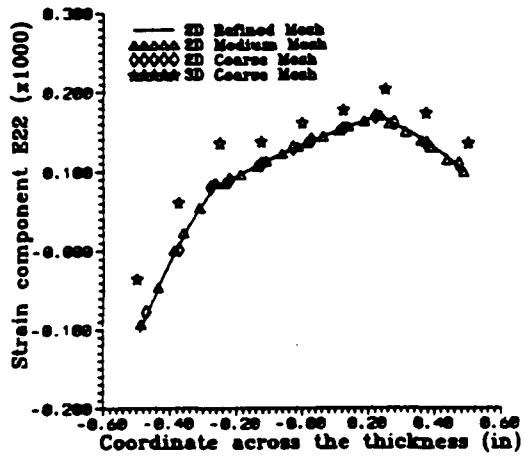
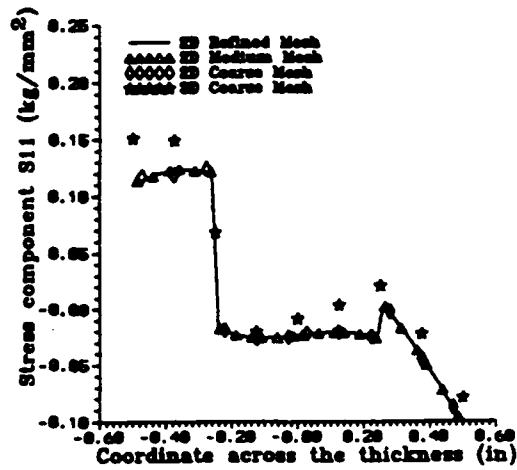
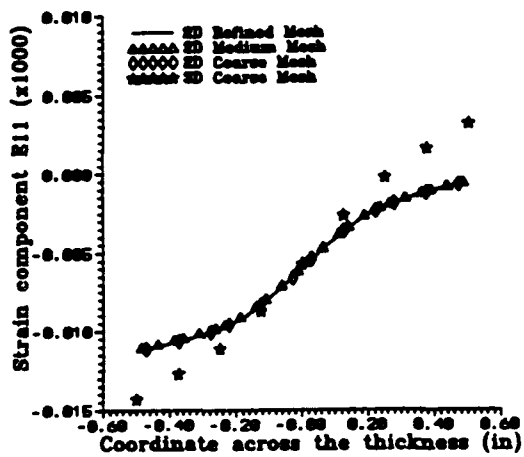


Figure 33: Cross-ply specimen. Some stress and strain components across the thickness at the center of the specimen.

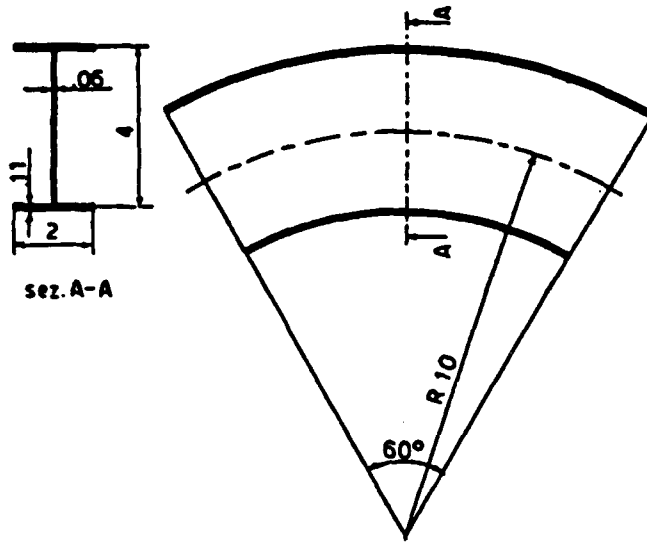


Figure 34: The curved composite I-shaped beam (dimensions are in inches).

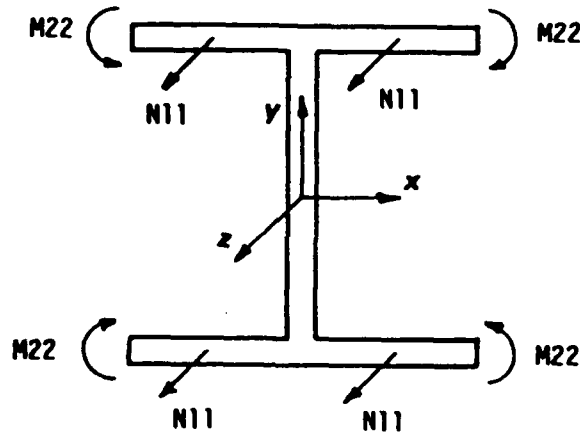


Figure 35: I-beam. Conventions for positive internal forces.

	Case	Layers	Thickness	Lamination
Web	all	12	.005 in.	$[6(\pm 45)]$,
Flange	1	22	.005 in.	$[3(0/90), 2(0), 3(\pm 45), 0/90, 0, 0/90, 0, 0/90]$
Flange	2	22	.005 in.	$[22(0)]$
Flange	3	22	.005 in.	$[9(0), 4(90), 9(0)]$
Flange	4	22	.005 in.	$[22(90)]$

Table 10: I-beam. Stacking sequences.

Orthotropic Young's modulus	E_L	=	2.63×10^7 lb in. ⁻²
Transversal Young's modulus	E_T	=	1.50×10^6 lb in. ⁻²
Tangential modulus	G_{LT}	=	1.04×10^6 lb in. ⁻²
Poisson's ratio	ν_{LT}	=	.28

Table 11: I-beam. Elastic properties.

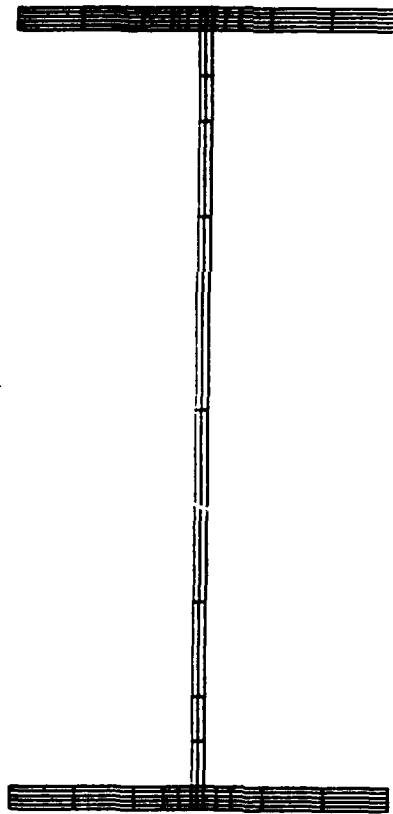


Figure 36: I-beam. Mesh of the cross-section.

Case	Axial rigidity (lb)	Bending rigidity (lb in. ⁻²)
1	5.2815×10^6	1.7305×10^7
2	5.8488×10^6	1.9591×10^7
3	5.4504×10^6	1.8466×10^7
4	1.5726×10^6	3.8004×10^6

Table 12: I-beam. Cross-sectional rigidities.

each flange (a plane element for each layer). All the elements are 8-node isoparametric elements. The total number of degrees of freedom is 5343: a three-dimensional discretization of the whole beam giving such detail would be computationally expensive.

Axial and bending rigidities in the analyzed cases are reported in Table 12: it has been observed that in the first three cases, although the stiffnesses are comparable in magnitude, the distribution of the axial force and the curling moment on the flanges are quite different.

The deformed cross-sections, the axial stress and the curling moment in the flanges due to tension and bending moment for Case 1 are shown in Figs. 37, 38 and 39. The axial tension is far from being constant along the flange span, showing that this kind of cross-section is not an optimum with respect to the maximum stress design criterium. This is mainly due to the interaction of the curling moment with the axial stress. Some strain components are plotted in Fig. 40 across the upper flange thickness (coordinates X and Y are measured with reference to the frame depicted in Fig. 35). It can be observed that while the extensional strain appears to be linear, the in-plane shear strain does not behave in such a way. This fact suggests that, for composite sections, it can be wrong to adopt a linear variation of the displacement through the thickness, which is usual in simpler approaches.

In Case 2 the flanges are made of uniaxial laminate with fibers along the beam axis, thus increasing the section axial and bending stiffness. Axial forces in the flanges come out to be about twice than Case 1 (see Figs. 42 and 43), but they can not spread along the flange width, due to the flange's poor stiffness to withstand the curling moment, which is lower than Case 1. That becomes evident from the deformed shape shown in Fig. 41 and is confirmed by the strains plotted in Fig. 44: the flanges do not deform significantly near their free edge and thus do not cooperate to the structural strength. This analysis stresses that the lamination of Case 2 is not a good choice as it would be for a straight beam.

Case 3 is similar to Case 2 but four layers have fibers along the flange span thus giving some capability to withstand the curling moment. That yields a more uniform distribution along the flange span of the axial stress, see Figs. 46 and 47.

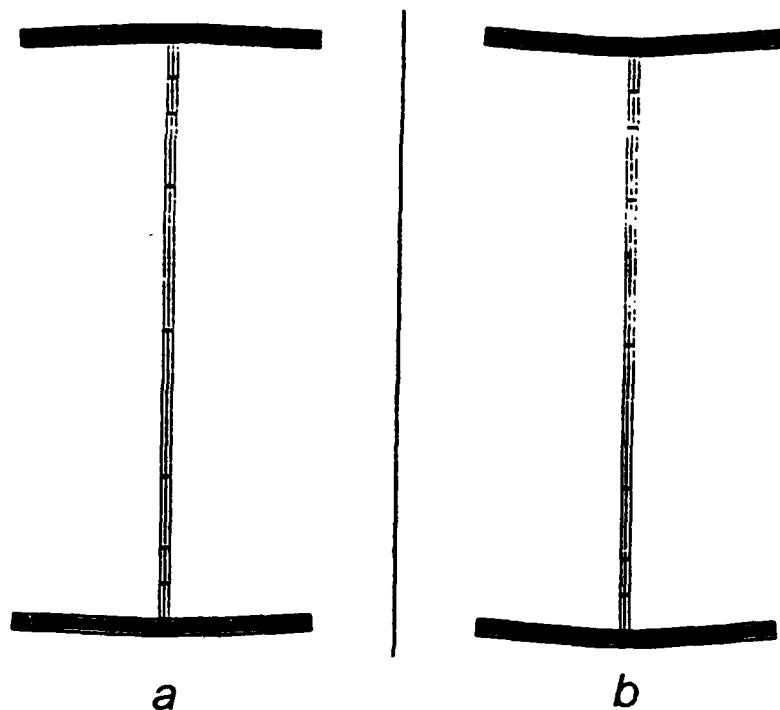
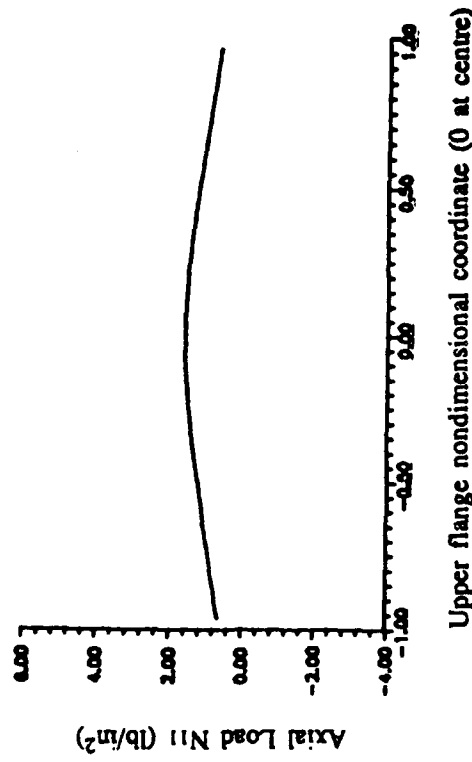
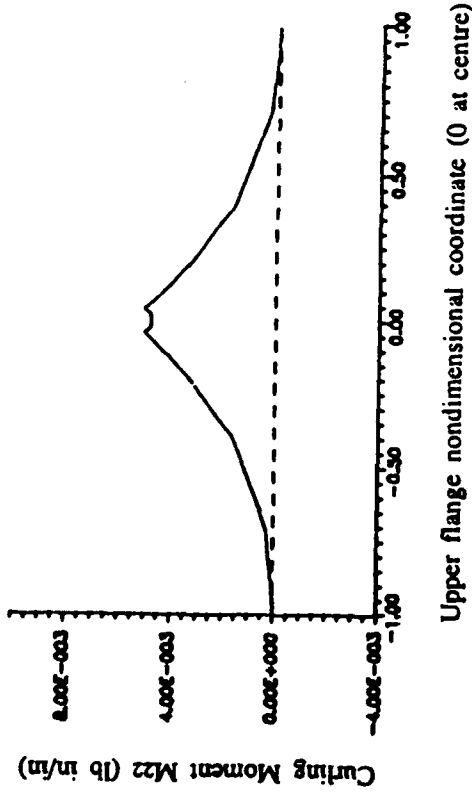


Figure 37: I-beam, Case 1. Deformed cross-section under (a) tension, (b) bending moment.

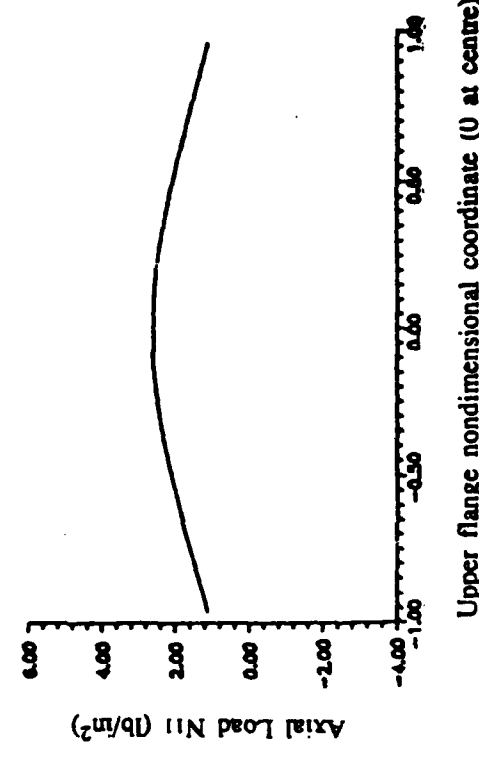
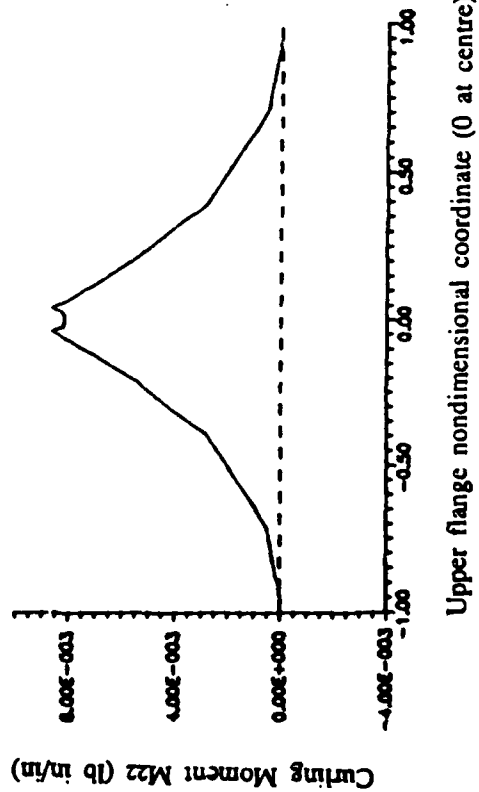
Nevertheless, the improvement is poor with respect to Case 2, since the transverse plies are located at the middle of the flange thickness: it can be seen from the deformation results in Figs. 45 and 48 that a wide area of the flange does not work significantly. After all, the axial and bending stiffness of the section is reduced with respect to Case 2.

In Case 4 all the plies lie along the flange span: this is the best configuration as regards to withstand the curling moment, but it lowers the axial strength of the flanges. As a consequence, the flanges do not quite work at all under tension and bending and the web is called to carry axial and bending loads. The results for Case 4 are shown in Figs. 49 to 52.

The present results were compared with the three-dimensional analysis by Peck (1991) on the beam model shown in Fig. 53. The MSC-NASTRAN mesh consists of 350 8-node plate elements and amounts to 9000 DOFs. In the central cross-section the applied loads give a compression axial force of 1593 lb and a bending moment of 9558 lb in. The axial stress and the curling moment in the flanges are shown in Fig. 54 together with the results of the present approach.

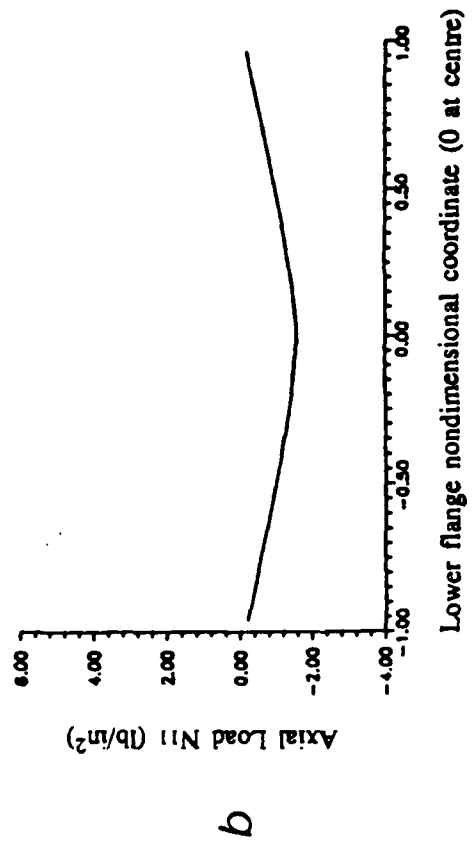
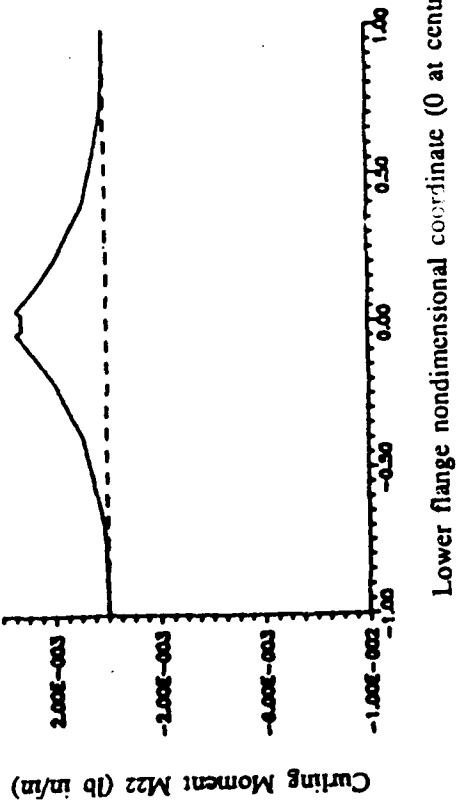


b

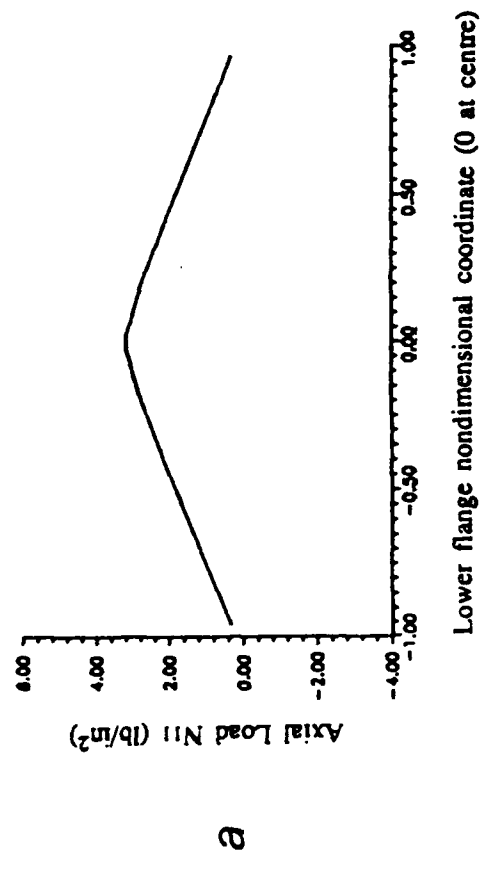
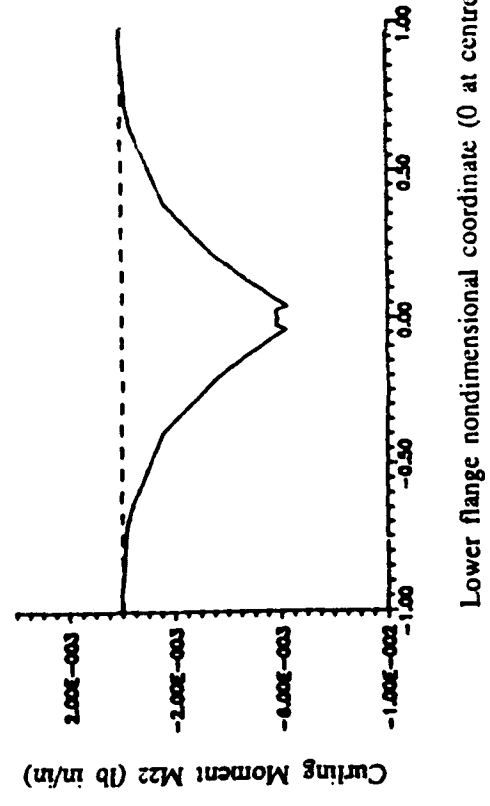


a

Figure 38: I-beam, Case 1. Internal forces in upper flange due to: (a) tension, (b) bending moment.



b



a

Figure 39: I-beam, Case 1. Internal forces in lower flange due to: (a) tension, (b) bending moment.

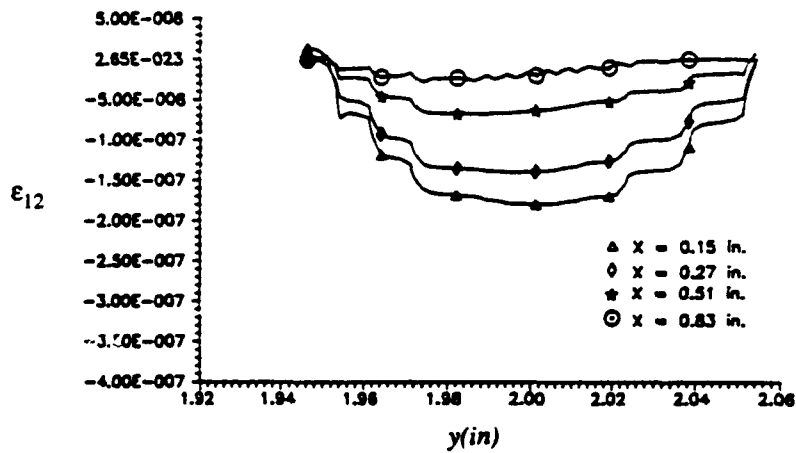
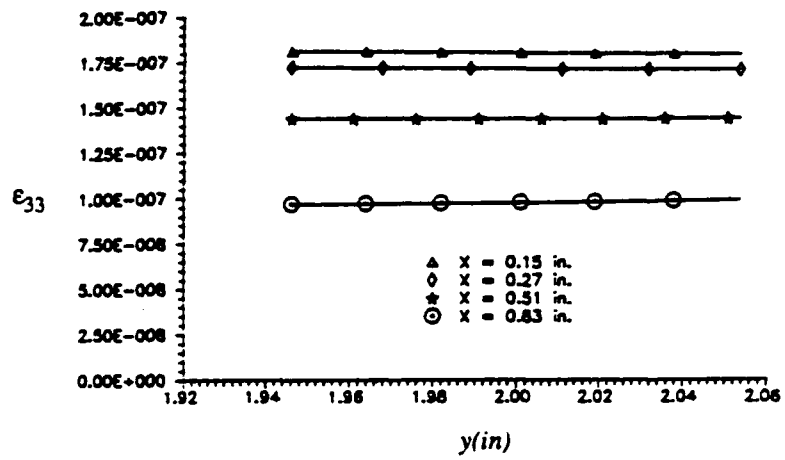
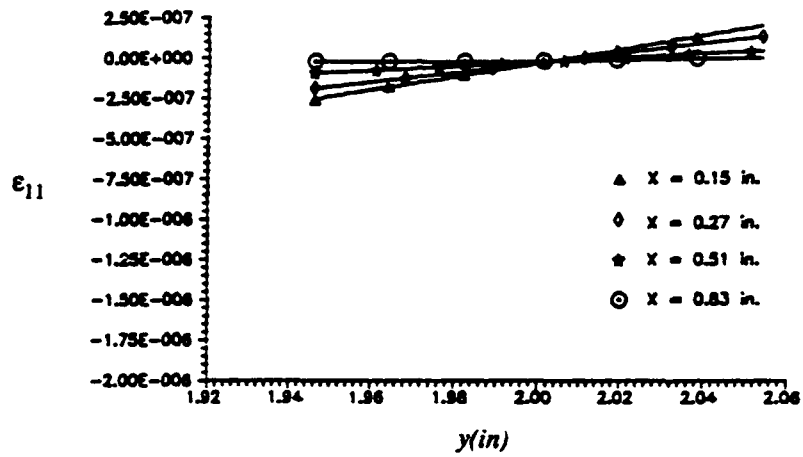


Figure 40: I-beam, Case 1. Some strain components across the thickness of the upper flange due to tension.

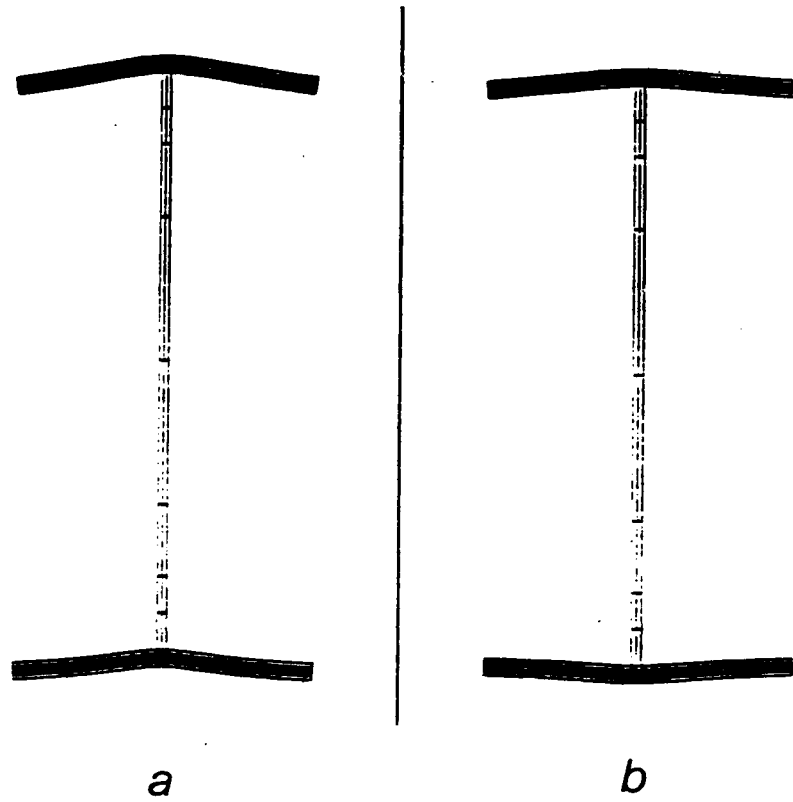


Figure 41: I-beam, Case 2. Deformed cross-section under (a) tension, (b) bending moment.

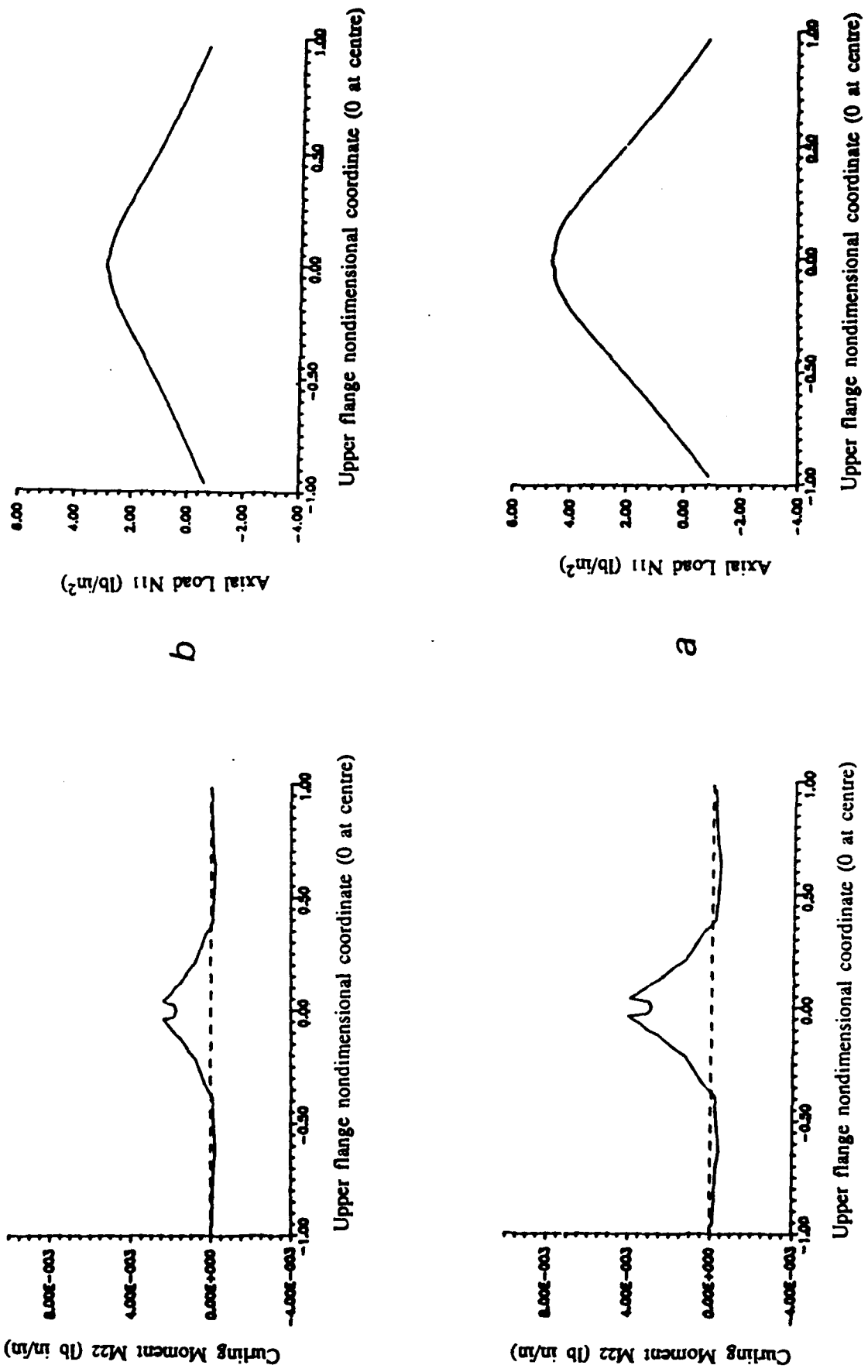
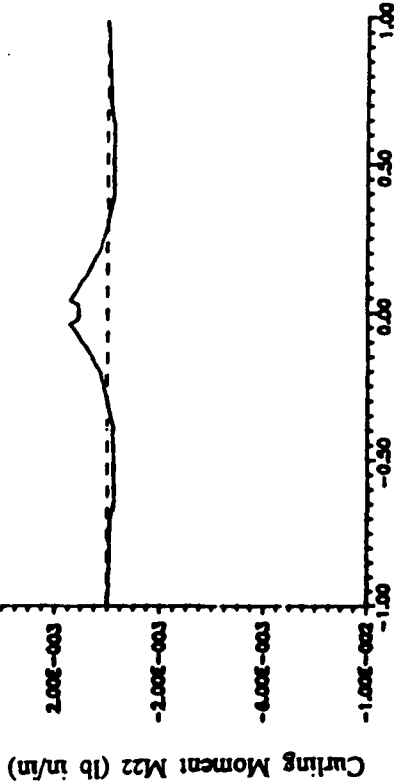
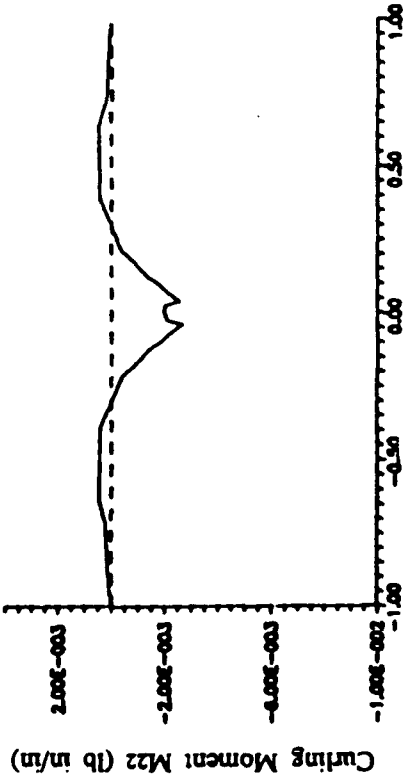


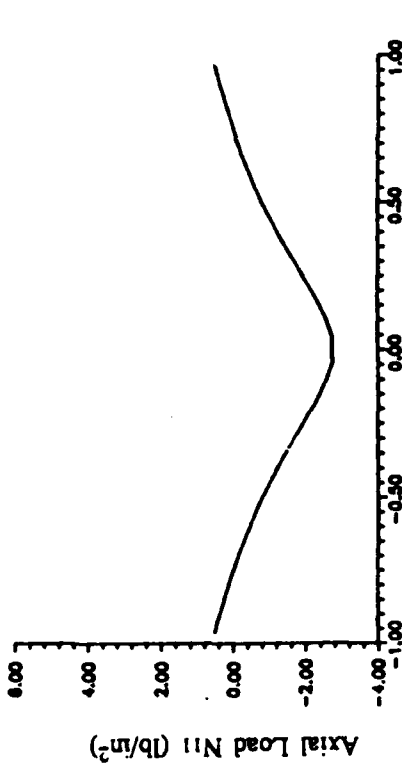
Figure 42: I-beam, Case 2. Internal forces in upper flange due to: (a) tension, (b) bending moment.



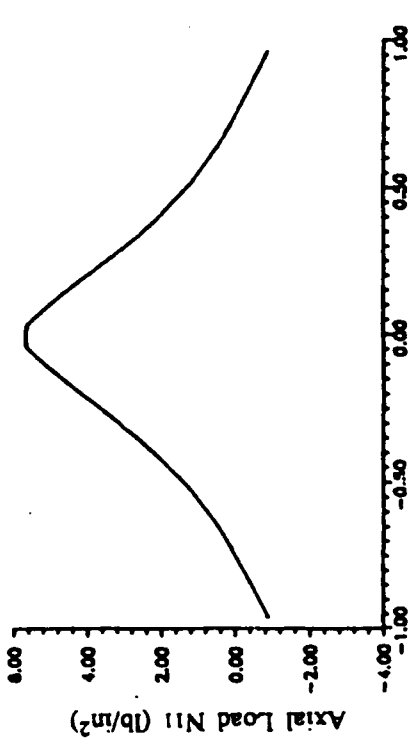
Lower flange nondimensional coordinate (0 at centre)



Lower flange nondimensional coordinate (0 at centre)



Lower flange nondimensional coordinate (0 at centre)



Lower flange nondimensional coordinate (0 at centre)

b

a

Figure 43: I-beam, Case 2. Internal forces in lower flange due to: (a) tension, (b) bending moment.

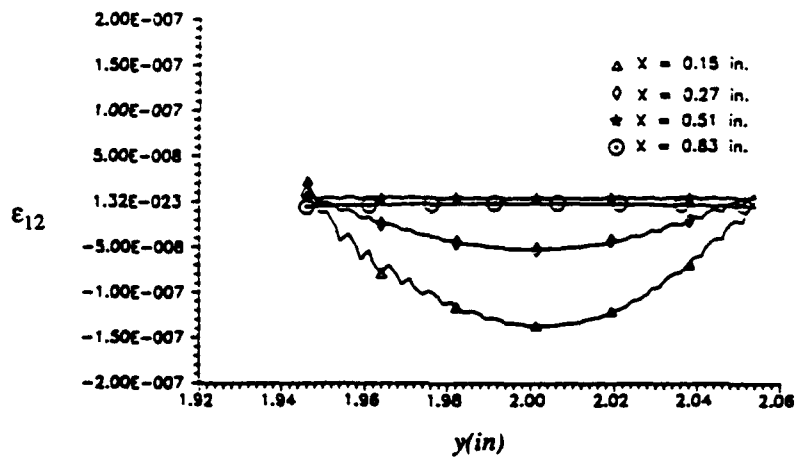
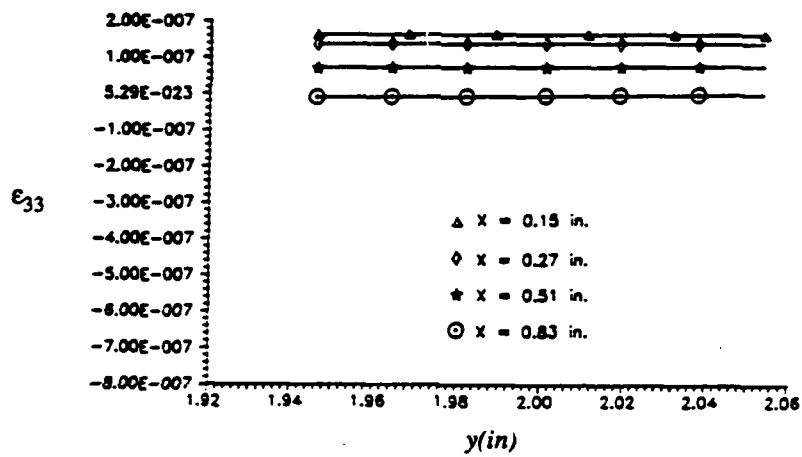
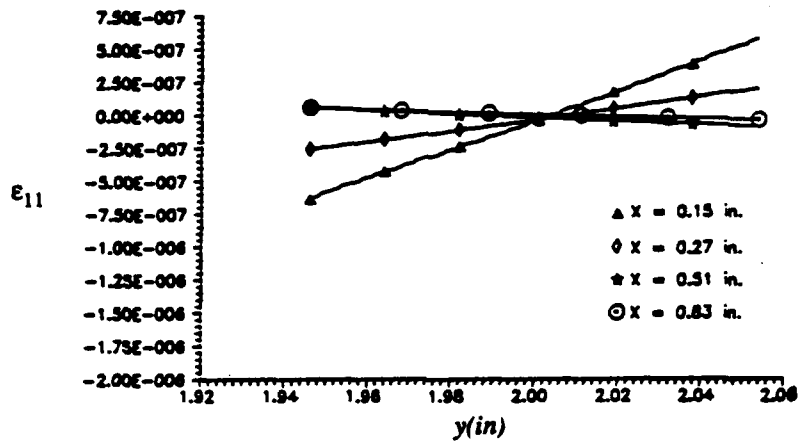


Figure 44: I-beam, Case 2. Some strain components across the thickness of the upper flange due to tension.

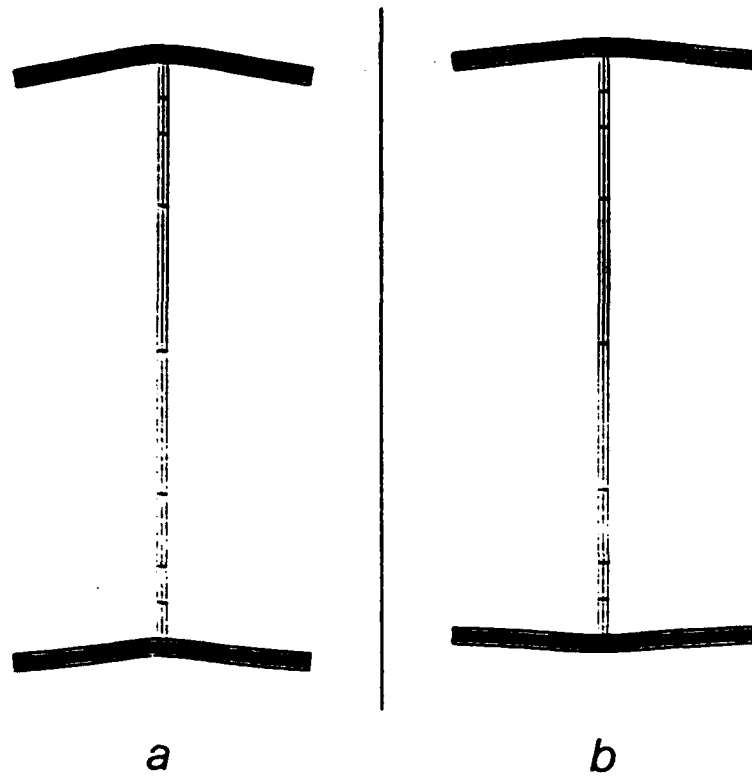


Figure 45: I-beam. Case 3. Deformed cross-section under (a) tension, (b) bending moment.

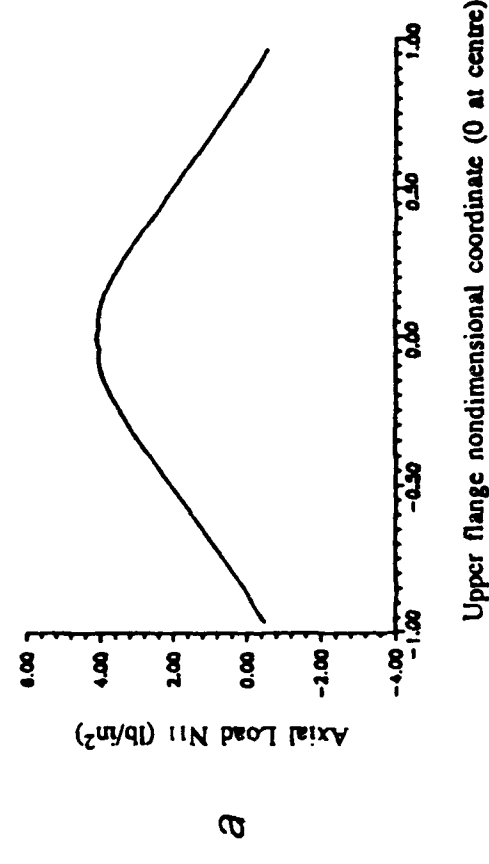
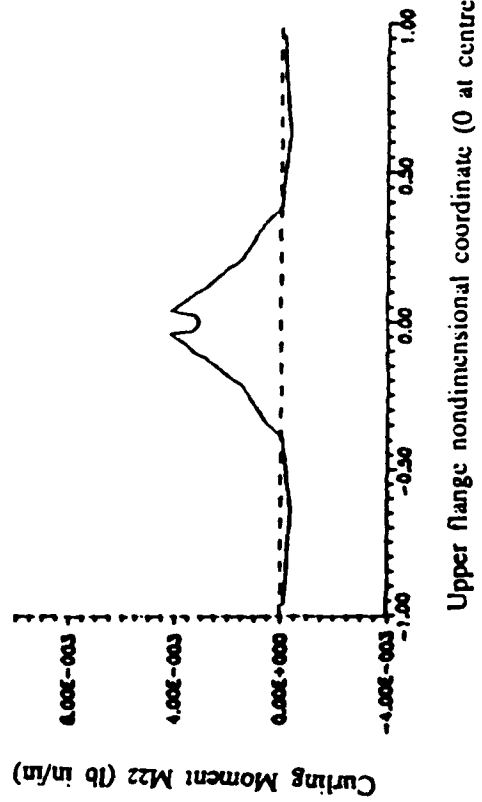
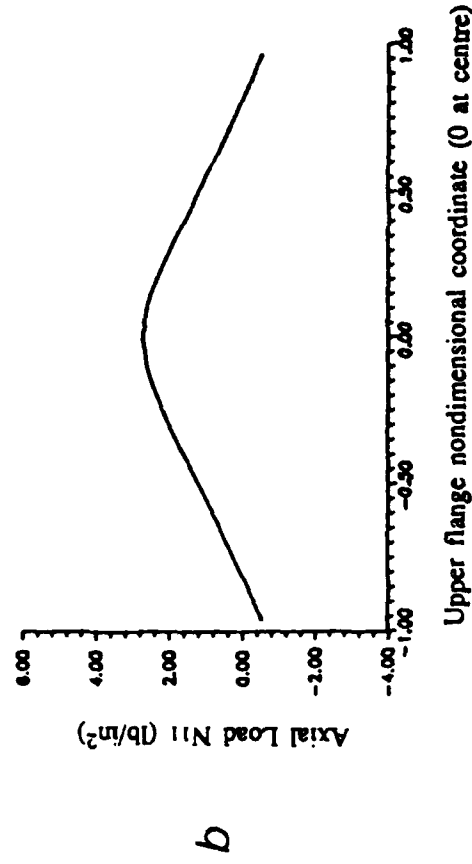
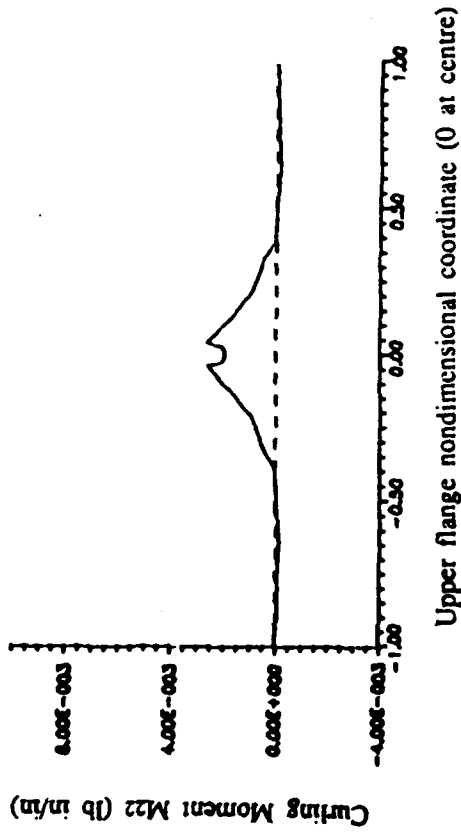
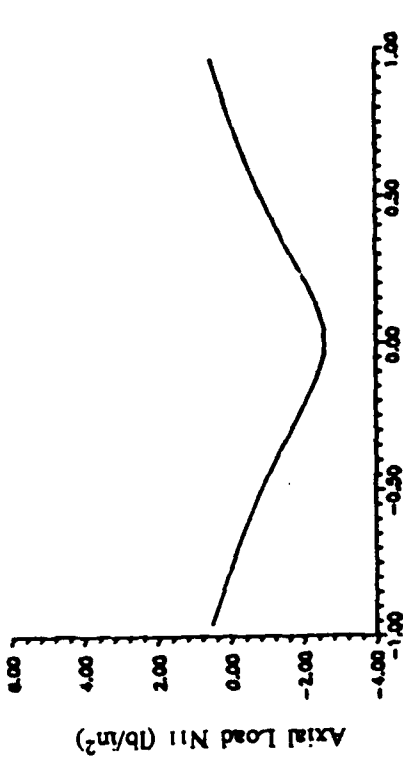
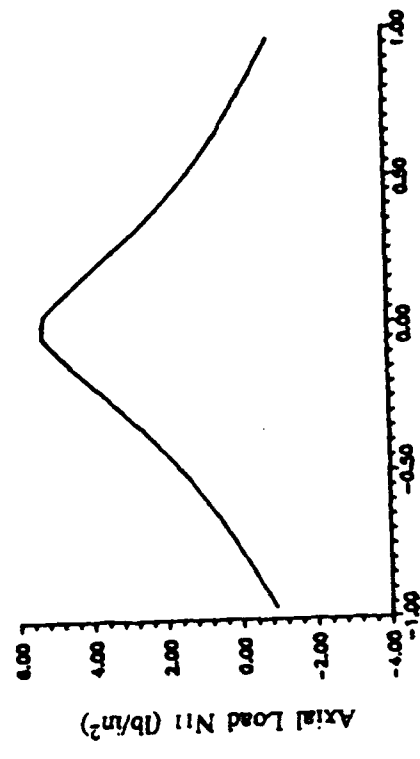


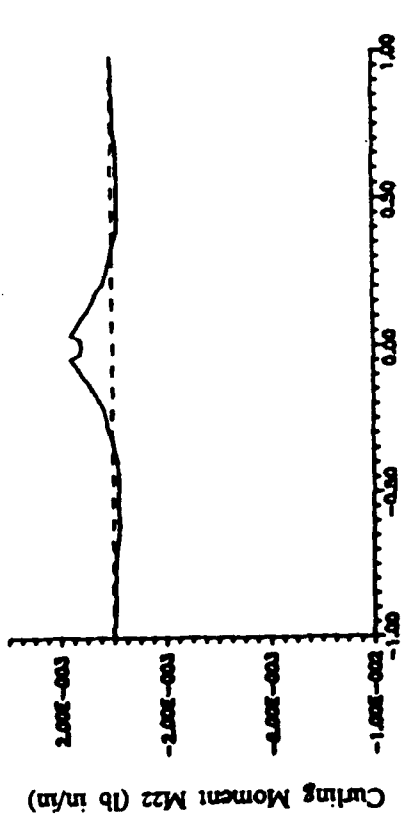
Figure 46: I-beam, Case 3. Internal forces in upper flange due to: (a) tension, (b) bending moment.



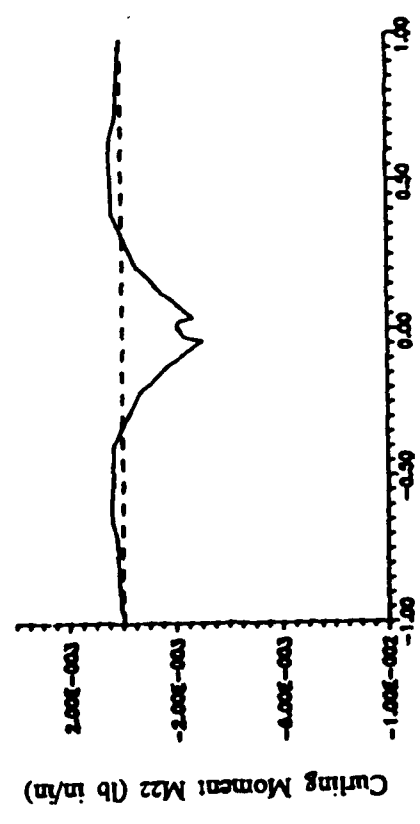
(a) tension



(b) bending moment



(a) tension



(b) bending moment

Figure 47: I-beam, Case 3. Internal forces in lower flange due to: (a) tension, (b) bending moment.

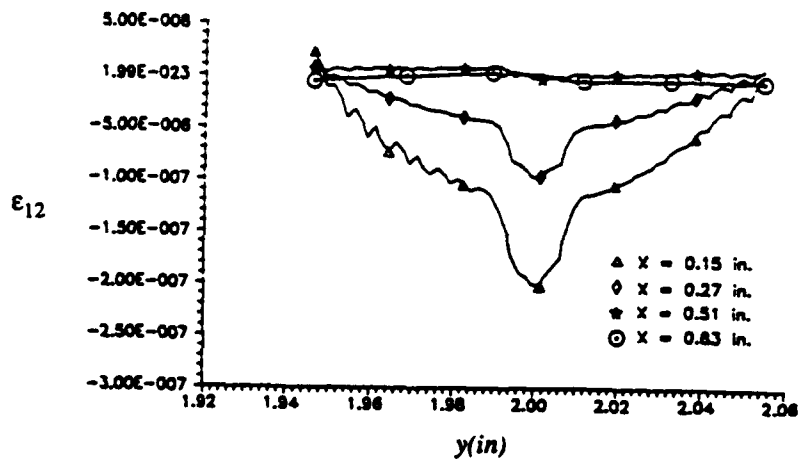
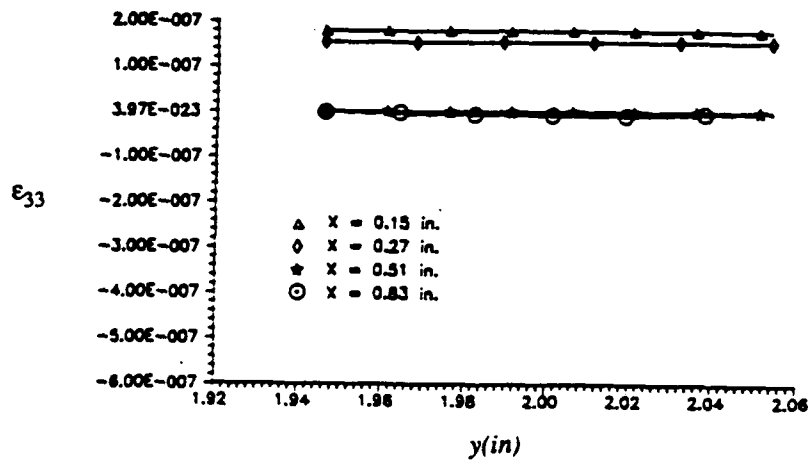
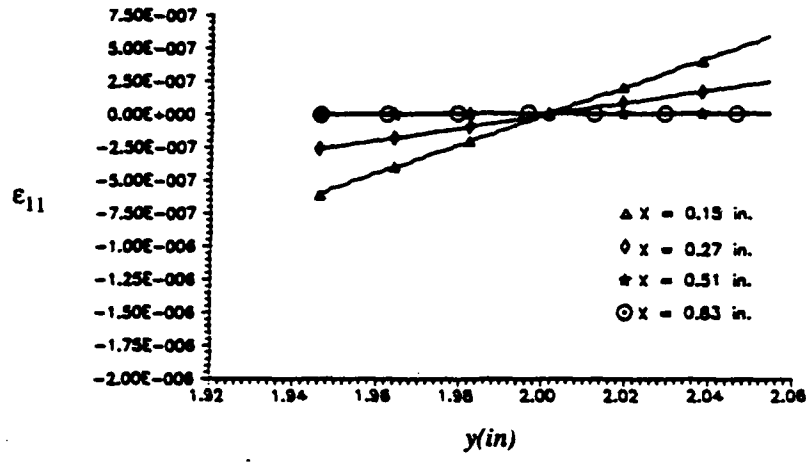


Figure 48: I-beam, Case 3. Some strain components across the thickness of the upper flange due to tension.

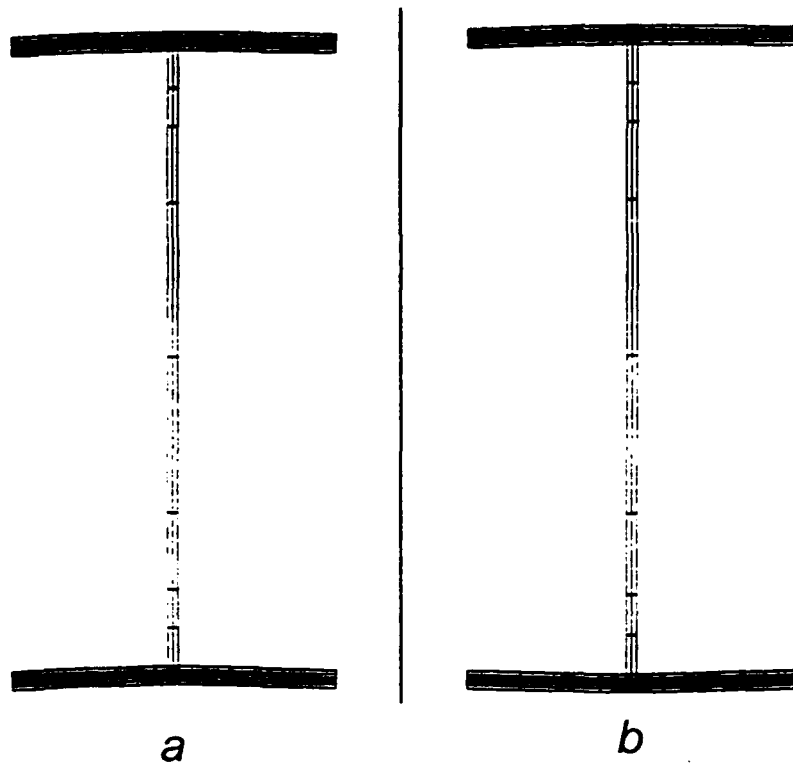


Figure 49: I-beam, Case 4. Deformed cross-section under (a) tension, (b) bending moment.

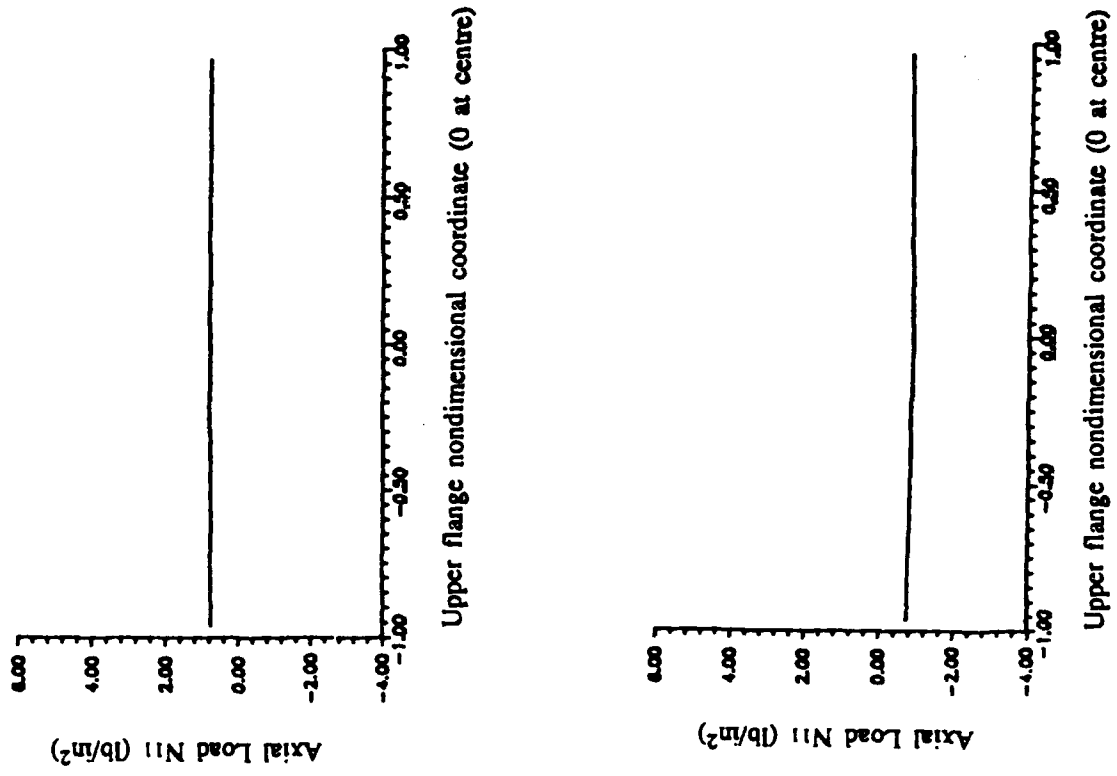
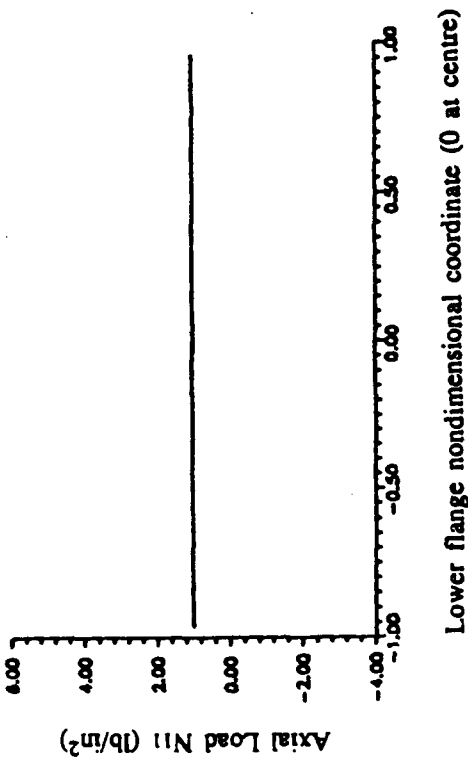
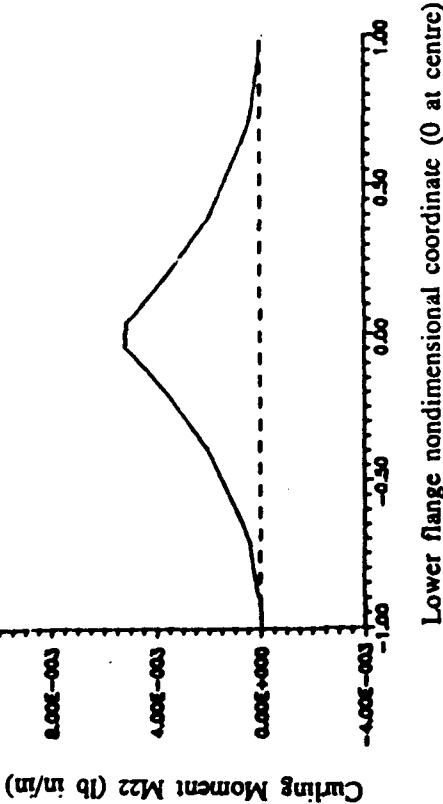
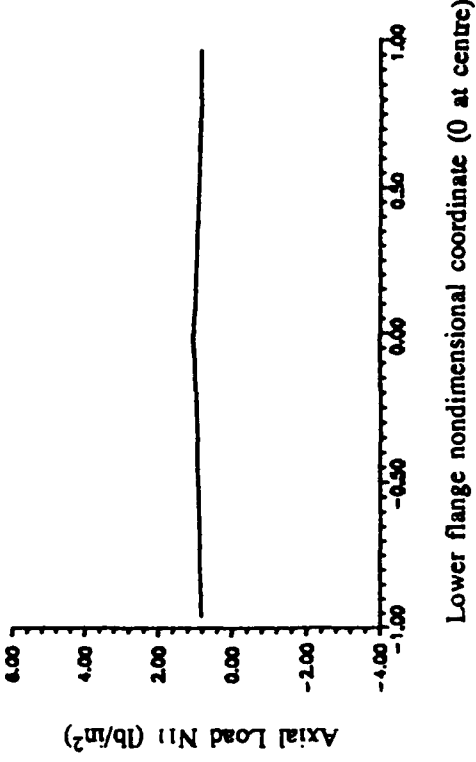
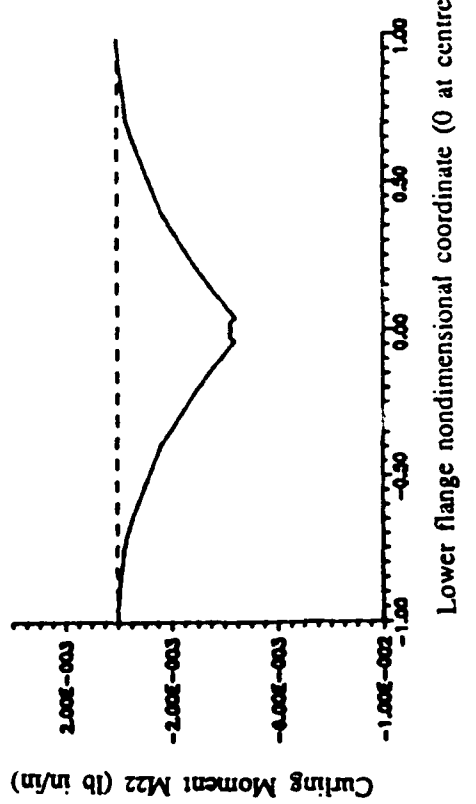


Figure 50: I-beam, Case 4. Internal forces in upper flange due to: (a) tension, (b) bending moment.



b



a

Figure 51: I-beam, Case 4. Internal forces in lower flange due to: (a) tension, (b) bending moment.

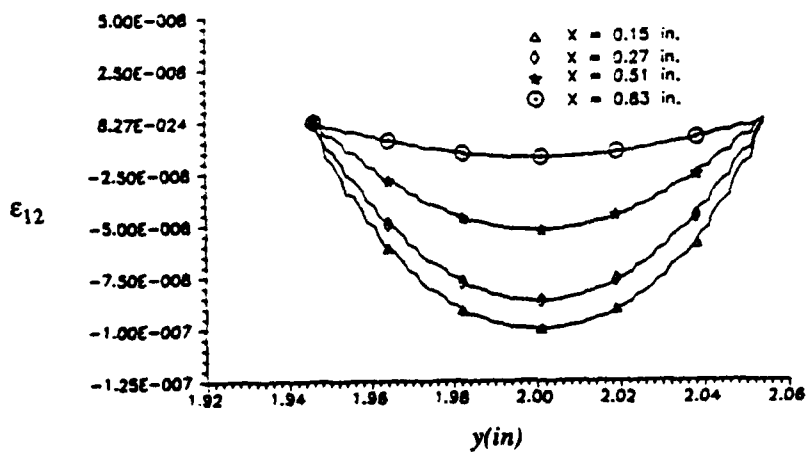
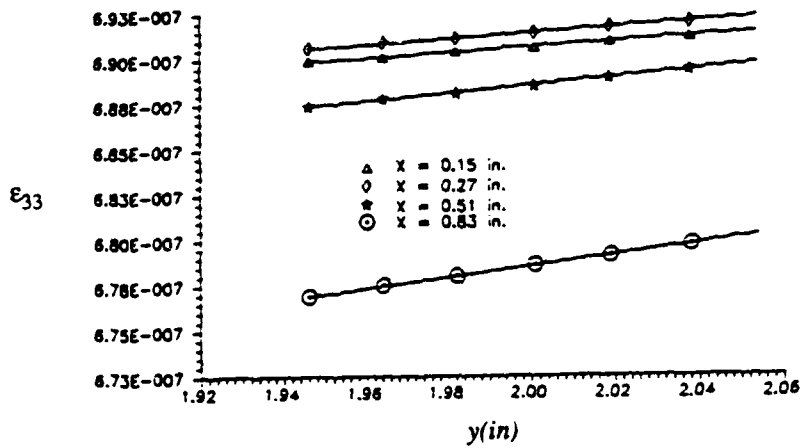
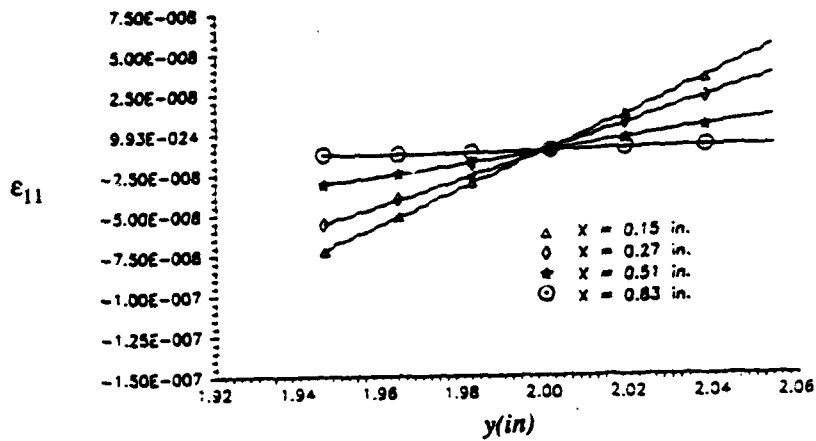


Figure 52: I-beam, Case 4. Some strain components across the thickness of the upper flange due to tension.

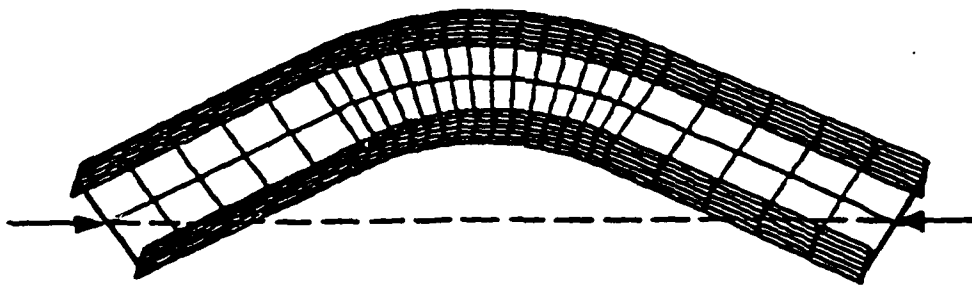


Figure 53: I-beam. MSC-NASTRAN mesh (Peck, 1991).

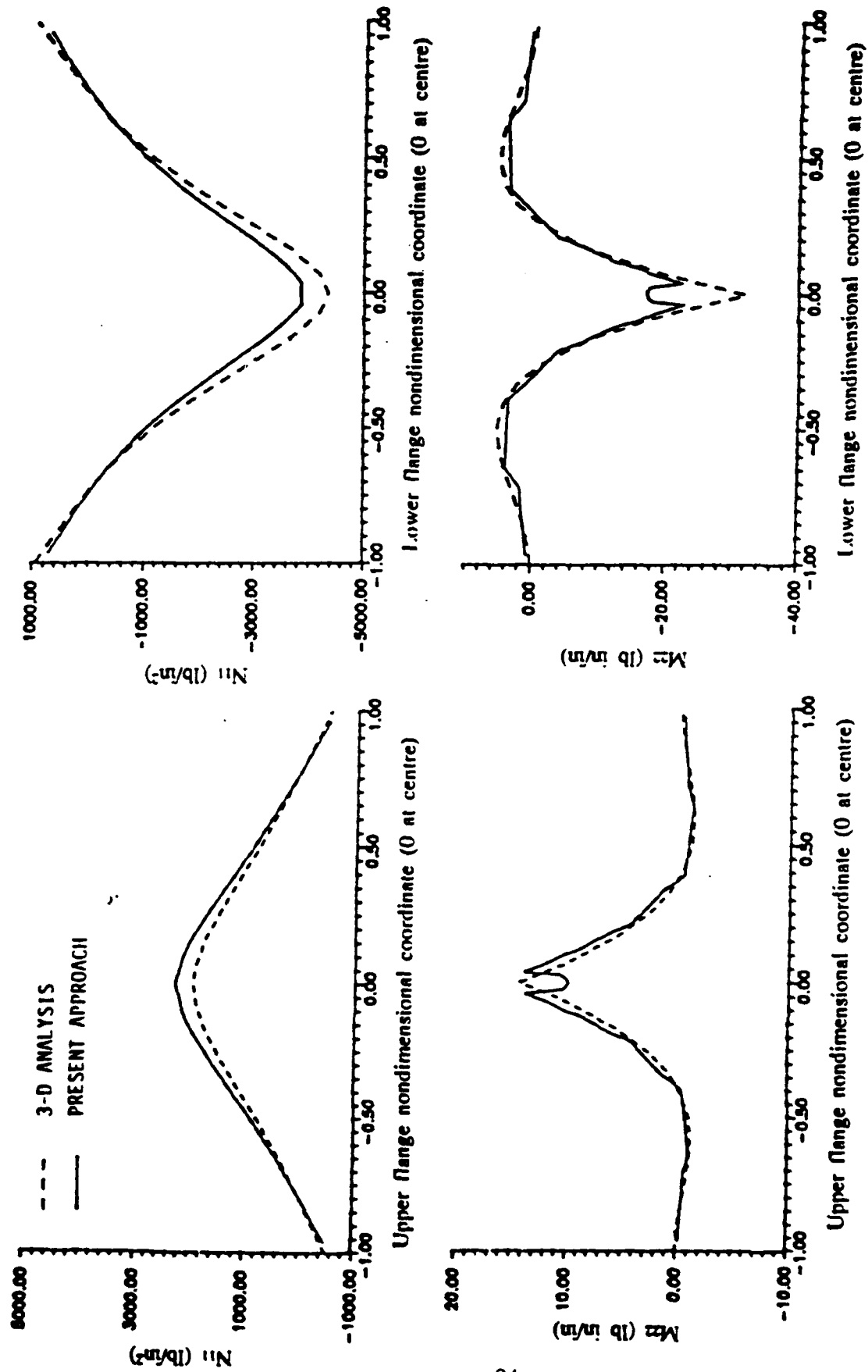


Figure 54: I-beam. Axial stress and curling moment on the flanges. Comparison with MSC-NASTRAN results (Peck, 1991).

6 Conclusions

The method developed to obtain the cross-sectional constitutive equations of naturally curved and twisted anisotropic beams is consistent with the three-dimensional theory of elasticity. No specific simplifications have been introduced except constancy of section, curvature and twist, which are commonly used in beam theory. The potential of the method is implied in the fact that it requires a two-dimensional approximation, thus achieving a degree of detail which is considered unfeasible with a three-dimensional approach. The finite element analysis of the beam cross-section constitutes a good step towards the understanding the complexity of composite beams and a useful mathematical tool for the tailoring of real designs.

The scope of the research, contained in the proposal, has been reached. Nevertheless, additional research work in this direction should be done: in particular, it is in the authors' opinion that it would be extremely useful and profitable to choose as benchmark some significant test case taken from real design; these should be submitted to different research centers and helicopter industries in order to assess the state of the art in the computation of composite blades.

7 References

- Atilgan, A. R. and Hodges, D. H. (1990). Unified nonlinear analysis for nonhomogeneous anisotropic beams with closed cross sections. *AIAA JI* 29, 1990-1999.
- Atilgan, A. R., Hodges, D. H. and Fulton, M. V. (1991). Nonlinear deformation of composite beams: unification of cross-sectional and elastica analyses. *Appl. Mech. Rev.* 44(11), part 2, S9-S15.
- Bauchau, O. A. (1985). A beam theory for anisotropic materials. *J. Appl. Mech.* 52, 416-422.
- Bauchau, O. A. and Hong, C. H. (1987). Large displacement analysis of naturally curved and twisted composite beams. *AIAA JI* 25, 1469-1475.
- Bauchau, O. A. and Hong, C. H. (1988). Nonlinear composite beam theory. *J. Appl. Mech.* 55, 156-163.
- Berdichevsky, V. L. (1981). On the energy of an elastic rod. *Prikl. Mat. Mek.* 45, 518-529.
- Berdichevsky, V. L. and Staroselsky, L. A. (1983). On the theory of curvilinear Timoshenko-type rods. *Prikl. Mat. Mek.* 47, 809-817.
- Borri, M. and Mantegazza, P. (1985). Some contributions on structural and dynamic modeling of helicopter rotor blades. *Aerotec. Missili Spazio* 64, 143-154.
- Borri, M. and Merlini, T. (1986). A large displacement formulation for anisotropic beam analysis. *Meccanica* 21, 30-37.
- Cardona, A. and Geradin, M. (1988). A beam finite element non-linear theory with finite rotations. *Int. J. Num. Meth. Engng* 26, 2403-2438.
- Danielson, D. A. and Hodges, D. H. (1987). Nonlinear beam kinematics by decomposition of the rotation tensor. *J. Appl. Mech.* 54, 258-262.
- Danielson, D. A. and Hodges, D. H. (1988). A beam theory for large global rotation, moderate local rotation, and small strain. *J. Appl. Mech.* 55, 179-184.
- Ghiringhelli, G. L. and Sala, G. (1986). Interlaminar edge stress analysis of composite cross-ply flat specimens. *Meccanica* 21, 151-158.
- Ghiringhelli, G. L. and Sala, G. (1990). Influence of stacking sequence and interlaminar layer on stress singularities at free edge of composite laminates. *Meccanica* 25, 32-39.
- Giavotto, V., Borri, M., Mantegazza, P., Ghiringhelli, G. L., Caramaschi, V., Maffioli, G. C. and Mussi, F. (1983). Anisotropic beam theory and applications. *Comput. Struct.* 16, 403-413.
- Hodges, D. H. (1987a). Finite rotation and nonlinear beam kinematics. *Vertica* 11, 297-307.
- Hodges, D. H. (1987b). Nonlinear beam kinematics for small strains and finite rotations. *Vertica* 11, 573-589.
- Hodges, D. H. (1990a). A mixed variational formulation based on exact intrinsic equations for dynamics of moving beams. *Int. J. Solids Structures* 26, 1253-1273.

Hodges, D. H. (1990b). Review of composite rotor blade modeling. *AIAA JI* 28, 561-565.

Hodges, D. H., Atilgan, A. R., Cesnik, C. E. S. and Fulton, M. V. (1991a). On a simplified strain energy function for geometrically nonlinear behavior of anisotropic beams. *Proc. 17th European Rotorcraft Forum*, Berlin, Germany, 24-27 Sept. 1991.

Hodges, D. H., Atilgan, A. R., Fulton, M. V. and Rehfield, L. W. (1991b). Free-vibration analysis of composite beams. *J. Am. Helicopter Soc.* 36(3), 36-47.

Iura, M. and Atluri, S. N. (1988). Dynamic analysis of finitely stretched and rotated three-dimensional space-curved beams. *Comput. Struct.* 29, 875-889.

Iura, M. and Atluri, S. N. (1989). On a consistent theory, and variational formulation of finitely stretched and rotated 3-D space-curved beams. *Comput. Mech.* 4, 73-88.

Kosmatka, J. B. and Dong, S. B. (1991). Saint-Venant solutions for prismatic anisotropic beams. *Int. J. Solids Structures* 28, 917-938.

Merlini, T. (1988). On the development of static modes in slender elements under end loads. *Aerotec. Missili Spazio* 67, 104-118.

Parker, D. F. (1979a). An asymptotic analysis of large deflections and rotations of elastic rods. *Int. J. Solids Structures* 15, 361-377.

Parker, D. F. (1979b). The role of Saint Venant's solutions in rod and beam theories. *J. Appl. Mech.* 46, 861-866.

Peck, A. W. (1991). Design and optimization of curved composite beams. Ph.D. Thesis, Rensselaer Polytechnic Institute, Troy.

Rehfield, L. W., Atilgan, A. R. and Hodges, D. H. (1990). Nonclassical behavior of thin-walled composite beams with closed cross sections. *J. Am. Helicopter Soc.* 35(2), 42-50.

Reissner, E. (1973). On one-dimensional large-displacement finite-strain beam theory. *Studies Appl. Math.* 52, 87-95.

Reissner, E. (1981). On finite deformations of space-curved beams. *ZAMP (J. Appl. Math. Physics)* 32, 734-744.

Simo, J. C. (1985). A finite strain beam formulation. The three-dimensional dynamic problem. Part I. *Comp. Meth. Appl. Mech. Engng* 49, 55-70.

Simo, J. C. and Vu-Quoc, L. (1988). On the dynamics in space of rods undergoing large motions - A geometrically exact approach. *Comp. Meth. Appl. Mech. Engng* 66, 125-161.

Smith, E. C. and Chopra, I. (1990). Formulation and evaluation of an analytical model for composite box beams. *Proc. 31st AIAA/AHS/ASME/ASCE/ASC Structures, Structural Dynamics and Materials Conference*, Long Beach, CA, April 2-4, 1990.

Stemple, A. D. and Lee, S. W. (1988). Finite-element model for composite beams with arbitrary cross-sectional warping. *AIAA JI* 26, 1512-1520.

Stemple, A. D. and Lee, S. W. (1989). A finite element model for composite beams undergoing large deflection with arbitrary cross-sectional warping. *Int. J. Num. Meth. Engng* 28, 2143-2160.